In Situ Monitoring of UV-Curing Kinetics of Acrylate Coatings by Combined Ultrasound Reflectometry and Near-Infrared Spectroscopy

Vom Fachbereich Chemie

der Technischen Universität Darmstadt

zur Erlangung des akademischen Grades eines

Doktor rerum naturalium (Dr. rer. nat.)

genehmigte

Dissertation

vorgelegt von

M. Tech. Suman Agarwal

aus Cuttack, Indien

Referent:	Prof. Dr. M. Rehahn
Co-Referent:	Priv.- Doz. Dr. I. Alig
Tag der Einreichung:	26 .11.2010
Tag der mündlichen Prüfung:	10.01.2011

Darmstadt 2011

D 17

Acknowledgement

In this section I would like to acknowledge all the people who contributed to this work.

My special thanks go to *Prof. Dr. Matthias Rehahn* for agreeing to be my supervisor. I thank him for his belief in me.

I express my deepest gratitude to *PD. Dr. Ingo Alig* for the encouragement, guidance and support from the initial to the final stage that enabled me to develop an understanding of the subject. I also thank him for the trust and confidence I was shown.

I would also like to thank *Prof. Dr. Florian Müller-Plathe* and *Prof. Dr. Bernd Stühn* for agreeing to be the reviewers of this thesis.

I am grateful to *Dr. Dirk Lellinger* for developing softwares for the analysis of NIR data, ultrasonic data and combination of ultrasonic and NIR data in real time. These were critical tools for my work. I am thankful to him for lot of discussions, scientific problem solving and ideations. His simplicity and willingness to help is highly appreciated.

I am thankful to *Dipl.-Ing. Harald Oehler* for helpful discussions and support throughout my work.

I owe my thanks to our project partners at IOM Leipzig. I would like to thank *Dr. Tom Scherzer* for playing an important role in sample selection. He was also prompt in his response to my questions regarding samples. I owe my thanks to *Katya Heymann* for abrasion tests and SEM measurements and *Mrs. Stefanie kriehn* for sample preparation.

I am thankful to *Mr. Wolfgang Boehm* for DMTA measurements and other practical help during my work.

I thank *Prof. Dr. Ralph Stengler* and *Dipl.-Ing. Mark Hartwich,* at Hochschule Darmstadt for allowing me to use the Universal Surface Tester. I also thank *Dipl.-Ing. Christoph Brinkmann* for GPC measurement and *Mrs. Christel Hock* for FTIR measurements, at DKI.

I thank *Mrs. Bärbel Schorlemmer, Mrs. Melanie Stein, Mrs. Anita Werner*, *Mrs. Cornelia Graefing and Dr. Hans Kothe* for their help in administrative matters.

Many thanks to *Dr. Ludmilla Scheffner* for the discussions and inputs in the manuscript. It was always a pleasant experience interacting with her.

I thank *Dr. Frank Boehm* for explaining me the method of construction of DMTA Master curves.

I thank all my colleagues for providing me an excellent work environment. It was a wonderful experience working at DKI.

Many thanks to *Dietrich Praclik* and *Dr. Irmgard Praclik* who have been playing the role of my guardians and friends in Germany. They made my stay in Germany very smooth and fun-filled. I would also like to thank *Dipl.-Ing. Shilpa Khare, Gholamreza Marzooghi* for their support and advice. They are the first set of friends that I made in Germany. I also thank Chitta Rajesh for the fun filled times spend together. I also thank to all my friends for their help and the fun we had together but whose names do not figure in this list.

I would like to shower my appreciation on my parents for their constant support, motivation and trust in me. I thank them for their blessings and love.

Last but not the least, I am grateful to my husband *Rahul Narayan* for his motivation and support throughout my work.

Suman Agarwal Darmstadt, November 2010

This study is a result of the work carried out from November 2007 to November 2010 at German Polymer Institute Darmstadt, under the supervision of Prof. Dr. Matthias Rehahn and PD. Dr. Ingo Alig.

“If I have the belief that I can do it, I shall surely acquire the capacity to do it even if I may not have it at the beginning.”

Mahatma Gandhi, 1869-1948

1 Zusammenfassung

Das Ziel dieser Arbeit war die Untersuchung der Kinetik der UV-induzierten Härtung und der Bildung von Netzwerken von UV-härtbaren Acrylat-Harzen. Hierzu wurden kombinierte Ultraschall/NIR-Echtzeitmessungen durchgeführt. Dies ermöglicht die gleichzeitige Erfassung des chemischen Umsatzes und des mechanischen Moduls (in diesem Fall Schubmodul) an derselben Probe. Hierdurch werden Fehler minimiert, die ggf. bei zwei getrennten Experimenten auftreten können. Zudem kann man die gegenseitige Abhängigkeit der chemischen Reaktion und der rheologischen Eigenschaften während der Aushärtung studieren. Diese sich ergänzenden Informationen sind von Interesse, da sie ermöglichen, den Zusammenhang zwischen Reaktionskinetik und den daraus resultierenden mechanischen Eigenschaften herzustellen. Zudem liefert diese Methodenkombination Informationen für ein besseres Verständnis der UV-Härtungskinetik. So kann man beispielsweise das Einsetzen der diffusionskontrollierten Reaktionen oder den Übergang zwischen der „Lichthärtungsphase“ und der „Dunkelreaktion“ identifizieren. Mit der hohen zeitlichen Auflösung beider Messtechniken - Ultraschallreflektometrie (US) und Nahinfrarot-Spektroskopie (NIR) - war es möglich, die Härtung von reaktiven Acrylaten mit einer Zeitauflösung von Millisekunden zu untersuchen. Zusätzlich zur Härtungskinetik wurden wichtige Eigenschaften der Beschichtung wie Kratzfestigkeit, Abriebfestigkeit und Trübung sowie die frequenz-und temperatur-abhängigen viskoelastischen Eigenschaften im ungehärteten und gehärteten Zustand untersucht.

Es wurden zwei Acrylat-Systeme betrachtet: das harte und spröde Epoxidacrylat (EPA) und das weiche Elastomer Urethanacrylat (UA). Beide Harze wurden sowohl ohne als und mit dem Reaktivverdünner Tripropylenglykoldiacrylat (TPGDA) untersucht. Die Acrylat-Harze zeigen eine charakteristische Absorptionsbande bei 1621 nm im NIR-Bereich (900–2200 nm), welche der Acrylat-Doppelbindung zugeordnet werden kann. Wenn das Acrylat-Harz polymerisiert, verringert sich die Intensität dieser Bande. Der Umsatz wurde über die Abnahme der Fläche unter der Acrylatbande (im Fall von UA) bzw. über die Abnahme der Höhe der Acrylatbande (im Fall von EPA) berechnet. Um den Umsatz zu berechnen wurde das Spektrum von 1500 nm bis 1800 nm durch neun Gauß’sche und eine kubische Funktion (im Fall von UA) bzw. durch drei Gauß’sche und eine lineare Funktion (im Fall von EPA) angepasst. Die Ultraschall-Reflexionstechnik misst die Änderungen des akustischen Reflexionskoeffizienten für US-Transversalwellen, wenn diese an der Grenzfläche zwischen

der Probe und der US-Quarzglas-Messzelle reflektiert werden. Aus dem Reflexionskoeffizienten kann der Schubmodul der Probe errechnet werden.

Im Folgenden werden die Änderung der Härtungskinetik und der rheologischen bzw. mechanischen Eigenschaften in den untersuchten Acrylat-Harzen in Abhängigkeit von der Lackrezeptur und den Aushärtungsbedingungen zusammengefasst:

- *Einfluss des Reaktivverdünners*: Die Zugabe des Reaktivverdünners TPGDA in EPA verringert die Viskosität und erhöht die Mobilität der Reaktanden. Das führt zu einem Anwachsen der Polymerisationsrate und zu einem schnelleren Anstieg des Schubmoduls. Die Modul-Umsatz-Kurven zeigten, dass sich die Reaktionen mit zunehmender Verdünnung von einem eher diffusionsbestimmten Reaktionstyp zu einem zunehmend längeren Zeitintervall mit massenbestimmter Reaktion änderten. Sowohl der Endumsatz als auch die Endmodulwerte der Lackschicht wachsen mit dem Gehalt des Reaktivverdünners TPGDA. Die DMTA-Analyse zeigt, dass die Netzwerkdichte von EPA größer wird, wenn TPGDA mit geringem Molekulargewicht hinzugefügt wird. Das zeigt sich auch in einer Abnahme der Elastizität und einer Zunahme von permanenten Deformationen bei Prüfung der Kratzfestigkeit.
- *Einfluss des Photoinitiators und der Dauer der UV-Bestrahlung*: Die Zunahme der Konzentration des Photoinitiators und die Dauer der UV-Bestrahlung zeigen einen ähnlichen Effekt auf den Schubmodul und die Glasübergangstemperatur der ausgehärteten EPA/TPGDA-Lackschicht. Zunehmende UV-Bestrahlungszeit erhöht den Endumsatz und den Endmodulwerte der Schicht, ohne hingegen die Reaktionsgeschwindigkeit und den Zusammenhang zwischen Modul und Umsatz des reagierenden Harzes während der UV-Härtungsphase zu beeinflussen. Dagegen werden bei erhöhter PI-Konzentration sowohl die Polymerisationsrate als auch die Abhängigkeit des Moduls vom Umsatz geändert. Dies geschieht auf Grund der Erhöhung der Konzentration von Primärradikalen, die die Polymerisation beschleunigt und die Netzwerkdichte der Lackschicht erhöht.

Im Folgenden soll der Einfluss von funktionalisierten und anorganischen Nanopartikeln, ihrer Typen und ihrer Konzentration auf die Eigenschaften und die Aushärtungskinetik der EPA- und UA-Matrix zusammengefasst werden:

- *Einfluss verschiedener Typen von Nanopartikeln*: Eine Reihe von Experimenten mit ALMAL, ALOXAl, Aerosil, ALMA und SIMA (15 wt % bzgl. der Matrix) in EPA/TPGDA zeigte, dass der chemische Umsatz und der Schubmodul weitgehend

unabhängig vom Typ der Nanopartikel sind. Die Werte des Endumsatzes sowie der Glastemperatur unterscheiden sich nur unwesentlich von denen der ungefüllten Matrixmaterialien. Das zeigt, dass die Nanopartikel keinen wesentlichen Einfluss auf den Reaktionsverlauf haben. Der Schubmodul der EPA/TPGDA-Lackschicht steigt unabhängig von Typ der Nanopartikel mit zunehmender Nanopartikelkonzentration. Der kleinste Trübungswert konnte bei Filmen mit ALMA Nanopartikeln gemessen werden (<20 %). Diese Filme waren noch transparent, wohingegen alle anderen Filme höhere Trübungswerte zeigen. SEM-Aufnahmen zeigen, dass die ALMA Nanopartikel besser in der Matrix dispergiert waren und somit wenig Agglomerate vorlagen. SIMA Nanopartikel zeigten hingegen Agglomeratbildung (Agglomeratgroße: 200-400 nm). Verbesserte Kratzfestigkeit konnte nur bei Filmen mit ALOXAL Nanopartikeln nachgewiesen werden. Zussamenfassend kann geschlussfolgert werden, dass verschiedene Typen von Nanopartikeln verschiedene Endeigenschaften, jedoch nicht die Härtungskinetik beeinflussen.

- *Einfluss der Konzentration von Nanopartikeln*: Es wurde gezeigt, dass der Endmodul der EPA/TPGDA-Schichten mit der Konzentration von SIMA-Nanopartikeln anstieg, wobei die Kinetik der Netzwerkbildung und der Umsatz nicht verändert wurden. Die Abhängigkeit des Moduls vom Nanopartikelgehalt wird ausführlich anhand von seriellen und parallelen Modellen der Moduln diskutiert. Hierraus ergab sich, dass die experimentell bestimmten Modulwerte besser mit dem seriellen Modell beschrieben werden können. Nahezu unabhängige Werte der Glasübergangstemperatur für verschiedene Nanopartikelanteile deuten ebenfalls darauf hin, dass keine signifikante Änderung in der Struktur der Polymernetzwerke auftritt und dass es sich lediglich um einen Mischungseffekt handelt. Es wurde auch gezeigt, dass eine Zunahme der Nanopartikelkonzentration und der Schichtdicke die optische Transparenz der Lackschicht verringert und die Trübung erhöht. Ebenso wurde gezeigt, dass sich die mechanischen Eigenschaften der Lackschicht, wie die Moduln und die Volumen-Abriebfestigkeit mit der Nanopartikelkonzentration erhöhten.
- *Einfluss des Matrixmaterials*: Die Untersuchung der UV-Aushärtungskinetik bei zwei verschiedenen Matrixmaterialien - eine gummiartiges UA/TPGDA Netzwerk und ein glasartiges EPA/TPGDA Netzwerk - mit ALMAL-Nanopartikeln zeigte sowohl bei der Reaktionskinetik als auch bei den Änderung der mechanischen Eigenschaften einen ähnlichen Trend während der Aushärtung. Es konnte gezeigt werden, dass der Reaktionsverlauf bei beiden Materialien unabhängig von der Konzentration der

Nanopartikel ist. Die Endeigenschaften der Lackschicht wurden im Wesentlichen durch die Eigenschaften der jeweiligen Matrix bestimmt. Der Schubmodul des UA/TPGDA-Netzwerks bei Raumtemperatur zeigt entropieelastisches Verhalten, wohingegen der Schubmodul des EPA/TPGDA-Netzwerks durch die Energieelastizität im glasartigen Zustand bestimmt wird. Es konnte gezeigt werden, dass die Nanopartikel im Falle der weichen UA-Matrix einen größeren Einfluss auf die mechanischen Eigenschaften haben als bei der glasartigen EPA-Matrix. Die Nanopartikel verringerten die Oberflächenelastizität (bei der Kratzprüfung) der UA/TPGDA-Lackschichten, wohingegen kein signifikanter Einfluss bei EPA/TPGDA zu beobachten war. Unzureichende Härte und der Verlust des elastischen Verhaltens infolge der Zugabe Nanopartikeln führen zu einer Verringerung der Volumen-Abriebsfestigkeit der UA/TPGDA-Lackschichten. Im Fall von EPA/TPGDA führt das Hinzufügen von Nanopartikeln zu noch größerer Härte und einer Erhöhung der Volumen-Abriebfestigkeit der Lackschicht. Die gummiartigen UA/TPGDA Lackschichten zeigten eine höhere Trübung verglichen mit den glasartigen EPA/TPGDA Schichten. Das deutet auf ein höheres Maß an Agglomeration hin.

Es wurde gezeigt, dass Nanopartikel im Wesentlichen die mechanischen Eigenschaften der Polymerbeschichtung verbessern. Sie können hinzugefügt werden, ohne die Aushärtungskinetik zu beeinflussen. Um die gegenseitige Abhängigkeit zwischen den Moduln und dem Umsatz für homogene Systeme wie TPGDA und Mischungen von TPGDA und EPA zu beschreiben, wurde ein empirisches Modell auf Grundlage der Dibenedetto, Vogel-Fulcher und Havriliak-Negami Gleichungen angewendet. Die Grenzen des Modells wurden diskutiert und eine Erweiterung vorgeschlagen.

Table of Contents

1 Introduction

UV radiation curing is a novel technology in the field of organic coatings (*1, 2*). It involves curing of a reactive resin using the energy of photons in the wavelength region 200-400 nm. It is usually done at room temperature (*3*). The most attractive feature of this technology is its low space, low capital and low energy consumption (*4, 5*). The organic coatings can be cured within seconds in presence of UV light as compared to conventional thermal curing methods which take from hours to days for completion. UV curing involves low emission of volatile organic compounds (VOC's). Therefore, it is also an eco-efficient process and possesses low risk potential to the environment.

UV cured products have superior final properties like, high chemical and mechanical resistance, high gloss, improved scratch (*6, 7*) and abrasion resistance. They serve either as a protective (*8*) or a decorative coat for the underlying substrate. Traditionally, they were used for temperature sensitive substrates like wood, paper and plastics, for example, clear coats for parquet, furniture, vinyl flooring, on plastic substrates, compact discs, headlight lenses etc. But with expansion in UV curing market, they also find applications in other fields like biomaterials (dental applications) (*9*) metal coatings (can coatings, automotive coatings), adhesives, printing inks, printed circuit boards, optical coatings, coil coatings and exterior coatings like windows, bikes, appliances like refrigerators and washing machines (Figure 1).

The most commonly used resins in UV curing are the free radical polymerizable unsaturated polyesters, thiol-ene resins and acrylate functionalized resins. Additionally, cationically curable epoxide terminated oligomers and vinyl ethers are also used. This work concentrates mainly on the curing of radically polymerized epoxy acrylate (EPA) and urethane acrylate (UA) resins. The epoxy acrylates form hard and stable coatings which are mainly used for paper coatings, inks and wood coatings. The urethane acrylates (UA) combine the high abrasion resistance, toughness and tear-strength of polyurethanes with the superior optical properties and weatherability of polyacrylates. They are mainly used as coatings for PVC floor coverings, wooden parquet, screen inks and optical fibres.

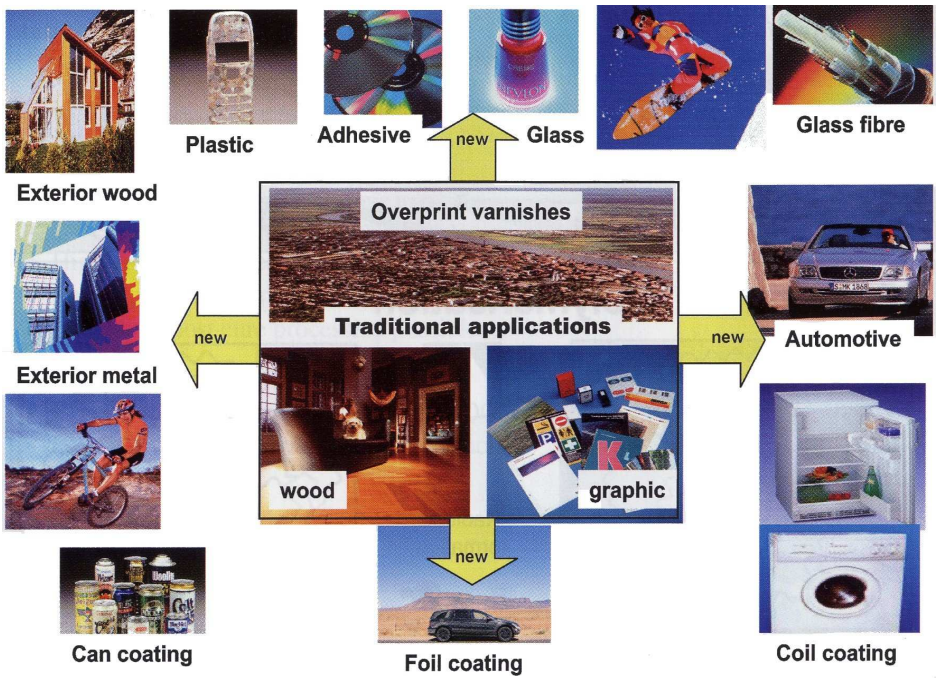

Figure 1. Schematic representation of applications of organic coatings (2).

The final properties and quality of the coatings depend largely on the underlying reaction kinetics and mechanism of network formation during curing. Therefore, in order to control the final properties of the coatings, it is important to understand the curing mechanism. In general, curing displays a complex interdependence of chemical kinetics and physical properties like gelation and vitrification (*10*). This is well known for curing of epoxies (*11, 12*) and holds true for acrylates as well. Therefore, in order to understand the curing mechanism, we need to understand the dependence of the mechanical properties and the underlying relaxation processes on chemical conversion. Different analytical methods like FTIR (*13, 14*), Photo-DSC (*15, 16*) Raman, NIR (*17, 18*) DMTA, microrheology (*19*) and ultrasound technique have been used by different research groups to monitor the cure kinetics of coatings. A lot of pioneering research in the field of UV curing can be found in the work of C. Decker et al. (*20-24*). However, methods like DSC which have a relatively slow acquisition rate, are not efficient enough to follow the curing of acrylates which have a reaction time in the range of few seconds. Therefore, for reactive systems like acrylates, we need a method which is fast enough and which can measure both chemical conversion and changes in mechanical modulus simultaneously. An attempt was made by Khan et al. (*25*) to study the real time chemical kinetics and rheology of thiol-ene polymers using RT-FTIR and in situ FTMS (Fourier Transform Mechanical Spectroscopy). However, the two methods were not combined in real time and the conversion and moduli were not measured simultaneously.

The FTIR spectrum was recorded in every 10 s and FTMS data in every 25 s, which is relatively slow for acrylates.

Later a method was developed by Alig et al. (*26*) in co-operation with DSM Research, Netherlands by combining two fast and *in situ* techniques, i.e., high frequency ultrasonic reflectometry (US) and real time near infrared spectroscopy (RT-NIRS). High frequency ultrasound technique is an efficient and a non destructive method to monitor the viscoelastic properties of polymers (*11, 27, 28*). It can be used to study the *in situ* changes in dynamic mechanical modulus of the coatings during UV curing (*29*). It has a high acquisition rate of more than 100 data points per second. Similarly, NIR spectroscopy is a highly efficient method to calculate average conversion in bulk materials. It can be provided with an ultra fast array detector and can collect an NIR spectrum in every 30 milliseconds. Chemical conversion can be calculated from the changes in acrylate band absorption at 1620 nm. These two techniques when combined together, can simultaneously measure both the dynamic modulus and the chemical conversion of a coating in real-time.

As the resin polymerizes, there is an increase in its molecular weight and its cross-link density. This change in the structure shifts the chemical kinetics from mass-controlled to diffusion-controlled regime, which is marked by slowing down of molecular relaxation and transport processes. This results in slowing down of the reaction kinetics. This phenomenon can be described as a “negative feed-back” between molecular diffusion and chemical reaction. The simultaneous measurement of dynamic mechanical modulus and chemical conversion during curing provides us a possibility to study this phenomenon of “negative feed-back”. Thus, the main objective of this work is to study the cure kinetics (conversion and mechanical modulus) of acrylates using the combined US/NIR method and to determine the interdependence of the chemical kinetics and the dynamic modulus (in this case dynamic shear modulus). This interdependence is illustrated in terms of modulus-conversion curves for each series of experiments.

This work includes a series of measurements done by varying the important parameters of curing, for example the reactive diluent concentration (TPGDA), photoinitiator concentration (TPO-L), base resin types and UV irradiation time. Additionally, a set of experiments are done to study the influence of different types and concentrations of nanofillers (inorganic and organically modified nanoparticles like Aerosil, SIMA, ALMA etc.) on the chemical conversion and the shear modulus of the coatings. In addition to the combined US/NIR experiments, a detail viscoelastic characterization (frequency dependent and temperature

dependent) of the uncured and cured resins is done using DMTA. Important informations on the change in distribution of molecular relaxation processes on going from a liquid state to a cured state are illustrated. Further, the modulus-conversion curves of the reactive diluent and the homogeneous polymer mixture of EPA and TPGDA are simulated with an empirical model and compared with the experimental data. The parameters of viscoelastic relaxation processes used for simulation are determined from DMTA measurements. Finally, the surface mechanical properties like, scratch resistance, abrasion resistance and the optical properties like haze of the coatings are also discussed.

2 Background

2.1 UV Radiation Curing

2.1.1 Components of UV Curing System

A typical UV curing formulation consists of three main components: an oligomer (25-90 %), a reactive diluent (15-60 %) and a photoinitiator (0.5-8 %). These components are mixed in a defined ratio, applied on the substrate and then irradiated with UV light under predefined conditions (temperature, light intensity, inert gas etc.). The composition of the curing formulation is usually selected depending on the final use of the coatings, like decorative or protective coatings. The final properties of the coatings can be tailored by varying the type and the concentration of each of these constituents (*30*), for example, a tri-acrylate monomer gives a harder coating than a mono-acrylate monomer, due to its higher cross-link density. The curing chemistry of most of the UV coatings is based on free radical mechanism (*31*). Thus, in this section the raw materials will be discussed with emphasis on free radical resins and photoinitiators.

Oligomer

In free radical photo-curing systems, usually oligomers with unsaturated carbon-carbon double bonds form the main constituent of the reaction mixture. The oligomers are responsible for the main properties of a film. The free radical reactive center reacts with the oligomer, opening up the carbon–carbon double bond and adding a molecule to the growing network. The three main types of free radical initiated resins are: (meth-)/acrylate, unsaturated polyesters and thiol-ene. Among these the acrylate resins are by far the most widely used oligomers for UV coatings. These resins have typically faster cure rates, with higher functional acrylates having higher viscosity and faster cure speed. The common types of acrylates used in free radical photopolymerization are epoxy acrylates, polyester acrylates (*13*), urethane acrylates (*32*), polyether acrylates, acrylated polyacrylates and acrylated oils. Figure 2 represents an example of two types of acrylate oligomers: epoxy acrylate and urethane acrylate.

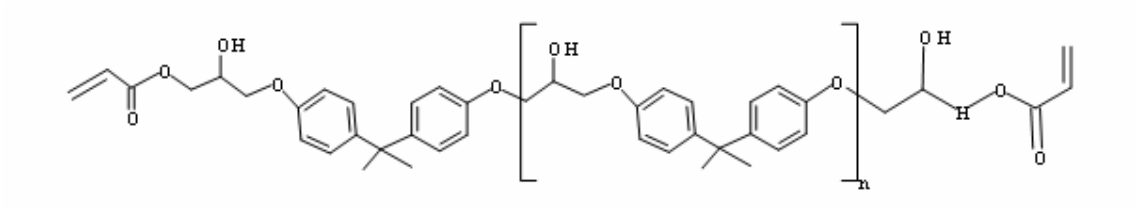

(a)

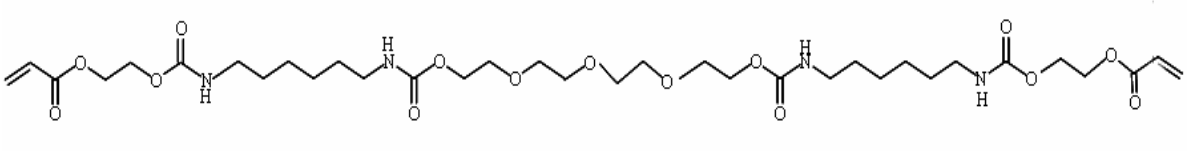

(b)

Figure 2. Schematic representation of an epoxy acrylate (a) and an urethane acrylate (b) oligomer.

Reactive diluent

As reactive diluents, usually monomer and low molecular weight oligomeric acrylates or vinyl ethers are used. They are usually used to reduce the viscosity of the oligomers. They ease the application of the UV curing resin and also participate in polymerization reaction, hence the term 'reactive'. They enhance the curing speed and through variation in cross-link density, control properties like hardness, flexibility and chemical resistance of the films (*33*). The most used acrylate monomers in free radical curing are di- and tri- functional acrylates, for example tripropylene glycol diacrylate (TPGDA), trimethylpropane triacrylate (TMPTA), propoxylated glycerol triacrylate (GPTA) and hexanedioldiacrylate (HDDA). Higher functional acrylates such as pentaerythritol tetraacrylate (PTA) or dipentaerythritol hexaacrylate (DPHA) are used only as minor ingredients as they form highly crosslinked, hard and brittle product. Vinyl ethers are also used in radical polymerizable systems as they are better diluents than acrylates and have lower toxicity (no labelling, no irritancy). The disadvantages are, they do not homopolymerize radically, but rather in an alternating polymerization i.e, they prefer acrylate double bonds over electron rich vinyl ether double bonds (*34*) and the unreacted residual vinyl ether groups are prone to acidic hydrolysis forming aldehydes. Therefore, the content of the vinyl ether reactive diluents should not exceed about 10 % in acrylate systems, in the range of 10-20% in epoxy systems and up to 50 % in unsaturated polyesters. The use of monomers, like styrene, N- vinyl pyrollidone and

monofunctional esters of acrylic acid despite being considered as best diluents, is consistently decreasing. This is because of their low molecular weight compared to oligomers, due to which they possess a higher risk of sensitization and irritation of skin, eyes, or respiratory tract. Since, their mono-functionality provides higher molecular weight between the cross-links resulting in better flexibility, monomers with lower volatility and odor, like isobornyl acrylate or trimethylol propane formal monoacrylate have been developed.

Photoinitiators

Photoinitiator plays an important role in free radical UV curing. Usually the oligomer and monomer are not efficient enough to start the polymerization on application of UV light. Sufficient number of carbon–carbon double bonds cannot be cleaved to produce the reactive species to carry out the chain initiation. For this purpose an initiator is often added (in a concentration of 1-5 %) to the UV curing resin that can absorb photons upon irradiation with UV light of specific frequency, producing sufficient number of free radicals. The photoinitiators govern both the rate of initiation and penetration of incident light into the sample. Selection of a photoinitiator is based on its three important properties: high molar extinction coefficient, high quantum yield and high reactivity of radicals with monomers.

The free radical photoinitiator system can be classified into two types of photoinitiators: type I and type II. The type I photoinitiator also called as Norrish type I, includes mostly the compounds containing benzoyl (phenyl-CO-) group. These are very versatile, exhibiting high efficiency due to unimolecular cleavage reaction. On absorption of photon of light these molecules cleave either at α or β position to form two free radicals. The commonly known type I photoinitiators are acylphosphine oxides (*35*-*38*), α-hydroxyl ketones (*39*), benzophenones, etc. Acyl phosphine oxides are longer wavelength absorbing photoinitiators and are efficient enough for thorough cure of pigmented coatings. The second class of type I photoinitiators are those that form biradicals through intramolecular hydrogen abstraction. This mechanism is commonly observed in ketones which form ketyl radical that participate in termination and the other radical initiates the chain reaction (Figure 3). The reactivity of free radicals depends on their chemical nature and their affinity towards the monomer. For example the benzoyl radical formed in almost every type I photoinitiators adds at a slower rate to the acrylate or methacrylate monomers, whereas the aliphatic ketyl or phosphinoyl radicals react at a two orders of magnitude higher rate with (meth)acrylate monomers (*40*). The type II photoinitiators are those that need a co-initiator to form a reactive species. These initiators in their excited state interact with second co-initiating molecule to generate radicals.

Due to their bimolecular nature of formation of radicals, their efficiency decreases as the resin vitrifies and reaction becomes diffusion controlled. The common type II photoinitiator class includes benzophenone derivatives, thioxanthanes, camphorquinones, benzyls and ketocoumarins (Figure 4).

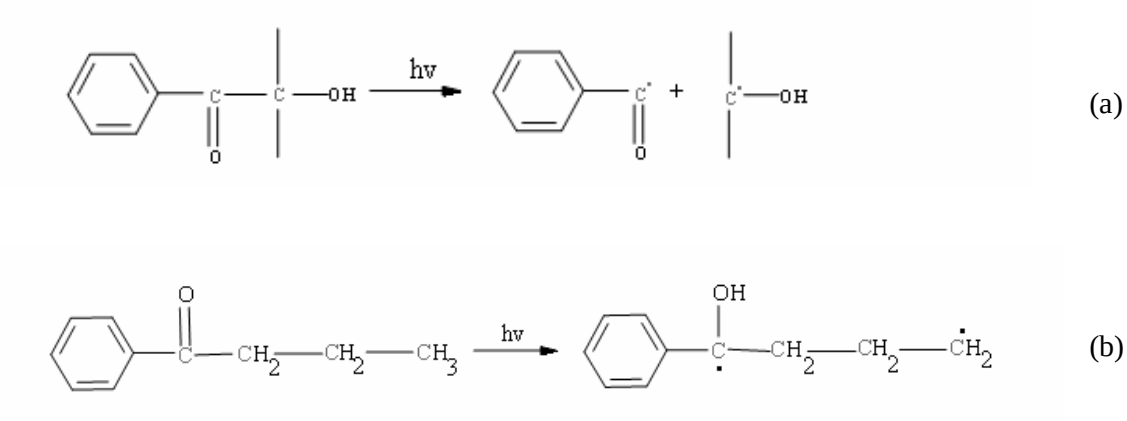

(a)

(b)

Figure 3. Schematic representation of type I photoinitiators forming free radicals by cleavage of α bond (a), by intramolecular hydrogen abstraction mechanism (b).

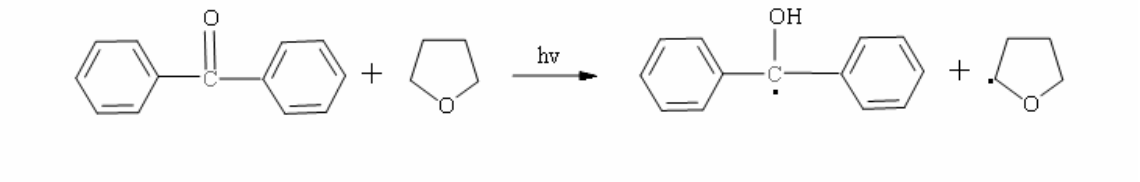

Figure 4. Schematic representation of type II photoinitiators: forming free radicals by intermolecular H- abstraction.

2.1.2 Curing Mechanism

UV curing mechanism can be divided into three main steps: initiation-during which the reactive species are produced and initiates the polymerization, propagation-during which the chain or the network grows and termination-during which active centers on the growing chain are destroyed or rendered inactive and further chain growth is stopped. Depending on the nature of the reactive species: a free radical or a cation, the photocuring mechanism can be classified as either free radical UV curing or cationic UV curing, respectively. The present work deals with free radical UV curing of acrylate resins. The basic mechanism of the three steps in UV curing can be compared with that of conventional free radical polymerization of linear unsaturated monomers (*31*), except that the photocuring is a much more complex

process, where the progressive increase in viscosity of the curing resin reduces the mobility of the reactive species, thus, affecting the curing kinetics of polymerization.

Initiation

Initiation of free radical UV curing can be considered to involve two steps. First step is formation of free radicals from photoinitiator and second step involves initiation of chain formation by reaction of radicals with monomers (Figure 5). Formation of free radicals can be explained with the help of a Jablonski diagram (Figure 6). When a photoinitiator molecule in ground state absorbs a photon upon irradiation with UV light, one of its electrons is excited to higher singlet states. This excited electron returns to the ground state by dissipating energy through various processes like radiationless internal conversion and evolution of heat or by intersystem crossing changing, its spin to triplet state. The reactive species are mostly formed from the molecule in triplet excited state, where there are two electrons, which leads to formation of radicals either by cleavage of photoinitiator molecule or by H-abstraction. One or both of the free radicals can participate in initiating the polymerization.

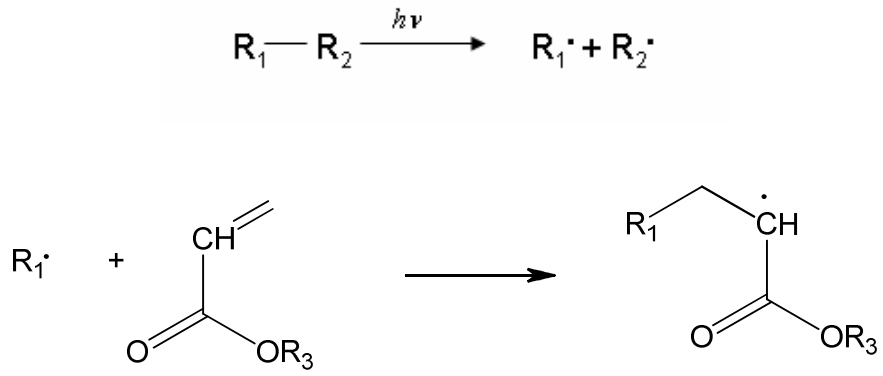

Figure 5. Schematic representation of initiation of free radical polymerization.

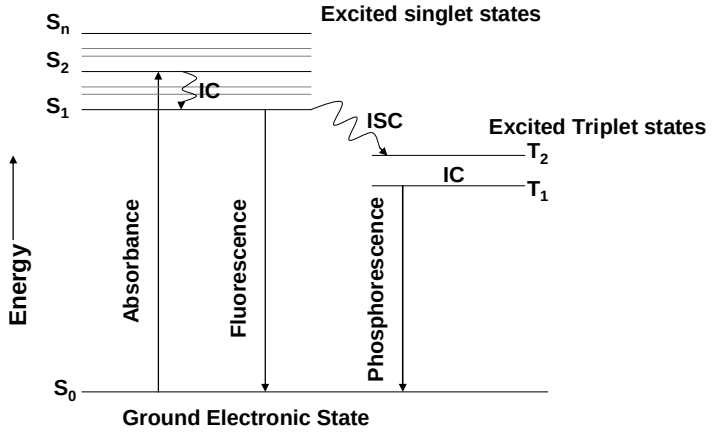

Figure 6. A Jablonski diagram representing the different excited states of an electron on absorption of a photon.

Propagation

Propagation involves addition of monomer/oligomer radicals formed in initiation step with other monomer/oligomer molecules (Figure 7), forming a cross-linked network. This is the key step to an efficient curing, as one radical formed can add more than 1000 monomer units within a fraction of a second. This step is marked by rapid increase in viscosity and modulus of the curing resin, resulting in formation of coatings with high chemical stability and rigidity. Generally, the higher the functionality of an oligomer or a monomer, the faster is the process of chain growth.

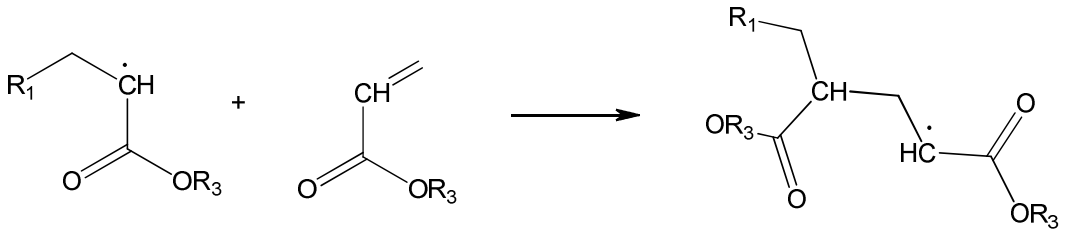

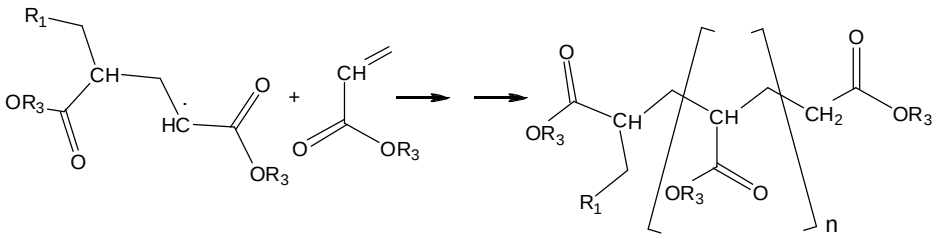

Figure 7. Schematic representation of propagation of network formation.

Termination

Termination can occur either by coupling or disproportionation (Figure 8 & 9). Coupling occurs when two growing chain radicals add together or when an initiator radical adds to a growing chain radical forming an inactive non radical species. Disproportionation occurs by abstraction of H-atom by one of the radical species from another radical or molecule forming a double bond. In case of UV curing, often due to increased viscosity and vitrification of the reacting mixture, many of the radicals are left trapped in cross linked networks (*41*) without being able to react further. For description of curing kinetics, this frustration of radicals and slowing down of the reaction rate by increased viscosity (hence, reduced molecular mobility) has to be incorporated by a diffusion controlled reaction regime.

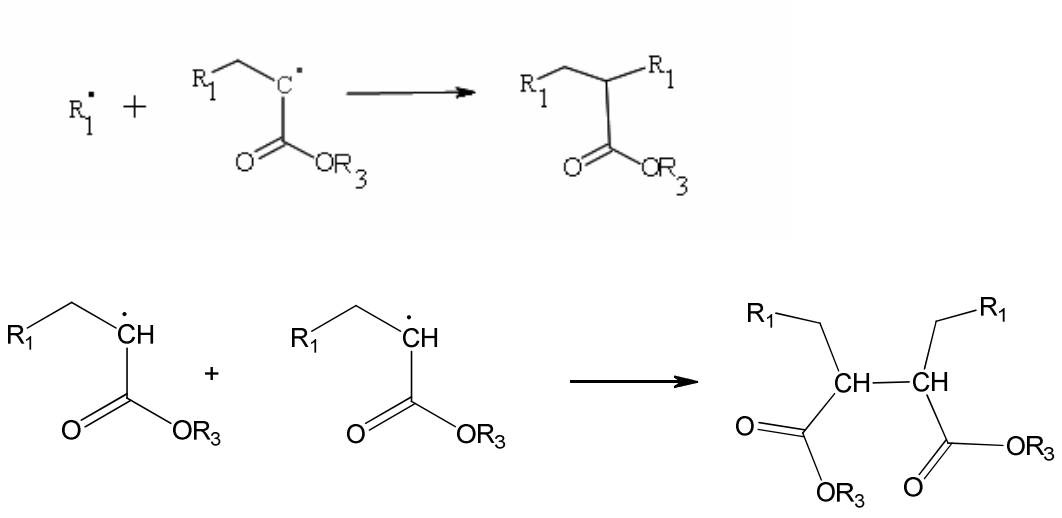

Figure 8. Schematic representation of termination by coupling.

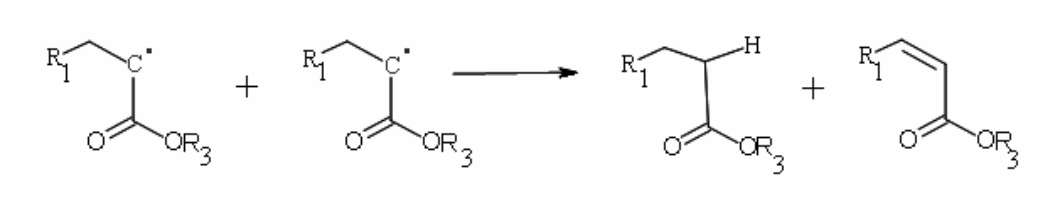

Figure 9. Schematic representation of termination by disproportionation.

Inhibition

Inhibition is an undesired phenomenon in free radical curing of UV coatings. Often oxygen in atmosphere and dissolved oxygen in resins react with free radicals forming less reactive peroxy radicals. This reduces the rate of polymerization and results in incomplete curing of coatings, which can be felt by sticky surface of coatings.

$$R_1^{\bullet} + O_2 \rightarrow R - O - O^{\bullet} \qquad (1)$$

This is one of the most commonly faced problems in coating industries. One way to solve this is to carry out UV curing in presence of inert gas. Other method could be to use high concentration of photoinitiators or high light intensity to increase the production of free radicals and to consume the oxygen present. Sometimes, inhibitors like hydroquinone and hydroquinone monomethyl ether are added to the formulation in very small quantities to increase the shelf life of highly reactive acrylate based formulations.

2.1.3 Reaction Kinetics

In this chapter, the first section describes the classical free radical polymerization kinetics in relation to light curing (during UV exposure) and dark reaction phases. These kinetic equations, however, describes the kinetics of curing in mass controlled regime (or chemical reaction controlled regime) only. But in case of polymers, for example acrylates, which form a highly cross-linked network on curing, diffusion plays a significant role in curing kinetics. Therefore, in the last section the discussion of reaction kinetics is further extended by incorporating the diffusion factor in the kinetic equations.

Curing kinetics under steady state reaction conditions

The rate of polymerisation R_p during light curing phase is given by assuming a steady state reaction condition. Steady state is defined as the condition when the number of radicals

produced equals to the number of radicals consumed with the total concentration of free radicals as constant. Under these conditions R_p can be given as following (*31*):

$$R_p = \frac{k_p}{(2k_t)^{0.5}}[M]r_i^{0.5} \tag{2}$$

where k_p, k_t are the propagation rate constant and termination rate constant respectively, $[M]$ is the monomer concentration and r_i is the rate of initiation. R_p can be derived from the slope of the conversion p versus time curve and initial double bond concentration as follows:

$$R_p = \frac{dp}{dt}[M] \tag{3}$$

The rate of initiation r_i is defined by the quantum yield of the initiation Φ_i and the irradiance absorbed I_a as following*:*

$$r_i = \Phi_i I_a \tag{4}$$

Taking the photoinitiator concentration [PI] into account, the above equation can be expressed as:

$$r_i = \Phi_i I_0 \left(1 - e^{-[PI]\varepsilon_{PI}\ell}\right) \tag{5}$$

where I_0 is the incident irradiance, ε_{PI} is the extinction coefficient of photoinitiator PI and l is the sample thickness. Substituting the value of r_i in equation 2 gives:

$$R_p = \frac{k_p}{(2k_t)^{0.5}}[M](\Phi_i I_0 (1 - e^{-[PI]\varepsilon_{PI}\ell}))^{0.5} \tag{6}$$

The kinetic chain length (KCL) i.e, the average number of monomer molecules polymerized per radical that initiates a polymer chain, can be derived from the ratio of rate of polymerization and rate of initiation as follows:

$$KCL = \frac{R_p}{r_i} = \frac{k_p[M]}{(2k_t)^{0.5} I_a^{0.5} \Phi^{0.5}} \tag{7}$$

Curing kinetics during dark reaction phase

As the UV exposure is stopped, the production of free radicals is also stopped and the polymerization is said to proceed in dark. During this phase the reaction is considered to be under non-steady conditions. Under these conditions the concentration of radicals decreases according to a hyperbolic law assuming a bimolecular termination with steadily decreasing rate of polymerization (*42*):

$$-d[PI^{\bullet}]/dt = 2k_t[PI^{\bullet}]^2 \text{ or } 1/[PI^{\bullet}] = 2k_t * t + 1/[PI^{\bullet}]_0 \tag{8}$$

where $[PI^{\bullet}]_0$ is the concentration of radicals at the end of UV light exposure:

$$(R_p)_{t_i} = k_p[PI^{\bullet}]_0[M]_{t_i} \tag{9}$$

where $[M]_{t_i}$ is the monomer concentration at the onset of dark reaction. The polymer radical concentration $[PI^{\bullet}]$ can also be expressed as a function of rate of dark polymerization $(R_p)_{t_i+t}$ at time $t_i + t$ as follows:

$$[PI^{\bullet}] = (R_p)_{t_i+t}/k_p[M]_{t_i+t} \tag{10}$$

By replacing $[PI^{\bullet}]$ and $[PI^{\bullet}]_0$ in equation 8, the rate equation of dark reaction can be given as:

$$\frac{[M]_{t_i+t}}{(R_p)_{t_i+t}} = \frac{2k_t}{k_p} * t + \frac{[M]_{t_i}}{(R_p)_{t_i}} \tag{11}$$

A plot of left hand term of equation 11 versus the duration of the dark reaction t gives a straight line. Its slope gives the ratio $2k_t/k_p$. Individual values of k_p and k_t can be calculated from the ratios $2k_t/k_p$ and $k_p/(2k_t)^{0.5}$ obtained under steady state and dark reaction conditions respectively.

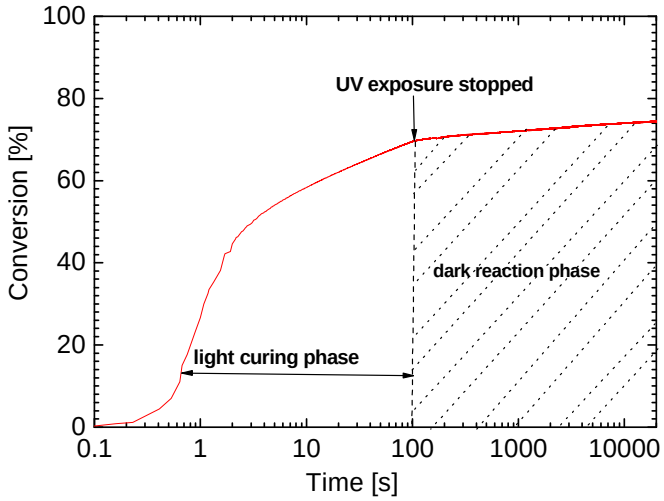

Figure 10. Conversion profile of a polymer blend EPA/TPGDA in a weight ratio 2:1 during the light curing and dark reaction phase.

Figure 10 shows the conversion profile of the polymer blend EPA/TPGDA cured under continuous irradiation for 100 s (UV dose 38.5 kJ/m^2). The change from light curing phase to the dark reaction phase is clearly marked by the bend in conversion curve at 100 s on stopping the UV light exposure at 100 s. This can be attributed to a sudden drop in the production of free radicals on removal of UV irradiation.

The classical kinetic equations assume that the polymerization is chemical reaction controlled and the average values of the reaction rate constants do not vary during the reaction time. But the curing of multifunctional monomers is a complex process and involve a number of anomalous behaviours which affect the curing kinetics (*43*, *44*):

1. Autoacceleration: This behaviour can be observed during very early stages of polymerization. It is found that at initial stages of irradiation, rate of polymerization increases considerably (Trommsdorff effect)**.** This is because of very fast increase in viscosity of the resin at about 5 % conversion, which leads the termination process to be diffusion controlled (*45*, *46*). This in turn increases the concentration of propagating radical, leading to acceleration of the rate of reaction.

2. Autodeceleration: This is mostly observed at later stages of curing, when the reaction becomes diffusion controlled. The decreased mobility of the propagating radical and of the functional groups leads to a slowing down of the polymerization process. The polymerization ultimately stops before reaching completion due to vitrification. The autodeceleration causes

the rate to decrease much more rapidly than can be accounted for by depletion of reactive groups.

3. Termination by "reaction diffusion": In cross-linking polymerization, radicals are mostly bound to 3-D network and move mainly by reacting with neighbouring functional groups until it combines with another radical. Termination is thus said to be "reaction diffusion" controlled and at this stage the termination rate constant is equal to propagation rate constant.

4. Volume shrinkage: At high initiation rate of UV radiation, volume equilibrium of the polymerizing resin cannot be maintained because volume shrinkage is slower than the chemical reaction. The time lag between these two processes, leads to excess free volume for the unreacted double bonds to move freely, increasing the degree of conversion as compared to the systems in volume equilibrium. This effect becomes more pronounced as the rate of polymerization increases dramatically (for example, by increasing the incident light intensity).

5. Formation of microgels: High concentration of pendant double bonds near the vicinity of radicals increases the rate of reaction forming microgels (*47*). These are considered as soluble intramolecular cross-linked macromolecules, with sizes comparable to linear or branched macromolecules and reactive groups at their surface or interior. The formation of microgels leads to heterogeneities in structural composition of the reacting resin during polymerization. This in turn affects the reactivity of the pendant functional groups, as described by Bowman et al. (*48*) with the help of a kinetic gelation model.

The dominance of any of these behaviours depends on the curing conditions like light intensity, temperature and on the curing formulation like type and concentration of functional groups, concentration of photoinitiator, viscosity of the resin, etc. In general, the curing kinetics of cross-linking monomers is found to be mainly influenced by autoacceleration, autodeceleration and termination by "reaction diffusion". Figure 11 shows the normalized kinetic rate $R_p/(100-p)$ of polymerization against the extent of reaction p of a diacrylate monomer TPGDA cured with 10 s of UV irradiation. It can be observed that the rate of polymerization increases dramatically with conversion at early stages of conversion. This can be attributed to autoacceleration of propagation mechanism. It then starts to decrease at later stages, i.e, after 40 % conversion. This can be due to start of vitrification of the resin, where the reaction becomes diffusion controlled.

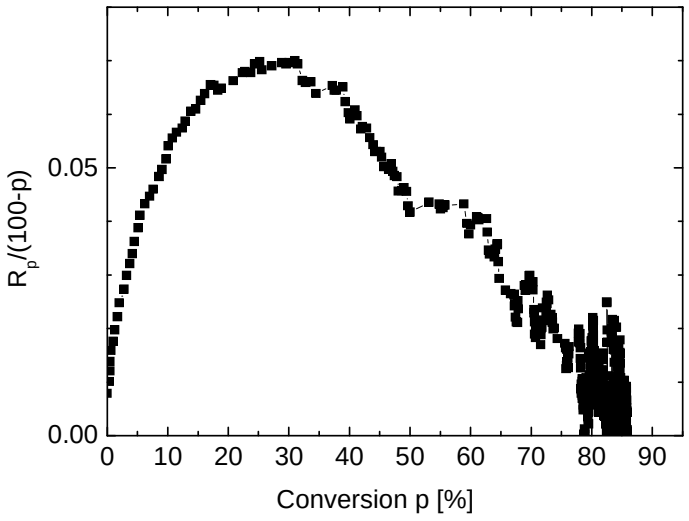

Figure 11. Normalized rate of polymerization $R_p/(100-p)$ as a function of conversion p of TPGDA cured under 10 s of UV irradiation.

Therefore, for reactive systems like acrylates, which passes through glass transition (chemical vitrification) during reaction, a diffusion controlled reaction regime has to be considered and a diffusion control factor has to be introduced in the kinetic equations. Various empirical models have been proposed by taking into account the characteristic cross-linking polymerization behaviours, to describe the curing kinetics of such complex systems (*49-53*).

Chern and Poehlin proposed a somewhat simpler semiempirical relationship based on free volume considerations (*51, 52*) for modelling of cure kinetics of epoxy resins. According to this model, when the degree of cure reaches a critical value p_c, diffusion control takes over and the diffusion controlled rate constant is given by:

$$k_d = k_c \exp[C(p - p_c)] \tag{12}$$

where, k_c is the rate constant for non-diffusion controlled reaction (in case of photopolymerization $k_c = \frac{k_p}{(2k_t)^{0.5}} r_i^{0.5}$), p is conversion, p_c is critical value of conversion and C is a constant. As p reaches its critical value p_c the reaction becomes diffusion controlled. According to Rabinowitch (*54*) the overall effective rate constant k_e can be expressed in terms of k_d and k_c as follows:

$$\frac{1}{k_e} = \frac{1}{k_d} + \frac{1}{k_c} \tag{13}$$

Combining equations 12 and 13, the "diffusion factor" $f_d(p)$ can be given as follows:

$$f_d(p) = \frac{k_e}{k_c} = \frac{1}{1+\exp[C(p-p_c)]} \tag{14}$$

This empirical model was also adopted by Choe et al. (*55*) to express the kinetics of photopolymerization in diffusion controlled regime as follows:

$$R_p = \frac{k_e(1-p)}{1+\exp[C(p-p_c)]} \tag{15}$$

The expression for diffusion factor was further simplified by Fournier et al. by replacing p_c by final degree of polymerization p_f which can be obtained from experimental data. He expressed $f_d(p)$ as follows (*49*, *56*):

$$f_d(p) = \frac{1}{1+\exp[(p-p_f)/b]} - 1 \tag{16}$$

Kurdikar and Peppas (*48*) proposed a model for diffusion controlled bulk cross-linking photopolymerizations. They used Smouluchowski theory (*57*) which relates the reaction rate constant k to the relative diffusional coefficient of the reacting species D to express the rate constants in diffusion controlled reactions. They expressed the propagation rate constant by considering that the monomer undergoes both translational and segmental diffusion processes before it can react with a radical. They considered these two diffusion processes to be in series and expressed k_p as follows:

$$\frac{1}{k_p} = \frac{1}{k_{p,trans}} + \frac{1}{k_{p,seg}} \tag{17}$$

where $k_{p,trans}$ and $k_{p,seg}$ are the translational and segmental propagation rate constant. These two quantities were further expressed as follows:

$$k_{p,trans} = 4\pi(r_r + r_m)D_m,\ k_{p,seg} = 4\pi(r_r + r_m)D_{seg} \tag{18}$$

Where D_m, D_{seg} are the translational and segmental diffusion coefficient respectively, and r_r, r_m are the reaction radii of the radical and monomer respectively. The termination rate constant k_t was expressed as:

$$k_t = 16\pi r_r D_{rp} \tag{19}$$

where $D_{rp} = \frac{2}{3} l^2 k_p [M]$ is the radical propagation diffusion coefficient. Here l is the bond distance and [M] is the monomer concentration.

2.2 Viscoelastic Properties of Polymers

Polymers exhibit both viscous and elastic properties and thus, are called as viscoelastic materials. The elastic properties of a polymer can be well described in terms of mechanical modulus and the viscous properties in terms of viscosity η.

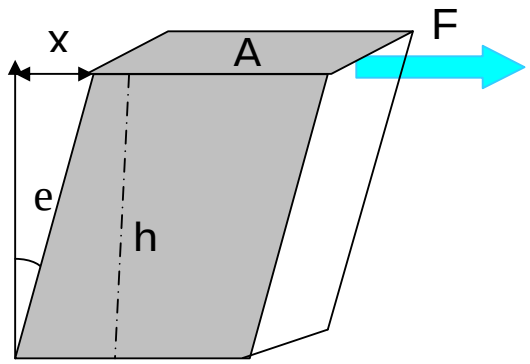

Figure 12. Effect of shear force F on an elastic object.

When a force F is applied parallel to a surface of area A of an elastic solid, the face opposite to it experiences a force –F in the opposite direction (Figure 12). The shear stress is then given as $\sigma = F/A$. The deformation is given either by the shear angle e or the value $X/h = \tan e$. In case of small deformations $\tan e \approx e$ so that, Hooke's law for an elastic solid is given as:

$$\sigma = Ge \tag{20}$$

where G is the shear modulus. Thus, a perfectly elastic body follows Hooke's law and strain is linearly proportional to the applied stress. A perfectly viscous body follows Newtonian law according to which the shear stress is linearly proportional to the shear rate, given as:

$$\sigma = \eta \dot{e} \tag{21}$$

where η is the proportionality factor called viscosity. Polymers exhibit properties in between these two limiting conditions-pure elastic and pure viscous object and hence, are viscoelastic.

Both viscous and elastic properties can be described in terms of a frequency dependent complex shear modulus. It is given by $G^*(\omega) = G'(\omega) + iG''(\omega)$, where $G'(\omega)$ and $G''(\omega)$ are the frequency dependent storage and loss moduli respectively.

The frequency dependent storage modulus $G'(\omega)$ is defined as the ratio of stress in phase with strain in a sinusoidal shear deformation to the strain (*58*). It is a measure of energy stored and recovered per cycle, when different systems are compared at the same strain amplitude. Mathematically, it is given by:

$$G'(\omega) = \frac{\sigma_0}{e_0}\cos\delta \tag{22}$$

where δ is the phase lag between stress and strain, σ_0 is the stress amplitude $\sigma = \sigma_0 \cos\omega t$ and e_0 is the strain amplitude $e = e_0 \cos(\omega t - \delta)$, ω is the angular frequency and t is the time.

The frequency dependent loss modulus $G''(\omega)$ is defined as the ratio of stress 90° out of phase with the strain to strain. It is a measure of energy dissipated or lost as heat per cycle of sinusoidal deformation, when different systems are compared at the same strain amplitude. Mathematically, it is given by:

$$G''(\omega) = \frac{\sigma_0}{e_0}\sin\delta \tag{23}$$

The ratio of loss modulus to storage modulus gives the tangent of the phase angle shift between stress and strain, or tan δ. It is a measure of the internal friction and damping property of a material.

As an alternative to $G^*(\omega)$, the complex shear viscosity $\eta^*(\omega) = \eta'(\omega) - i\eta''(\omega)$ is frequently used to describe the viscoelastic liquids, where $\eta'(\omega)$ and $\eta''(\omega)$ are the real and imaginary part of $\eta^*(\omega)$. $\eta'(\omega)$ is defined as the ratio of stress in phase with strain rate to the strain rate and $\eta''(\omega)$ is the stress 90 ° out of phase with the strain rate to the strain rate. The phase relations are the opposite of those for $G^*(\omega)$, and the individual components are given by, $\eta'(\omega) = G''(\omega)/\omega$ and $\eta'' = G'/\omega$.

A simple Maxwell model element as given in Figure 13, can serve to represent the viscoelastic behaviour of energy storage and loss in a linear viscoelastic material for specific measurement conditions (frequency, shear rate, etc.). It consists of an ideal elastic spring attached to an ideal dashpot in series (*59*). The spring represents the elastic part and the dashpot the viscous part of a viscoelastic material.

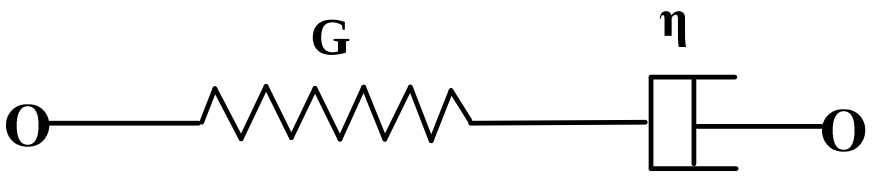

Figure 13. Schematic representation of Maxwell Model.

According to this model under an applied stress, the total strain γ_{total} and total stress σ_{total} is given as $\gamma_{total} = \gamma_d + \gamma_s$ and $\sigma_{total} = \sigma_d = \sigma_s$ respectively, where γ_d, γ_s are strain in the dashpot and spring respectively and σ_d, σ_s are the stress in the dashpot and the spring respectively. If the spring corresponds to shear rigidity G_i and the dashpot to a viscosity η_i then the relaxation time of the element is defined as $\tau_i = \eta_i / G_i$ and τ_i is a measure of the time required for stress relaxation. This model expresses the complex dynamic shear modulus and its components as follows:

$$G^*(\omega) = \frac{G_i i\omega\tau_i}{1 + i\omega\tau_i} \tag{24}$$

$$G'(\omega) = \frac{G_i \omega^2 \tau_i^2}{1 + \omega^2 \tau_i^2} \tag{25}$$

$$G''(\omega) = \frac{G_i \omega\tau_i}{1 + \omega^2 \tau_i^2} \tag{26}$$

According to this model, at short time intervals $t << \tau_i$ or at high frequencies, the material behaves like elastic and at longer times $t >> \tau_i$ or low frequencies, it behaves as a Newtonian liquid and at $t = \tau_i$, it is viscoelastic. Moreover, this model allows only a single value of the parameter τ_i (i.e a single relaxation time) which is true only for an ideal system with small deformations. This is comparable to the Debye relaxation model which proposes a single relaxation time for the relaxation of dielectric permittivity as a function of frequency. In reality, the polymers exhibit a much more complex behaviour than a single Maxwell element. The polymers exhibit a distribution of relaxation times due to their structural heterogeneities. To describe the distribution of relaxation times, a stretched exponential function first proposed by Rudolf Kohlrausch in 1854, now known as Kohlrausch-Williams-Watts (KWW**)** function (*60, 61*) can be used. It is given as follows:

$$\varphi(t) = e^{(-t/\tau_{kww})\beta} \tag{27}$$

where $\varphi(t)$ is the relaxation function, τ_{kww} is the Kohlrausch relaxation time and $0 < \beta \leq 1$ is a broadness parameter. Because, KWW function has no simple representation in the frequency domain, its use is limited to describe the time domain phenomena only. Therefore, its counterpart Havriliak–Negami (HN) fitting function is generally used to describe the frequency dependence of the shear moduli. Havriliak–Negami is an empirical function (*62*, *63*) and introduces two parameters β and γ describing the broadness and asymmetry of the relaxation spectra respectively. It can be expressed as follows:

$$\frac{G^*(\omega) - G_\infty}{G_\infty - G_0} = -\frac{1}{(1 + (i\,\omega\tau_{HN})^\beta)^\gamma} \tag{28}$$

where G_∞, G_0, are the high and low frequency limiting values of shear modulus and τ_{HN} is the HN characteristic relaxation time. Figure 14 shows the frequency dependent storage shear modulus and loss modulus of the TPGDA polymer film over a broad range of frequency ("Master curves") and its fit curve using HN fit function. It can be seen that HN function fits well the frequency dependent modulus of TPGDA polymer over a broad range of frequency. The principle and construction of "Master curve" is discussed in the following section.

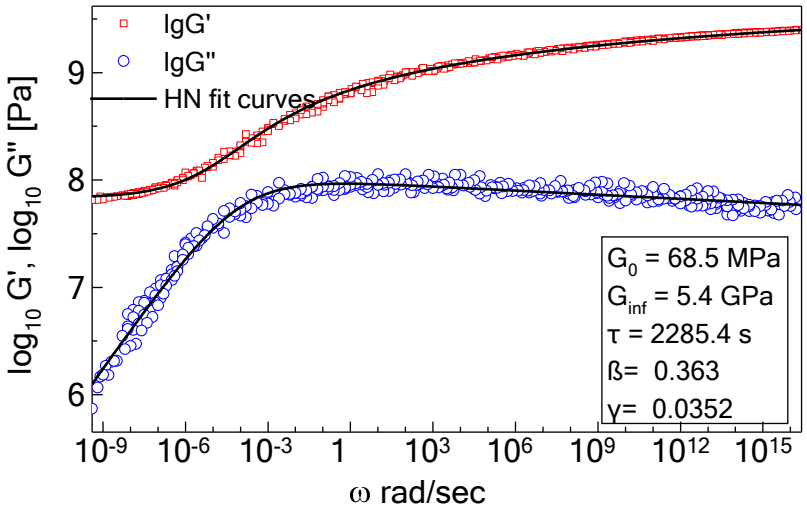

Figure 14. Storage modulus and loss modulus as a function of frequency for TPGDA polymer film and the HN fit curves.

Principle of Master Curve Construction

Viscoelastic functions like shear modulus, when plotted against frequency (or time), the ordinate covers an enormous range of magnitudes, changing over several powers of 10. Concomitantly, abscissa covers a still larger range of frequency to encompass these changes (*58*). Therefore, both the coordinates are usually plotted in logarithmic scale. Generally, such large range of frequencies is out of the frequency range of classical dynamic mechanical measurements. So, in order to have a complete spectrum of modulus as a function of frequency, often a "Master Curve" is created from a series of DMA measurements carried out at different temperatures.

The construction of master curves is based on "time temperature superposition (TTS)" principle. According to this principle, in case of thermo-rheological simple materials, the effects of frequency (time) and temperature are super imposable (*59*):

$$G^*(T,\omega) = G^*(T_0, a_T\omega) \tag{29}$$

where T_0 is the reference temperature, T is any temperature, a_T is the shift factor, ω is the radial frequency and G^* is the complex dynamic shear modulus. If the temperature of a flexible polymer is lowered, shear relaxation will take longer times than it would take at higher temperatures, i.e, increasing the temperature speeds the relaxation processes. Thus, changing temperature shifts the viscoelastic functions in frequency scale, without changing their shapes. Using the above principle, a continuous modulus-frequency curve over a large frequency range can be obtained for a particular reference temperature. This is done by shifting the modulus-frequency curves measured at different temperatures horizontally along the log ω axis by multiplying with a suitable shift factor a_T. Figure 15 shows the construction of master curve of an UA oligomer (EB270) at a reference temperature of 243 K, by overlapping the measured modulus curves at different temperatures. The shift factors as a function of temperature and the fit curve using Vogel-Fulcher equation are shown in Figure 16. It can be observed that the master curve gives the frequency dependence of storage modulus over a frequency range of more than 15 decades, which would have otherwise been not possible by any available measuring methods.

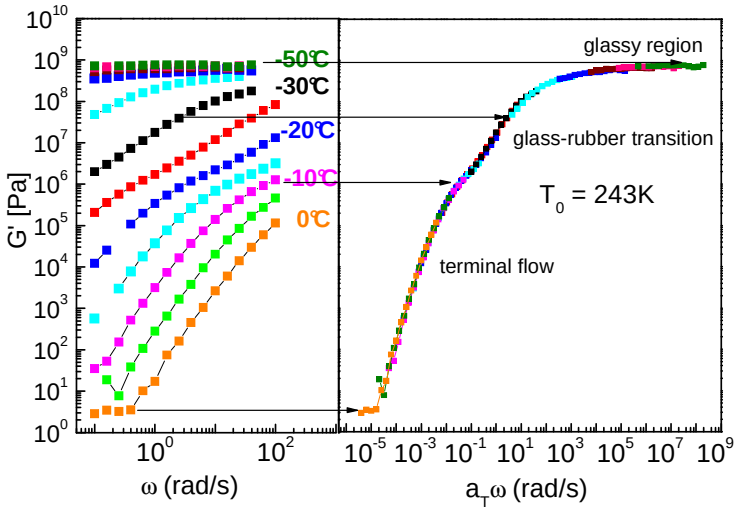

Figure 15. Frequency dependent storage modulus curves at different temperatures (left), master curve (right) at a reference temperature 243 K of un-crosslinked EB270.

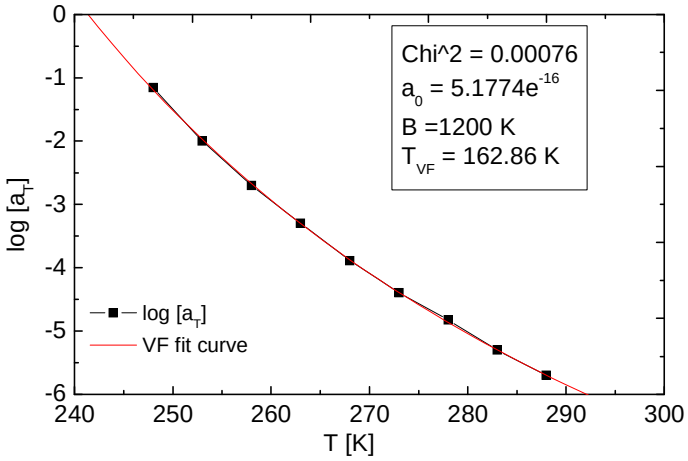

Figure 16. The shift factors plotted as a function of temperature above T_g, and the fit curve using Vogel-Fulcher equation ($a_T = a_0 \exp(B/T - T_{VF})$) for the master curve of EB270.

2.2.1 Frequency Dependence of Viscoelastic Properties

The master curves plotted logarithmically show a distinct pattern of certain zones on the frequency scale (Figure 15), where the viscoelastic functions have characteristic shapes. It can be observed from the above given master curve that the polymer resin passes through different relaxation regimes as the frequency is changed. Typically, the following regions can

be observed: a glassy region at higher frequency where the polymer behaves like a hard glass and has a high modulus (above 1 GPa), glass rubber transition region where its consistency changes to a rubber like matter, rubber plateau region (seen only in high molecular weight polymers), terminal flow region (seen in uncross-linked polymers) or a pseudo equilibrium zone (seen in cross-linked polymers) at lower frequencies. These zones can be associated qualitatively with different mechanical responses depending on the molecular weight, crosslink density, crystallinity or glass transition temperature of the polymer systems.

Figure 17 shows schematically the real part of the complex dynamic shear modulus as a function of frequency. This figure represents the viscoelastic behaviour in dependence of molecular weight and cross-linking density of polymers.

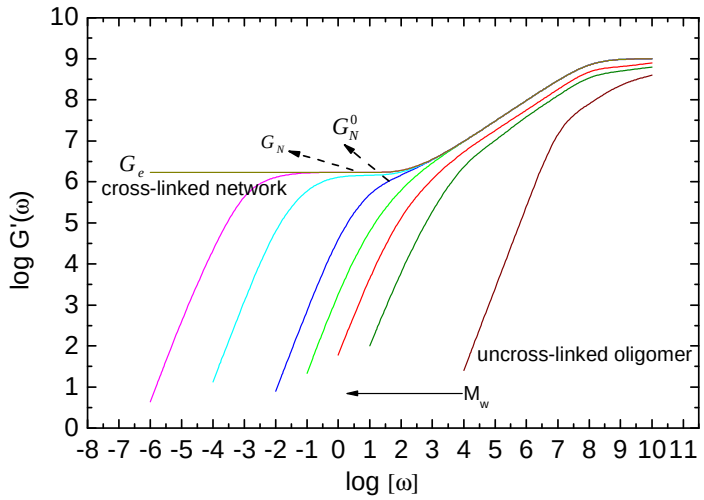

Figure 17 Schematic representation of frequency dependent storage shear modulus at different molecular weights and cross-link density of oligomer (or polymer). (Courtesy: Dr. Lellinger, DKI)

At sufficiently high frequencies, $G'(\omega)$ approaches a value of the order of 10^9 Pa, characteristic of a hard glass like solid. At these frequencies (regarded as glassy zone), the configurational rearrangements of the chain backbones is absent within the interval of the experiment. The plateau in between the high and low frequency storage modulus is related to "physical cross-links" called entanglements, which "disentangle" at low frequencies. The constant value of $G'(\omega)$ at intermediate frequencies is denoted as G_N^0 for the uncross-linked and G_N for the cross-linked polymers, often called as "plateau-modulus". At lower frequencies, $G'(\omega)$ for cross-linked networks with sufficiently long network chains between

cross-links, approaches values which are again nearly constant, written as G_e. This represents the equilibrium shear modulus as treated by the theory of rubber like elasticity (*64*). According to this theory, G_e is proportional to the number-average molecular weights of the network strands. A strand is often defined as a segment between cross-links. For uncross-linked polymers, however, $G'(\omega)$ falls rapidly with decreasing frequency and eventually vanishes at long times. This region is called as terminal region.

From the above discussions, it can be observed that the viscoelastic properties of the polymers depend on the chemical structure and physical arrangements of the polymer segments and thus, can be used as a tool to determine the internal structural arrangement of the polymers. It should be noted that the above discussions is restricted to small deformations of the systems only (linear viscoelasticity).

2.2.2 Glass Transition Temperature in Polymers

Glass transition temperature (T_g) is often defined as a temperature below which a polymer is hard and brittle and behaves like a glass and above which it is soft and flexible like a rubber. However, since the molecular mobility of polymers follows a frequency–temperature superposition principle, the "glass transition temperature" is expected to depend on the probe frequency. On a molecular level, this can be explained by the fact that the rearrangements of the polymer segments need time ("relaxation") and that this relaxation is temperature dependent. In order to avoid this difficulty the glass transition temperature as an operational quantity is measured under well defined experimental conditions (frequency, heating or cooling rate etc.).

The rubber elasticity originates from the activity of α modes, a major group of relaxation processes in polymer fluids. If the external force is varied too rapidly (i.e, at higher frequencies), the deformation cannot follow and the polymer system acts as a glass. Similarly, when the temperature of the sample is lowered, the mobility of the α modes decreases, i.e the relaxation time τ increases. This progressive increase in τ with decrease in temperature finally leads to 'freezing' of the α modes. The dependence of the characteristic relaxation time of the α modes τ_α on temperature T for the polymer systems is described by the Vogel-Fulcher (VF) equation as follows:

$$\tau_\alpha = \tau_0 \exp\left(\frac{B}{T - T_{VF}}\right) \tag{30}$$

where τ_0 and B are constants and T_{VF} is the Vogel-Fulcher temperature. The value of T_{VF} usually lies about 50 K below its calorimetric T_g.

Glass transition temperature can also be defined as the temperature at which the viscosity η of the polymer melt equals to 10^{13} poise. The typical relaxation time at this viscosity is reported to be 10^2 s (*59*).

The glass transition temperature is related to the chemical structure, the arrangement of polymer segments and the degree of cross-linking of polymers. The dependence of the glass transition temperature on the extent of cure p can be given by the DiBenedetto equation as follows:

$$T_g(p) = \left(\frac{\lambda \cdot p}{1-(1-\lambda)\cdot p} \cdot \left(T_{g,1} - T_{g,0}\right) \right) + T_{g,0} \tag{31}$$

where $T_g(p)$ is the glass transition temperature at conversion p, $T_{g,0}$ and $T_{g,1}$ are the glass transition temperature of the uncured polymer resin ($p = 0$) and a fully cured polymer ($p = 1$) respectively and λ is a material parameter.

The glass transition temperature also depends on the composition of the polymer blends. The T_g of an uncured polymer blend decreases with addition of low molecular weight reactive diluent, due to decrease in its viscosity. Whereas, the T_g of a cured polymer film increases with increase in the concentration of reactive diluent. This is due to increase in the cross-link density of the polymer network on addition of low molecular weight molecules.

The thermal glass transition T_g can be measured by methods like DSC or DMTA. Its value can be determined either from the maximum of the loss modulus or $\tan\delta$. As stated above, the T_g values for different methods depend on the probe frequency and cooling rate of the experiments. Therefore, the T_g values of ultrasonic experiments (at about 1 MHz) are typically 30-40 K above than those of the DMA experiments (at about 1 Hz).

3 Methods

3.1 NIR Spectroscopy

Near-infrared (NIR) spectroscopy corresponds to the wavelength region of 800 to 2500 nm (4000-12500 cm^{-1}) of the electromagnetic spectrum. It was developed in the 1960s (*65*) and is increasingly used in chemical industry for process monitoring and other commercial applications. In the field of polymer research, it has been used widely for the characterization of thermal curing of epoxies (*66, 67*), batch and solution polymerization of styrene (*68*), anionic polymerization of butadiene (*69*), inline analysis of polymer melt (*70*) and polymerization kinetics of acrylates and methacrylates (*71*). An infrared spectrum is based on the change in dipole moment of a molecule on interaction of molecular vibrations with electromagnetic radiations. The absorption bands in NIR spectrum consist of overtones and combination of IR fundamental vibrations. The occurrence and the spectral properties of NIR bands are due to the anharmonicity of molecular vibrations. It is dominated by absorption associated with XH_n functional groups, due to large anharmonicity of vibrations of light hydrogen atom. The predominant bands which can be analysed include: the methyl C-H stretching vibrations, methylene C-H stretching vibrations, aromatic C-H stretching vibrations, and O-H stretching vibrations (*71*).

In the present study, NIR measurements were performed by a Multispec NIR spectrometer (tec5, Germany) with a fast array detector based on extended InGaAs technology and high dynamic range of up to 16 bit. The spectral range extends from 890-2200 nm with a wavelength accuracy of 0.6 nm. It is capable of recording each spectrum in every 30 milliseconds. This feature makes it well suited for studying the photopolymerization reactions occurring in a time frame of few seconds. The photopolymerization of acrylates is monitored by following the decrease in the area of the characteristic acrylate CH_2=CH- stretching band at 1621 nm (Figure 27).

3.2 Ultrasound Reflectometry

3.2.1 Principle

Ultrasonic techniques have been known from long as excellent tools for non destructive characterization of materials. Ultrasonic shear wave reflection technique was first developed by Mason *et al.* in 1949 (*72*) to measure the complex dynamic shear modulus G^* of polymer liquids. This technique was further developed by Alig *et al.* by combining it with high frequency digital analysis, making it possible to have automated dynamic measurements (*73, 74*). By using ultrasonic transducers which allow simultaneous generation of shear and longitudinal waves, it is possible to measure both the complex dynamic shear modulus G^* and complex dynamic longitudinal modulus L^* simultaneously during the film formation (*28*). From the values of G and L other quantities like, Young's modulus E, compression modulus K and poison ratio ν of the polymer can also be calculated. Ultrasonic reflectometry has been used successfully to study the time and temperature dependent viscoelastic properties of polymers (*27*). Furthermore, it has been used to study the processes like isothermal film formation, crystallisation of polymer dispersions and curing and aging of coatings (*73, 74*). In order to study the changes in modulus during UV curing, the US reflectometry was combined with a UV lamp (*29*). More recently, the method was combined with an NIR spectrometer to allow simultaneous measurements of the chemical conversion and mechanical properties of UV curable materials (*26*).

The measuring principle of ultrasonic shear wave reflection technique used in this study is based on the differences in acoustic properties of the sample and the substrate. Fused quartz glass is the first choice as a substrate because of its low ultrasonic attenuation. An ultrasonic shear wave of single high frequency (5 MHz) is transmitted by a transducer into a fused quartz bar. The shear wave is reflected from the interface between the sample (polymer film) and the quartz substrate and collected by a second transducer attached at the other end of the quartz bar. The shear wave is polarised so that the particle motion is parallel to the plane of the interface and only shear waves are reflected from this surface. Since the attenuation in the fused quartz is very low, a long series of fading reflected pulses appears on the receiving end after pulse excitation of the transmitter. Among these series of pulses, only the first echo is evaluated in the present study (Figure 18).

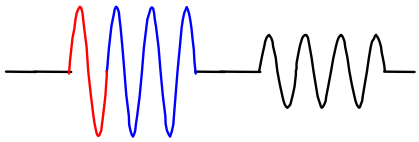

Figure 18. Sequence of echoes at the receiving end. Red denotes the first echo.

As a polymer resin vitrifies during polymerization, the changes in polymer architecture and molecular relaxation processes changes the acoustic properties of the polymer. This influences the reflection coefficient r and the phase shift ϕ of the reflected waves (Figure 19).

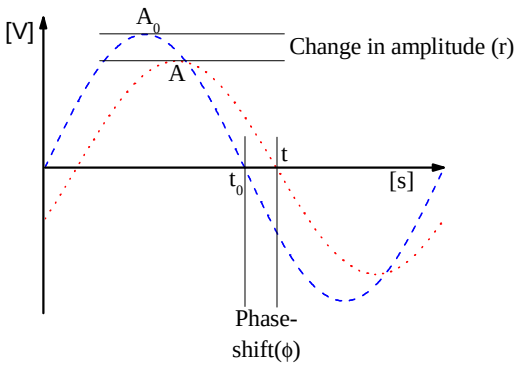

Figure 19. Changes in properties of reflected waves as a sample polymerizes.

For viscoelastic materials the reflection coefficient is a complex quantity and is given by $r^* = r \cdot e^{-i\cdot\phi}$ with an absolute value of $r = |r^*|$ and a phase shift ϕ. The absolute values of the reflection coefficient r and the phase shift ϕ for the first signal are given by, $r = A_{us} / A_{0,us}$, $\phi = \Delta t \omega$, where A_{us} and $A_{0,us}$ are the amplitudes of the ultrasonic shear waves with and without sample, respectively, Δt is the time difference between the corresponding signals with and without sample and ω is the ultrasonic angular frequency. For an ultrasonic wave reflected off a quartz-air interface, it can be assumed that $r = 1$ and $\phi = 0$. The measured amplitude and phase shift of the reflected wave without the sample is taken as the reference measurement. For isotropic and homogeneous materials r^* can be expressed in terms of the complex acoustic impedances of the substrate Z_1^* and the sample Z_2^*:

$$r^* = \frac{Z_1^* \cos\theta - Z_2^* \cos\theta'}{Z_1^* \cos\theta + Z_2^* \cos\theta'} \tag{32}$$

where θ (=79.03 deg.) and θ' are the angles of the incident and the refracted waves to the normal of the interface. Because of the negligible ultrasonic attenuation in quartz glass, its acoustic impedance can be considered to be a real quantity ($Z_q = Z_1$). For the acoustic impedance of the viscoelastic sample a complex value ($Z_s^* = Z_2^* = R + iX$) has to be taken. R and X are the resistive and the reactive components of the complex dynamic shear impedance, respectively. Z_s^* is defined as the complex ratio of the shear stress and the rate of change of displacement transverse to the direction of wave propagation. Under these assumptions one can derive from equation 17:

$$Z_s^* = Z_q \frac{\cos\theta}{\cos\theta'} \frac{1 - r^2 + i2r\sin\varphi}{1 + r^2 + 2r\cos\varphi} \tag{33}$$

The complex dynamic shear impedance Z_s^* of the sample is then related to the complex dynamic shear modulus G^* (=G'+iG") by:

$$Z_s^{*2} = (R + iX)^2 = \rho(G' + iG'') \tag{34}$$

where ρ is the density of the sample, G' and G'' are the storage and the loss component of the complex dynamic shear modulus which can be solved as:

$$G' = \frac{R^2 - X^2}{\rho},\ G'' = \frac{2RX}{\rho} \tag{35}$$

3.2.2 Ultrasonic Measuring Cell

A typical ultrasonic measuring cell is depicted in Figure 20. It was first developed at DKI in 1997 (*27*). It consists of two transducers-one for transmitting the shear waves and one for receiving the reflected shear waves, and a medium for sound wave propagation.

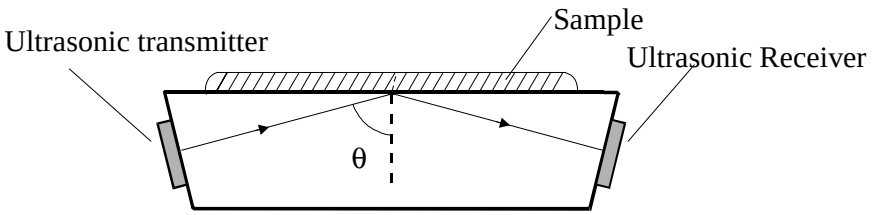

Figure 20. Schematic drawing of an ultrasonic cell.

A quartz crystal (crystal cut direction Y-cut, diameter d = 15 mm, thickness D ≈ 0.385 mm, frequency f = 5 MHz) coated with gold layer on both sides is used as an ultrasonic transducer. A fused quartz bar (height h=20 mm, width b=35 mm, Length l_1=107 mm, Length l_2=99.25 mm) acts as a sound propagating medium. Each of the oblique faces of the quartz bar (20 mm · 35 mm) is coated with a chromium layer of specific resistance less than $50\,\Omega$. The piezoelectric transducers are attached at each of these oblique faces of the fused quartz bar. The rear side of the transducer and the chromium layer act as an electrode. The transducer is connected to the circuitry board through springs (Figure 21). The piezoelectric transducer can be excited to oscillation by an external electrical pulse and emits polarised transversal (shear) pulses into the quartz bar. Further, to control a defined temperature during curing, a SMD-platinum-temperature sensor of the type "PT100" is attached to one of the oblique side of the quartz bar.

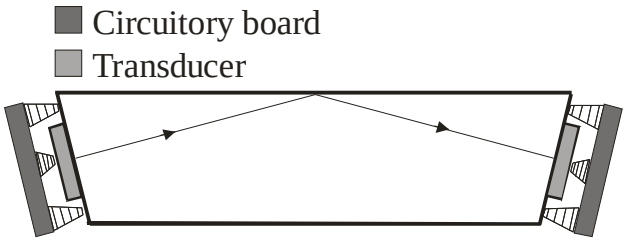

Figure 21. Schematic representation of contact of the ultrasonic transducers with circuitory board.

The described components are integrated in a measuring cell shown in Figure 22. The transducers are connected to the coaxial cables leading to the excitation pulse or induced electric voltage. The sample can be applied on the top surface of the quartz bar. The

advantage of this type of construction of the measuring cell is that the sample can be studied under varied curing conditions.

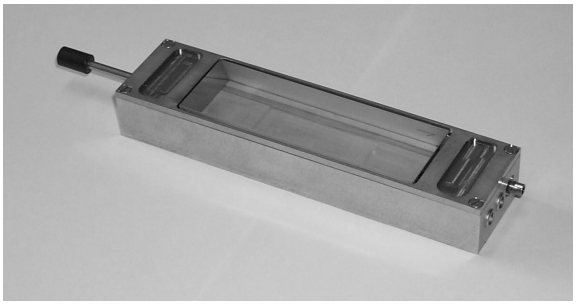

Figure 22. Ultrasonic cell for measuring shear modulus (74).

3.2.3 Ultrasonic Measurement System

The Ultrasonic part of the measurement system used in this work consists of an ultrasonic measuring cell, housing for the cell and a thermostat (Lauda RC 20 CP-edition 2000). A pulse generator-receiver plug-in card (U.S. Ultratek, PCIPR300) and a digitizing plug-in card (Acqiris, DP235) installed together in a fast PC (CPU: 3 GHz), are the main electronic components of the US system. The pulse generator–receiver plug-in card generates electrical impulses to stimulate the piezoelectric transducer of the cell at intervals of about milliseconds. A typical needle pulse has a voltage of 70 V and a rise time of 5 ns. It stimulates the transmitting transducer to generate ultrasonic signal, which is reflected at the sample–substrate interface and converted back to electric signal by the receiving transducer. The electric signal is further amplified by a signal amplifier. The amplified signal is then digitized by the data acquisition board. The data transfer from the plug-in card to PC is performed by special software (DKI_MEAS) developed at DKI. The measuring software analyses the digital data according to the procedure described in chapter 3.2.1. By this method about 100 measurements per second can be obtained.

3.3 Combined NIR Spectroscopy and US Reflectometry

3.3.1 Further Improvement in US Measuring Cell

The ultrasonic measuring cell was further developed by coating it with gold layer at the bottom to reflect the NIR radiations (*26*). The gold was deposited by thermal vapour deposition technique (device type: Univex 450). Before deposition of gold, the cell surface

was cleaned properly, first with ethanol in ultrasonic bath and then by plasma etching process. This ensures a better adhesion of gold layer to the quartz surface.

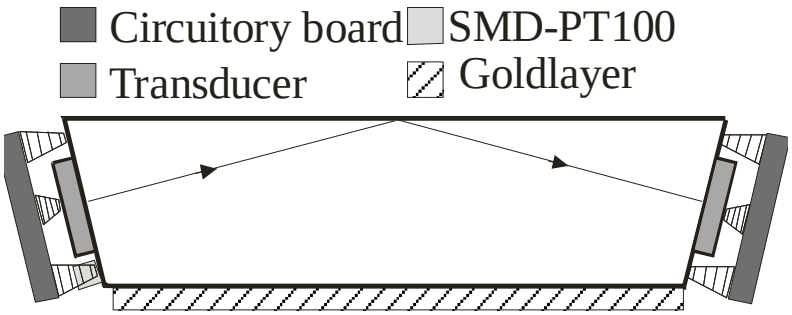

Figure 23. Ultrasonic Measuring cell with gold layer at the bottom.

3.3.2 Coupling of NIR Spectrometer with US Measurement

The experimental set up used in this study was similar to the one described in reference 24. It is presented schematically in Figure 24. The US measuring cell was kept in a closed aluminium box provided with a quartz glass window transparent to UV radiations. An inert gas (e.g. Nitrogen gas) can be flooded into this housing through an inlet for inert gas. The gas supply was regulated by an adjustable valve from KEY Instruments (MR300 series flow meter). A water circulating thermostat (Lauda RC 20 CP - edition 2000) is connected to the housing and the temperature of the cell can be controlled between 15-50 °C. The NIR spectrometer is coupled with the combined US-NIR cell via fibre optics. The inside of the aluminium box is provided with an optical system consisting of lenses and mirror system. The NIR radiations are guided from the source (halogen lamp) in the spectrometer towards the aluminium box via glass fibres. The NIR radiations are then focussed onto the sample via a condenser lens. The NIR beam is then reflected from the gold layer of the quartz cell and falls on the mirror in the box. This is then further reflected towards the sample. The process is repeated and the NIR beam passes 6 times through the sample. The NIR beam is finally collected by the second condenser lens in the box and guided to detector through the glass fibres. The mirrors are placed laterally offset so as not to interfere with UV light. The multiple beam path increases the sensitivity of the beam regarding small chemical changes during curing of thin films.

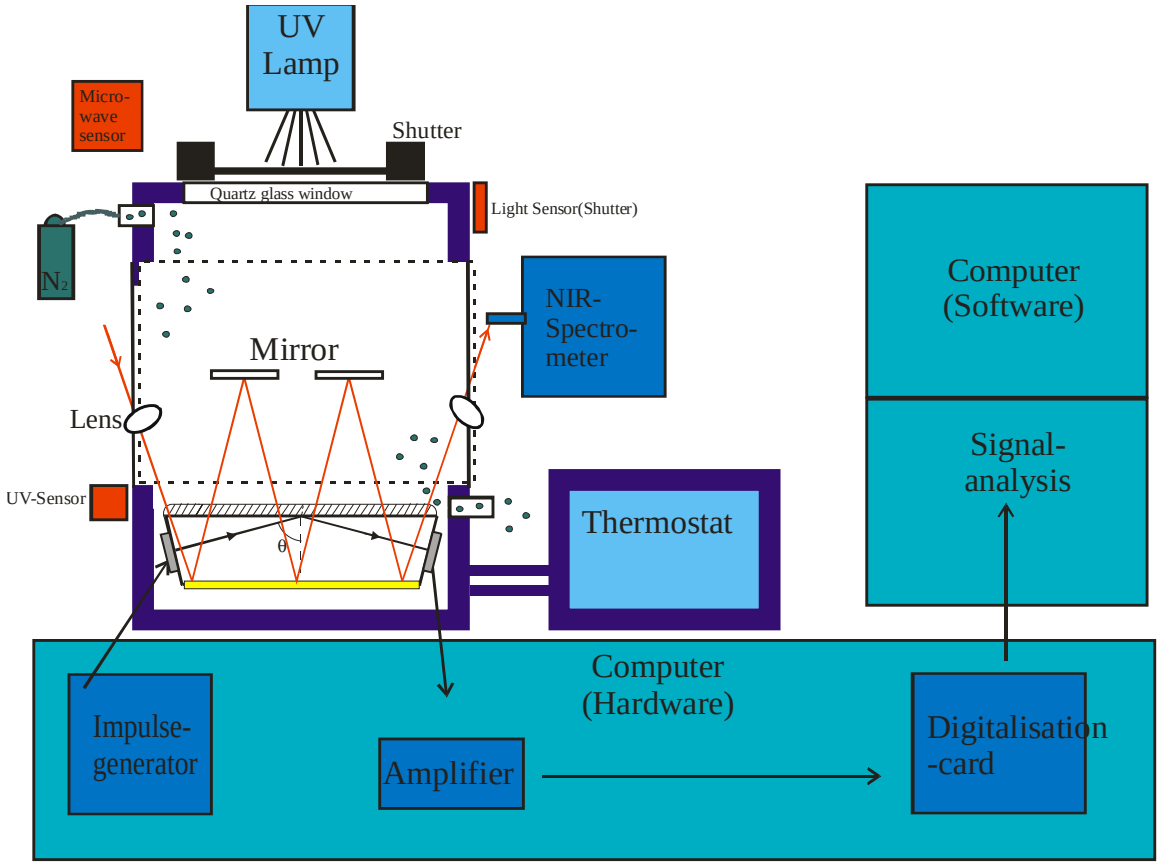

Figure 24. Schematic representation of combined US/NIR method.

The coatings are irradiated with a continuous Mercury vapour UV-Lamp (Nordson UV, UV Mac 6 curing System). The spectrum of a typical Mercury vapour lamp is given in Figure 25. It uses microwaves as an energy source to discharge mercury gas. As compared to other conventional electrode techniques of radiation, this UV light source provides more than several thousand hours of UV light with constant intensity.

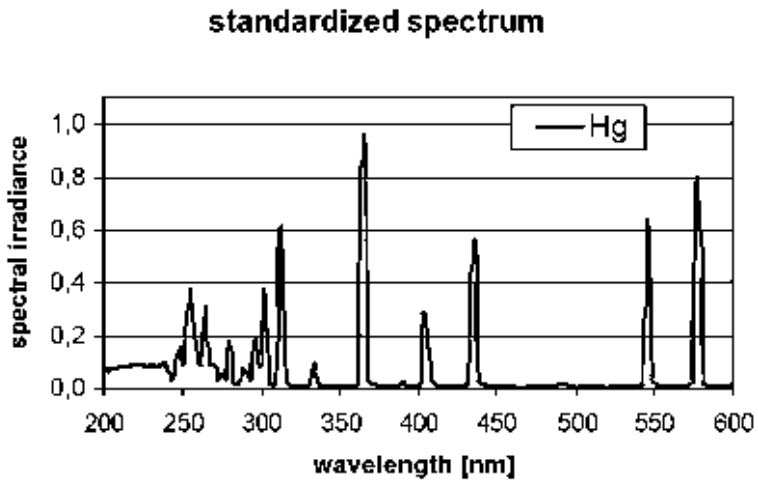

Figure 25. Spectrum of a Mercury Vapour Lamp.

Other components of the radiation unit are an electronically controlled aperture (shutter, Prontor, PRONTOR magnetic E-100), a light sensor (DKI) and a UV sensor (Polytec, Radiometer IL-1700). The shutter is located between the UV lamp and the US- NIR measuring system. The opening and closing of the shutter is controlled electronically. The UV sensor measures the intensity of UV radiation falling at the measuring cell. The maximum of its spectral sensitivity lies in the range 320-400 nm. The light sensor is used exclusively as a control sensor to detect the opening of the shutter. A microwave sensor is used as a protective measure against any leakage of microwave radiations used in UV lamp. It turns off the UV lamp automatically in case of any danger. The combined UV curing unit was placed in a chamber provided with good air suction facility. This removed any excess ozone generated during UV curing of polymers. Further, the walls of the chamber were covered with aluminium foil to block any UV radiation either entering or coming from the curing chamber.

3.3.3 Optimisation of the Set Up

Shielding of NIR Radiations Coming From UV Lamp

During the combined US-NIR measurements, additional NIR radiation was detected coming from the UV lamp. This additional NIR radiation was found to interfere with the NIR light coming from the NIR spectrometer and in turn obscured an accurate calculation of acrylate double bond conversion. To solve this problem, a filter was required in between the UV lamp and the measuring cell which filters out the NIR radiations and allows only UV radiations to pass through it. To find a suitable filter that fits well to the measuring set up, several options

were tried. First option was the copper sulphate solution, which is well known to absorb NIR radiations (*75, 76*). For this a 21 % solution of copper sulphate in distilled water was prepared. This solution was taken in a Petri dish and kept below the shutter. The UV lamp was turned on and the intensity of NIR radiations was measured. Figure 26 shows the intensity of NIR bands coming from the UV lamp in absence of any filter and in presence of copper sulphate solution. And it can be seen that the strong NIR bands visible in absence of any filter have disappeared in presence of copper sulphate solution. Then the $CuSO_4$ solution was tested for UV light transparency. Unfortunately, it was found that the Petri dish which contained the solution decreased the UV light intensity by a factor of 3.5. So, this option was discarded and a second option was tried with distilled water and Millipore water (conductivity 0.05 µs/cm). It was possible to fill these two types of water directly in the quartz window of the aluminium box (chapter 3.3.2). The intensity of NIR radiations recorded in presence of water filter is shown in Figure.26. It could be seen that both the distilled water and the Millipore water showed similar NIR intensity spectrum. Though, the NIR radiations are not completely blocked as in case of CuSO4 solution, the NIR radiations in the region of interest (1500-1800 nm) can be blocked by the water filter. This “water filter” was found to be UV light transparent.

From the above experiments and observations, the water filter with Millipore water in quartz glass was used as an NIR filter for combined US-NIR measurements. Millipore water was selected over distilled water because of its extra purity, so that the quartz glass is not etched with time.

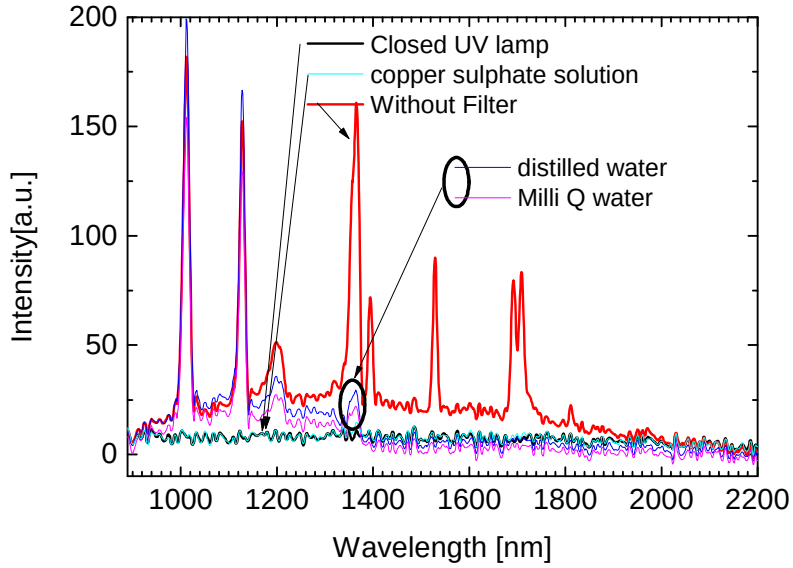

Figure 26. NIR intensity spectra in presence of different NIR filters.

Temperature Effect of the UV Lamp on Ultrasonic Modulus

US measurements were found to be highly sensitive to temperature changes. The temperature of the US measuring cell increases on absorption of radiation (UV and IR) by the sample and the cell during UV irradiation or by the heat generated during exothermic polymerization reactions. The increase in temperature of the cell not only changes the amplitude of the ultrasonic waves but also the time taken by the shear waves to travel within the cell (time of flight: TOF). Thus, the initial measured reference values of amplitude and TOF are no longer valid if the cell temperature changes and the calculated modulus values deviate from the original values.

From the preliminary analysis of the set up, it was found that through active temperature control (water circulating thermostat), the temperature of the measuring cell could be maintained constant (± 2 K) even in presence of UV light. The relative deviation of signal amplitude is in the range of < 3 %. The relative error in the calculated real part of complex dynamic shear modulus (G') under these conditions is estimated to be less than 10 % during the time period of UV irradiation (for 100 s) and till the temperature is constant again (~30 min). The error in the phase lag, however, lies in the measuring region (i.e R < 10 ns). Therefore, the measured loss modulus cannot be believed till the temperature of the measuring cell deviates by more than 0.1 K from the set temperature. These effects, however

disappear when the UV lamp is turned off and the measuring cell attain a constant set temperature. Therefore, the $G''(t)$ values are not shown and interpreted in the following chapters.

3.3.4 Synchronization of NIR Spectrometer and US Measurement Set Up

Ultrasound reflectometry and NIR spectroscopy are two independent measuring techniques. When these two methods are combined to monitor photocuring, it is important to ensure that the data collected by both the methods are synchronized in time. As long as both the measurement softwares were installed on the same computer, the internal time of the computer could be used for synchronization. But, the resolution of the internal clock of this computer was only 70 ms which is too low to monitor fast photopolymerization process. In addition, the computer has to share the CPU time between both the methods. For these reasons the two measurement softwares were installed separately on two different computers. But in this case the problem was further worsened, as the internal clocks of both the computers were not synchronized. This problem was solved in multiple steps with the help of Dr. Lellinger (DKI). At first, it was tried to use the start point of the curing reaction for synchronization. This is the most critical step in curing process and can be distinguished well in both the measurement techniques. The ultrasound software records the time of opening and closing of the shutter for UV light irradiation. But the shutter takes a while till it actually opens (~30 ms). For this reason a light sensor was fixed to the quartz window that measured the intensity of incoming UV light in real time. This gives a signal as soon as the shutter opens and light falls on the sample. This point was taken as the start (t_0) of the curing process in US reflectometry. In case of NIR measurements the start of curing can be easily distinguished by a sudden decrease in the area of the absorbance band at 1621 nm (acrylate band). The spectra are saved with a name, date and time (accuracy of 10 ms). Both these informations can be used to synchronize the methods. But as the internal clocks of these two computers are different, a software module had to be programmed in ultrasonic software which can monitor the computer network connection between both the computers. This calculates the time difference between the internal clocks of the two computers in every two seconds. With a smoothing procedure the undesired scattering of time data could be eliminated and the US and NIR data can be accurately synchronized. As a verification of the above procedure of synchronization a second method was used. In this method the small portion of NIR radiations that are transmitted along with the UV light from the UV lamp was exploited. This part of NIR radiation is scattered on the sample or reflected from the sample

and is detected by the NIR spectrometer. A characteristic band of UV lamp can be seen at 1012 nm in NIR absorbance spectra. When the amplitude of this band is plotted against measurement time, one can see exactly when the UV lamp was turned on and off. This can be used further to verify the above method of synchronization.

3.3.5 Calculation of Conversion

The NIR absorbance spectra were collected in the wavelength range from 900-2200 nm. Due to scattering effects and noise of the absorption bands, only a part of the complete wavelength region is selected for calculating the conversion of polymer resin. This selection is based on the characteristic absorption of the reacting resin. An absorption band is either created or disappears during the course of polymerisation. In case of acrylates, such an absorption band is seen at 1621 nm which corresponds to the characteristic overtone of CH_2=CH- acrylate double bond. As the polymerisation proceeds, the concentration of acrylate double bonds decreases and the area under the absorbance band at 1621 nm diminishes (Beers law) Figure 27. From the change in area of the acrylate band, the percentage of conversion can be calculated as follows:

$$p(t) = \left(1 - \left(\frac{X_t}{X_0}\right)\right) \cdot 100 \tag{21}$$

where X_0 is the area at time t_0 and X_t is the area at time t under the acrylate band at 1621 nm.

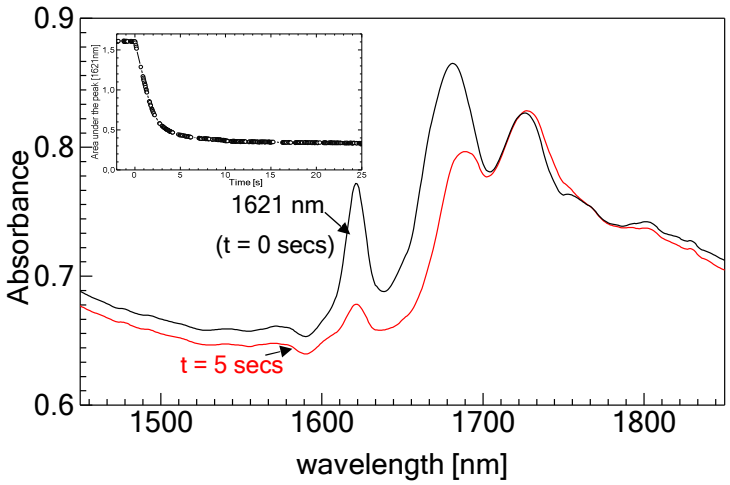

Figure 27. Characteristic CH_2=CH- acrylate band absorption at 1621 nm in NIR spectrum, calculated area under the peak (in inset).

The accurate calculation of area under the acrylate band (1621 nm) is affected by many factors like, baseline shift of the absorbance spectra and overlap of neighbouring bands (for example: 1680 nm) whose intensity changes in the course of polymerization. Therefore, several options were tried to calculate the conversion accurately.

The first possibility was the use of chemometrics for the quantitative analysis of the spectra. Common chemometric methods, for e.g. "Partial Least Square Analysis" (PLS) can be used to evaluate absorption spectra. In this method, however, a calibration data set (minimum 10 data points) with a series of well defined conversion is needed. But in case of UV photopolymerization, it is difficult to cure coatings with an exact predetermined conversion value. The only defined conversion values available are at time t_0 (no reaction) and time t_∞ (final state). Nevertheless, a separate calibration is required for each acrylate formulation, which can be a complex and laborious task. Therefore, chemometrics was not used for evaluating acrylate conversion data.

The second simple and less time consuming possibility was fitting the spectrum with analytical functions. For this the fit functions developed by Dr. Lellinger (DKI) for UA and EPA systems were used. In this method the wavelength region from 1500 nm to 1800 nm of the spectrum was selected for fitting. In case of urethane acrylate system, the acrylate band and the neighbouring bands were simulated with 9 Gaussian functions (Figure 92 in the appendix). The changing base line was modelled with a cubic function. Each individual spectrum was then fitted with 9 Gaussian and one cubic non linear fit model. The area under

the acrylate band (1621 nm) was calculated from height and width of the corresponding Gaussian function. The absorption band at 1725 nm was taken as the reference band. The conversion was calculated using the following formula:

$$p(t) = 1 - \left(\frac{X_{1621}(t) / X_{1725}(t)}{X_{1621}(t_0) / X_{1725}(t_0)} \right) \tag{22}$$

where $X_{1621}(t)$, $X_{1621}(t_0)$ are the area under the peak 1621 nm at time t and time t_0 and $X_{1725}(t)$, $X_{1725}(t_0)$ are the area under the peak 1725 nm at time t and time t_0 respectively.

The above model seemed to be too complex for epoxy acrylate system. So, it was simplified to a nonlinear fit function with three Gaussian and one linear fit function ($y = a + bx$). The peaks at 1621.7, 1648.5 and 1671.2 nm were fitted with Gaussian functions each and the base line was fitted with one linear function. The widths of the 3 Gaussian functions were fixed at 7.7, 6.2 and 13.4 nm respectively. The height and the parameters a and b for the baseline correction were set as free parameters. As the widths of the Gaussian functions were fixed, the conversion was calculated from the change in height of the acrylate double bond peak at 1621 nm:

$$p(t) = 1 - \left(\frac{X(t)}{X(0)} \right) \tag{23}$$

where, $X(t)$ is the height of the Gaussian function of the band at 1621 nm at time t and $X(0)$ is the height of the Gaussian function of the band at 1621 nm at time $t = 0$.

Besides the above mentioned facts, under identical curing parameters like irradiation time, UV intensity etc., the calculated conversion also depends on the type of substrate used. Conversion is largely influenced by the thermal properties like heat capacity and thermal conductivity of the substrate. In case of acrylates cured on ultrasonic measuring cell made up of quartz bar, the final conversion is less than as compared to other substrates like paper or laminates with lower thermal conductivity. Because of relatively high thermal conductivity and heat capacity of the quartz bar, the heat released during polymerization process is almost immediately dissipated and the temperature of the quartz cell does not exceed more than 22 °C. So, there is only a small influence of temperature changes due to released heat of reaction on conversion for a quartz substrate. Whereas, if the same sample is cured on a paper substrate with poor thermal conductivity and low heat capacity, the substrate gets heated up

during UV curing. This facilitates further reaction by heating the sample above its glass transition temperature giving a higher final conversion.

The value of measured conversion also depends on the analytical technique used. In case of ATR, the penetration depth of the infrared radiation into the sample, which is defined as the depth in which the amplitude of the electromagnetic wave is only 1/e of its value at the interface, is typically in the range between 1 and 2.5 µm. So, the measured conversion corresponds to only a very thin layer of the film, in contrast to the NIR measurements where the conversion corresponds to the conversion of double bonds in the entire depth of the film (200- 300 µm). This is made clear from conversion values measured by NIR and ATR spectroscopy on the same film of mixture of epoxy acrylate EPA and a reactive diluent TPGDA in the weight percentage ratio 80/20. The conversion on both the sides of the coating was measured separately by ATR. And it was found that conversion values (calculated from area under acrylate band at 1405 cm^{-1}) on either side of the coating differed markedly. The surface of the coating facing the UV light had undergone higher conversion (63%) as compared to the bottom layer of the coating (39%), which is true considering the phenomenon of light induced frontal polymerisation (*77*). The conversion value obtained from NIR was an average over the entire depth of the film and amount to about 47% of conversion of double bonds.

3.4 Dynamical Mechanical Thermal Analysis (DMTA)

For the rheological characterization of uncured and cured polymers, a rheometer of model ARES (Advanced Rheometric Expansion System) from TA Instruments-Waters LLC was used. These measurements were done with the help of Mr. W. Boehm at DKI. Monitoring of the instrument and data collection is done by a computer and the program TA Orchestrator Version V7.2.02. It can be used to measure the glass transition temperature, viscosity, gel point, temperature dependent and frequency dependent properties of the polymers.

Dynamical mechanical testing measures the response (here: shear deformation) of a material to periodic forces applied by a motor. The motor deforms the sample by applying a shear strain either in dynamic (sinusoidal) or steady mode. A transducer measures the stress generated by the sample during deformation by the motor. The sample is mounted between the motor and the transducer using various tools depending on the physical state of the sample. A low viscosity fluid can be measured in cuvettes, a solid polymer film can be measured using torsional-rectangular geometry with a sample dimension of

12 mm · 10 mm · 0.7 mm and a polymer melt or thermosetting resin can be measured using plate–plate geometry using plates of different diameters. The given sample geometry is critical for correct modulus value calculations. The measuring environment can be controlled from very low -150 °C (liquid nitrogen atmosphere) to very high 600 °C (air convection oven) temperatures. The viscoelastic properties of a sample can be measured over a frequency range from $1.59 \cdot 10^{-6}$ Hz to 32 Hz.

3.5 Other Analytical Test Methods

3.5.1 Universal Surface Tester

The Universal Surface Tester (INNOWEP, UST®) is used for measuring the micromechanical properties of a material surface. It can be used to measure abrasion, scratch resistance, wear, microfriction, structure and haptic parameters. In this work it was used to measure the scratch resistance of the coatings (at Hochschule Darmstadt).

This instrument analyzes the surface properties using a patented MISTAN®-Process. For measuring the scratch resistance, the sample is fixed on a specimen holder (vacuum table) and the coating surface is scanned mechanically with a tip (diamond tip, 120° cone angle) along a straight line in three steps (Figure 28). The tip moves along a length of 10 mm with a span length of 2 µm and a velocity of 0.2 mm/s. During the first step, the tip scans the surface profile with a minimum load of 0.7 mN. During the second step, the load on the tip is increased stepwise from 1 to 100 mN in steps of 10 mN. In the third step, the tip scans the surface again with a constant load of 0.7 mN. Any deformation of the surface profile during scanning and increasing the load is recorded in situ.

A measure of permanent deformation due to increasing load is given by the difference between the depth of deformation recorded during first scan and the third scan. A measure of elastic deformation is given by the difference between the depth of deformation recorded during second scan and the third scan. The elastic deformation describes the elasticity of the viscoelastic polymer coatings and the plastic deformation describes the plasticity of the coatings.

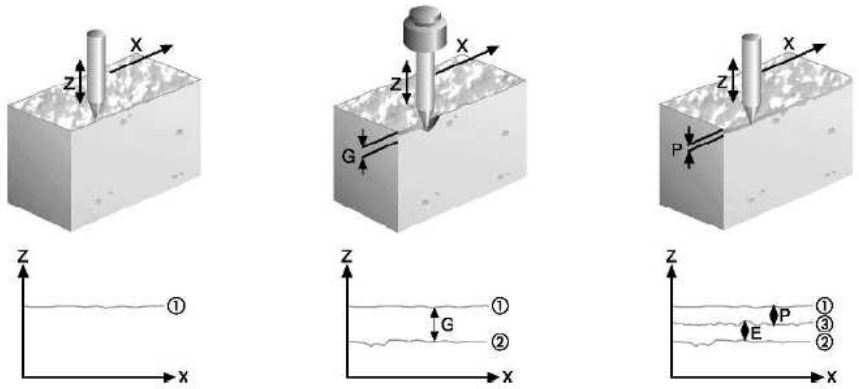

Figure 28. Schematic description of Scratch resistance measurement by UST (78).

3.5.2 Haze Measurement

The haze was measured with Haze- Gard-*plus* (BYK Gardener GmbH) at DKI. It is a measure of the transparency of the films. In this measurement, a unidirectional light beam is directed onto the film specimen. After being transmitted by the film, it enters an integrating sphere where a photo detector measures the total light transmitted by the film and the amount of transmitted light that is scattered more than 2.5 °. This percentage of light transmitted through the film that is deflected more than 2.5 ° from the direction of the incoming beam is termed as haze of a particular film specimen. Haze value below 20 implies that the film is transparent for visible light. The value of haze depends strongly on the polymer type, degree of curing and the thickness of the film.

3.5.3 Taber Abraser

Abrasion resistance tests were done with DIN 68861.2 Taber Abraser (Taber Industries, NY, USA) at Institute for surface modification (IOM), Leipzig. Coatings of thickness 50 µm were coated on a furniture decorative paper and cured with UV light. In this test the polymer coatings were subjected to the wearing action of sandpaper for a specific time (given by the number of rotations of the abrasive wheel). The evaluation criterion was the amount of sample abraded during the process. Coatings were subjected to tests with a total of 4000 rpm. The weight of the sample was taken after every 400 rotations and the emery paper was regenerated (regeneration was through 25 rotations with S/CW/P paperT9 150). The sand paper was changed after every 2000 rotations and the test was stopped after 4000 rotations. In case the sample was destroyed with less than 4000 rotation cycles, the test was stopped and the abrasion resistance at 4000 cycles was calculated graphically. In graphical analysis, generally

the total mass abrasion is plotted against the number of rotations. The lesser the steepness of the curve, lower is the value of mass abraded at 4000 rotations and greater is the stability of the sample against mass abrasion. For practical relevance, volume of abrasion is more important than the mass of the abraded sample, so that a correlation can be made with loss of thickness of the sample. Since the investigated coatings were of different densities (especially the one with nanoparticles) the volume abrasion was calculated from mass abrasion as:

$$V_{Abrasion} = \frac{m_{Abrasion}}{\rho} \tag{36}$$

where ρ is the density of the film. As the density of the film is difficult to measure, density of the uncured resin was used here. The density in both the cases is assumed to be the same as there is no evaporation of solvents and the shrinkage is very small during UV curing. The density of various acrylates and nanoparticles is provided in chapter 4.

3.5.4 Attenuated Total Reflection Spectroscopy

Attenuated Total Reflection spectroscopy (ATR) was used to measure the final conversion of cured acrylate films and compare it with that of the value calculated from NIR measurements done *in situ* during film curing. An ATR spectrometer of the model Nicolet, Typ- Nexus at DKI was used for this purpose. The sample was pressed on a diamond crystal and an average of 100 scans per measurement was taken. The conversion was calculated from the area under the acrylate double bond peak at 1405 cm^{-1} of the uncured sample and the cured polymer film, given as, $p(t) = 1 - \left(\frac{X_\infty}{X_0} \right)$, where X_∞, X_0 are the area under the acrylate double bond peak of the cured film and the uncured sample respectively.

3.5.5 Scanning Electron Microscopy

Scanning electron microscopy (SEM) of the type “Carl Zeiss ULTRA 55” was used to study the size distribution of the nanoparticles in polymer nanocomposites. The SEM images were taken at a voltage of 1 kV at IOM, Leipzig.

3.5.6 UV/Visible Spectroscopy

UV-Visible absorption spectrum was measured using the UV-Visible spectrometer of the type Lambda 40 from Perkin Elmer at DKI. The UV absorption spectra of the components of UV curing system were measured to ensure that photoinitiator is the main UV radiation absorbing

component and all other components in the formulation are transparent to the wavelength of irradiated UV light. For measuring a UV-Vis absorption spectrum, each component of the UV curing formulations - the oligomer, the reactive-diluent and the photoinitiator were diluted to concentrations of 1 wt%, 0.1 wt%, 0.01 wt% in ethanol. Each of these solutions was taken in a quartz cuvette with an internal width of 1 cm. A complete UV- Vis absorption spectrum of each component was obtained from the absorption spectrum at each concentration of the samples.

4 Sample System

4.1 Acrylate Oligomer

The selection of the samples and the preparation was performed in close co-operation with IOM, Leipzig. For the experimental studies, the two most commonly used acrylate oligomers: epoxy acrylate (EPA) and urethane acrylate (UA) were taken. Epoxy acrylate and urethane acrylate were bought from Sartomer and Cytec respectively. Epoxy acrylates are usually manufactured by reacting epoxides with acrylic acid and urethane acrylates are manufactured by addition of multifunctional isocyanates with polyols and hydroxyalkyl acrylates. The exact chemical structure of these acrylates is not revealed by the suppliers.

Ebecryl 270 (UA) is an aliphatic urethane diacrylate oligomer with a number average molecular weight of $\overline{M}_n$ = 2294 g/mol. Its GPC spectrum is given in Figure 93 in the appendix. The polymer films from urethane acrylate are well known for their flexibility, abrasion resistance, exterior durability and good adhesion to various substrates. These are used as protective coatings for wood, plastics and metal coatings.

CN104 (EPA) is a difunctional bisphenol A based epoxy acrylate with a number average molecular weight of $\overline{M}_n = 1022$ g/mol. Its GPC spectrum is given in Figure 93 in the appendix. The epoxy acrylate films are hard, good adhesives and resistant to chemicals. They are used as inks, adhesives and as a coating material for metal, wood, plastic and floor.

The names of suppliers of the oligomers, reactive diluent, photoinitiator and additives are given in Table 1 and the physical properties of the acrylates are summarised in Table 2.

4.2 Reactive Diluent

Tripropylene Glycol Diacrylate (TPGDA) is a difunctional monomer with acrylate end groups (Figure 29). It is a low molecular weight liquid monomer ($\overline{M}_n = 480$ g/mol). Its GPC spectrum is given in Figure 93 in the appendix. It is used as a thinner for viscous acrylate oligomers. Provided with the same end groups, it also copolymerizes with the acrylate oligomers during UV curing. Figure 30 shows the extinction coefficient of TPGDA diluted with ethanol, in the wavelength range of UV irradiation. This was measured to ensure that the monomer does not interfere with absorption of UV light by photoinitiator.

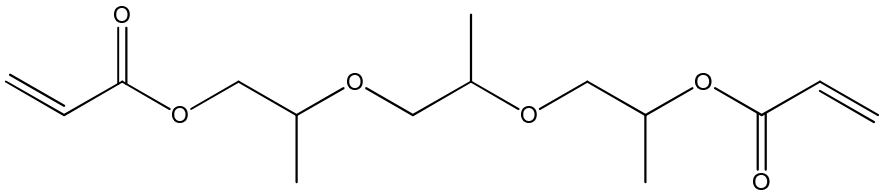

Figure 29. Chemical structure of Tripropylene glycol diacrylate (TPGDA).

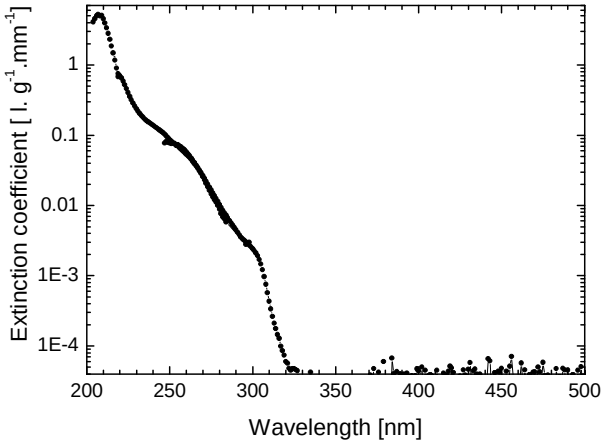

Figure 30. Extinction coefficient of monomer TPGDA diluted with ethanol as determined by UV/VIS spectroscopy.

Table 1. List of chemicals used in UV curing.

Chemicals used	Supplier	Commercial name	Abbreviated name used in text
Aliphatic Urethane diacrylate	Cytec	EB270	UA
Bisphenol-A-Epoxydiacrylate	Sartomer	CN104	EPA
Tripropylene glycol diacrylate	Sartomer	TPGDA	TPGDA
Hydroquinone monomethyl ether	Merck	4-Hydroxyanisol	MEHQ

Dispersing agent	BYK-Chemie	Disperbyk 108	Disperbyk 108
Ethyl(2,4,6-trimethylbenzoyl)-phenylphosphinate	BASF	Lucirin TPO-L	PI

Table 2. List of the physical properties of acrylates used in UV curing.

Acrylates	Functionality.	T_g [°C]	η [Pa·s]	ρ [g·cm^{-1}]	Appearance
UA	2	-33	3 (60 °C)	1.1	Colourless fluid, highly viscous
EPA	2	-4	18.9 (49 °C)	1.15	Colourless fluid, highly viscous
TPGDA	2	-80	0.015 (25 °C)	1.05	Colourless fluid

4.3 Reactive Blends

In the present work, apart from the pure acrylate resins, reactive blends were made by mixing acrylate oligomers and the reactive diluent in different weight ratios, as listed in Table 3.

Table 3. List of reactive blends used in the present study.

Reactive Blends	Ratio of oligomer to reactive diluent (wt %/wt %)
EPA/TPGDA	67/33 (2:1)
EPA/TPGDA	80/20 (4:1)
UA/TPGDA	67/33 (2:1)

4.4 Photoinitiator

Lucirin TPO-L (Ethyl(2, 4, 6–Trimethylbenzoyl)phenylphosphinate) from BASF was used as received. This is liquid in form and can be easily mixed with different types of polymer resins. This has many advantages over other photoinitiators (*79*). It absorbs from far UV light to near visible light with an absorption maximum at 370 nm. Figure 31 shows the extinction coefficient of TPO-L in ethanol at different wavelengths. Due to absorption in longer wavelength region, it has proved to be extremely useful in through cure of thicker and pigmented coatings and thus lessening the yellowing effect usually seen with other photoinitiators. It also allows curing in presence of UV absorber which is important for the stability of exterior coatings.

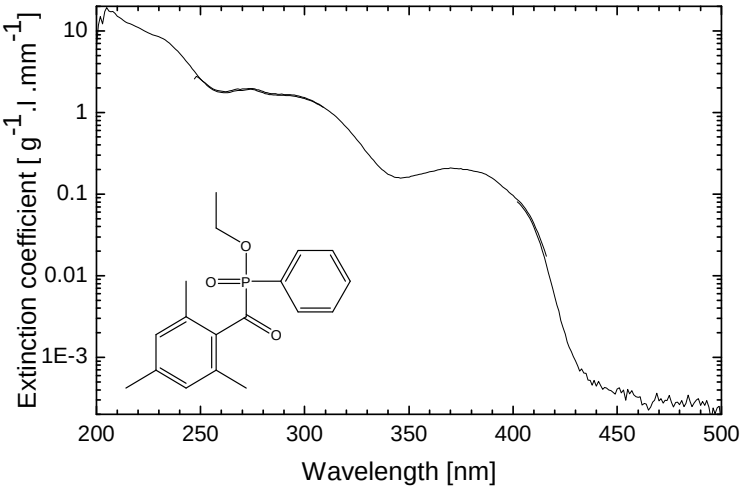

Figure 31. *Extinction coefficient of TPO-L in ethanol determined by UV/VIS spectroscopy.*

4.5 Dispersing and Stabilising Agents

Disperbyk 108 is a hydroxy functional carboxylic acid ester with pigment affinic groups and act as a dispersing agent. This deflocculates the pigments through steric stabilisation of the small particles of the pigments, thus, improving the final gloss, colour strength and transparency of the polymer film. Dispersing agents reduce the viscosity, increasing the loading level of pigments in the polymer matrix.

MEHQ is hydroquinone monomethyl ether, used as a stabilising agent in the UV curing formulation. It inhibits spontaneous polymerisation due to UV light and thus, stabilises the polymer coatings against degrading effects of UV radiation.

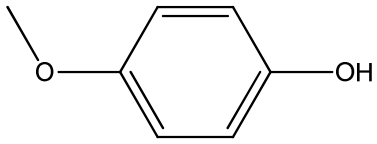

Figure 32. Chemical structure of Hydroquinone monomethyl ether (MEHQ).

4.6 Nanoparticles

Inorganic nanoparticles like silica and alumina have been used since long to improve the mechanical properties of the polymers (*80-82*). Because of their nanometer size (10-50 nm) and high active surface area, it is expected that the polymer nanocomposites have improved properties as compared to the conventional polymers. They are believed to have increased modulus, toughness, transparency, low gas permeability, scratch resistance, abrasion resistance, solvent and heat resistance. Further, the viscoelastic properties of the polymer nanocomposites can be improved by improving the particle-oligomer interaction. This is done by grafting different organic functional groups on to the nanoparticle surface.

In the present work, both the inorganic nanoparticles (Aerosil) and organically modified nanoparticles such as SIMA, ALMA, ALOXAL and ALMAL were used. These nanoparticles were provided by IOM, Leipzig. The method of synthesis of these organically modified (methacrylate and maleate) silica and alumina nanoparticles was developed at IOM, Leipzig (*83-86*).These surface modified nanoparticles with the same end groups as the oligomer and monomer are matrix compatible and link covalently with the matrix. Due to their small size they are expected to improve the viscoelastic properties of the cured polymer film without affecting its optical properties. Table 4 summarises the nanoparticles used as fillers in the present work.

Table 4. Particle size of the nanoparticles used

Nanoparticles	Particle diameter *d* [nm]			Supplier
	Data sheet, Powder	SEM, Powder	SEM, Composite	
ALMAL		40–80	51–94	Synthesized at IOM
ALOXAL		42–91	21–94	Synthesized at IOM
AEROSIL OX 50	40	35–70	59–133	Degussa
ALMA		31–90	51–145	Synthesized at IOM
SIMA		35–78	59–73	Synthesized at IOM

4.6.1 Route of Synthesis of Functionalised Nanoparticles

ALMAL-Nanoparticle

About 1.4 mol.lit^{-1} of aluminium 2-propoxide and 700 ml of isopropanol was taken in a 2 L batch reactor and stirred continuously at a temperature of approximately 82°C. After complete dissolution of aluminium 2-propoxide, a solution of 0.5 mol of maleic acid or maleic anhydride in 80 ml water was added to the above solution by a peristaltic pump for 90 mins with continuous stirring. The basic aluminium maleate, bis-aluminium dihydroxy-maleate is obtained quantitatively as a white coloured precipitate. The solvent is removed in a rotary evaporator under reduced pressure and the nanopowder is obtained by drying the precipitate for 24 hrs at 120 °C. These nanoparticles are called as ALMAL nanoparticles (*86*) by IOM, Leipzig.

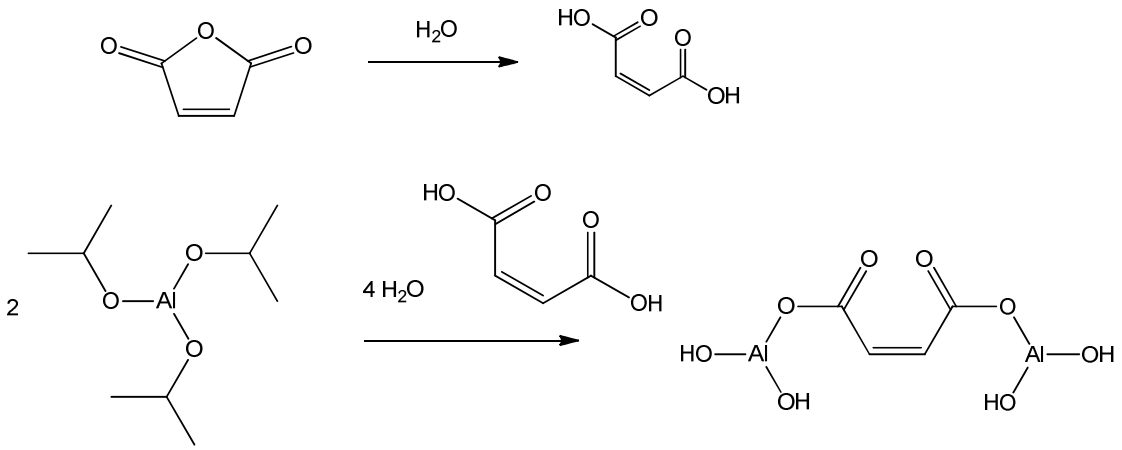

Figure 33. Route of synthesis of ALMAL nanoparticles (86) at IOM, Leipzig.

ALOXAL-Nanoparticle

The synthesis of ALOXAL nanoparticles is similar to that of ALMAL nanoparticles, except that the maleic acid is replaced by a suspension of oxalic acid dihydrate in 120 ml water. The bis-aluminium dihydroxy oxalate (ALOXAL) is obtained quantitatively as white coloured nanopowder.

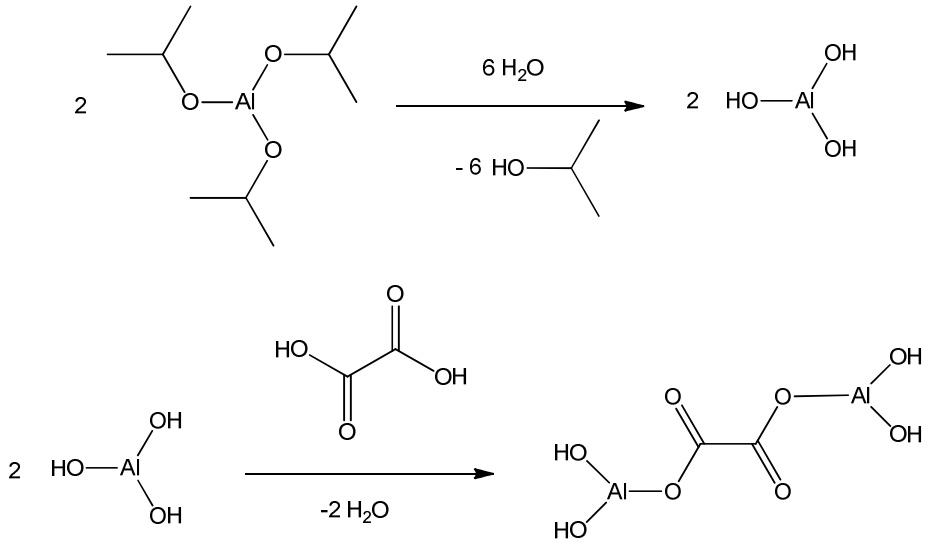

Figure 34. Route of synthesis of AlOXAL nanoparticles at IOM, Leipzig.

ALMA-Nanoparticle

For the synthesis of ALMA nanoparticles, about 150 g of aluminium oxide nanoparticles ($d \approx 40$ nm) were suspended in 1.5 l of boiling acetone and stirred intensively. To this

solution, 3-methacryloxy(propyl)trimethoxysilane was added with continuous stirring followed by a solution of 2.25 g of maleic anhydride in 15 ml water. This mixture was refluxed for 2 h under air. After the mixture was cooled to room temperature, the solvent was removed using a rotary vapour under reduced pressure. The white precipitate thus obtained quantitatively was dried under vacuum and identified as ALMA nanoparticles by IOM, Leipzig.

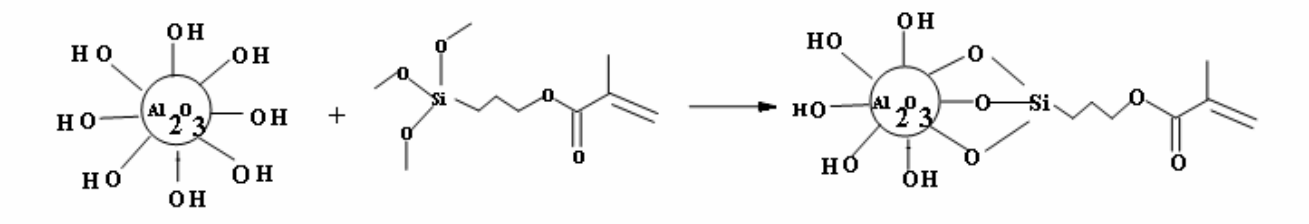

Figure 35. Route of synthesis of ALMA nanoparticles at IOM, Leipzig.

SIMA-Nanoparticle

SIMA nanoparticles are methacrylate modified silicon dioxide nanoparticles (*83*). The synthesis of SIMA nanoparticles is similar to that of ALMA nanoparticles. Here the aluminium oxide nanopowder is replaced by the silicon dioxide nanopowder ($d \approx 13$ nm).

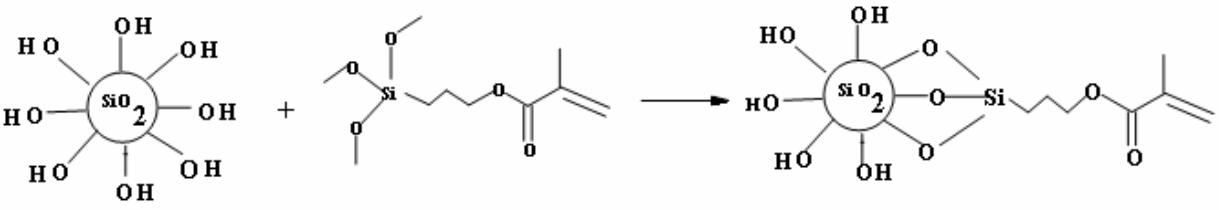

Figure 36. Route of synthesis of SIMA nanoparticles at IOM, Leipzig.

4.6.2 Homogeneous Mixing of Nanoparticles in Polymer Matrix

Preparation of the Base Matrix

The oligomer, reactive diluent, stabilising agent (0.3 %) and dispersing agent (1.2 %) were mixed in a temperature controlled batch reactor. For a thorough mixing, the mixture was heated up to 60 °C and stirred for 15 min at a rate of 1000 rpm.

Preparation of Polymer Nanoparticle Mixture

Formulations of polymer - nanodispersion with different concentrations of nanoparticles were provided by IOM, Leipzig. These were made by adding nanoparticles in the above base resin and dispersing them with continuous stirring at a rate of 4000 rpm at a temperature of 60 °C for about 3 h. Any kind of particle agglomerate is supposed to break down with such an intensive stirring. The resultant is a milky nanodispersion. The photoinitiator (TPO-L) is added at the end and mixed properly. The mixture is finally kept in ultrasonic bath (approx. 45 minutes) to get a homogeneous and air bubble free formulation. Table 4 gives the densities of the homogeneous mixture of EPA /TPGDA resin with ALMAL nanoparticles. Table 5 describes the densities of each of the different types of nanoparticles at a concentration of 15 % in the EPA / TPGDA matrix.

Table 5. Densities (g /cm^3) of mixtures of EPA/ TPGDA (2:1) resin with ALMAL nanoparticles.

Nanoparticle concentration	0%	5%	10%	15%	20%	25%
ALMAL	1.11	1.14	1.16	1.19	1.22	1.25

Table 6. Densities of different types of nanoparticles at a concentration of 15 wt % in EPA/TPGDA.

Nanoparticle type	ALMAL	ALOXAL	ALMA	SIMA	AEROSIL
Density	1.19	1.19	1.19	1.19	1.17

5 Results and Discussion

The first section of this chapter deals with a detail viscoelastic characterization of each of the acrylate resins and the reactive blends used in this work (TPGDA, EPA, UA, blend of EPA/TPGDA, blend of UA/TPGDA), as studied by DMTA. The second section presents the results of the combined US/NIR method. At first the conversion-modulus curves of each of the acrylate resins and their blends are discussed. Then the effect of variation of curing parameters (UV dose, photoinitiator concentration, etc.) on the curing kinetics and modulus of EPA/TPGDA blend is discussed. The following sections deal with the effect of nanoparticles and their concentration on the curing kinetics (conversion and modulus in real time) of blends of EPA/TPGDA and UA/TPGDA. The final properties of the UV curable acrylate resins are also discussed. This chapter also presents an empirical model, which is applied to fit the combined conversion-modulus curve of single phase polymer systems.

5.1 Viscoelastic Characterization of Uncured Acrylate Resins and Cured Films

Reactive Diluent: TPGDA

The temperature dependent shear modulus curves of TPGDA in both uncured and cured state measured at 1 Hz frequency are given in Figure 37. The monomer resin was mixed with 0.1wt % of PI and irradiated for 10 s (equivalent to UV dose of 3.85 kJ/m^2) to get the cured film. It can be seen in the figure that, as TPGDA is converted from a low viscosity liquid monomer to a polymer film on UV irradiation, the step in G' and the maximum in G'' shear modulus curve shift to higher temperatures. Both the G' and G'' curves are considerably broadened with a significant increase in T_g from 193 K to 320 K indicated by the maximum in G''. A high value of T_g and presence of a rubber plateau of about 100 MPa at temperatures above 60 °C in case of cured TPGDA indicates a highly cross-linked polymer network. For a detailed analysis of frequency dependence of shear modulus, master curves were constructed. Figure 38 shows the master curves of the uncured (left) and cured (right) TPGDA. For the uncured TPGDA, measurements were conducted for a series of temperatures from 183 K to 233 K and the master curve was constructed at a reference temperature of 193 K (T_g of the uncured TPGDA). In case of cured TPGDA, measurements were conducted for a series of temperatures from 193 K to 343 K and the master curve was constructed at a reference temperature of 293 K (temperature of cure). The temperature dependence of the shift factors

of both uncured and cured TPGDA is shown in Figure 94 in the appendix. It can be seen that, the master curve of cured TPGDA covers a frequency range of about 27 decades as compared to only 10 decades in uncured state. The broadening of the modulus–frequency curves indicates that, cured TPGDA has a broad distribution of relaxation times. This can be possibly due to heterogeneity in its network structure, which can be due to broad distribution of molecular weight of the strands between the cross-links.

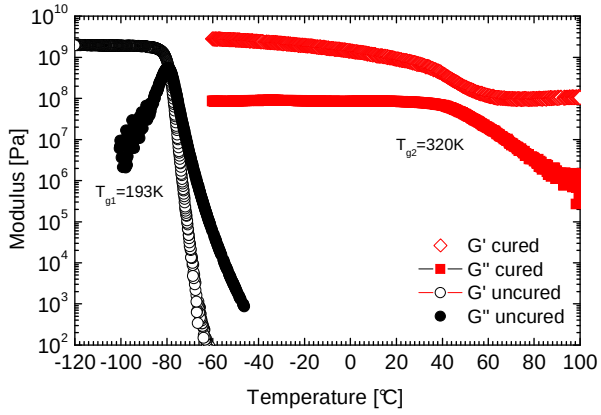

Figure 37. Temperature dependent modulus curves of TPGDA (uncured and cured) measured by DMTA at 1 Hz frequency.

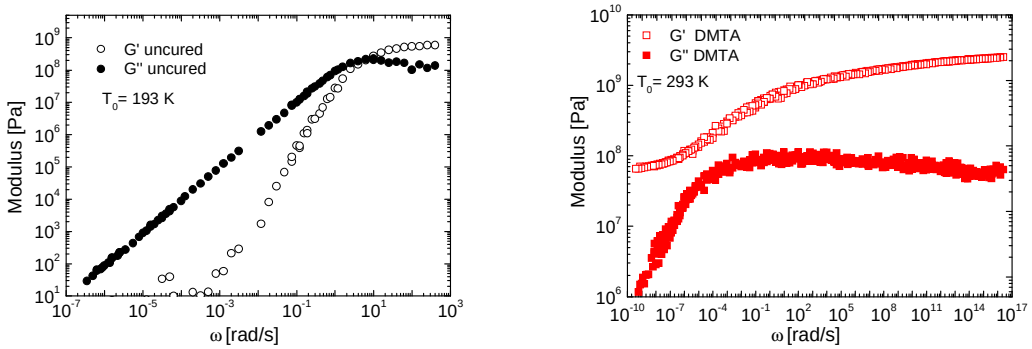

Figure 38. a. Master curves of uncured TPGDA (left) at a reference temperature of 193 K, b. Master curves of cured TPGDA (right) at a reference temperature of 293 K.

Epoxy Acrylate (EPA)

The temperature dependent modulus curves of uncured and cured EPA are given in Figure 39. The sample was mixed with 0.1% PI and irradiated with UV light for 10 s (equivalent to UV

dose of 3.85 kJ/m^2) at room temperature. Figure 39a shows that, the storage shear modulus of uncured EPA exhibit a high modulus at lower temperatures (glassy zone) which falls rapidly at higher temperatures. In case of cured EPA, however, the storage modulus attains a constant value of about 10^5 Pa (rubber plateau) at higher temperatures. This indicates that, EPA forms a cross-linked polymer network on UV curing. Moreover, the glass transition temperature on curing increases by 13 K. The master curve of the uncured EPA is shown in Figure 39b. It was constructed at a reference temperature of 268 K for a series of measurements from 263 K to 277 K. It resembles that of a typical uncross-linked resin system with a glassy zone at higher frequencies and a terminal zone at lower frequencies, without any rubber plateau in between. The temperature dependence of the shift factors is given in Figure 95 in the appendix. The master curve of cured EPA was difficult to measure for broad frequencies due to the high network density of the film.

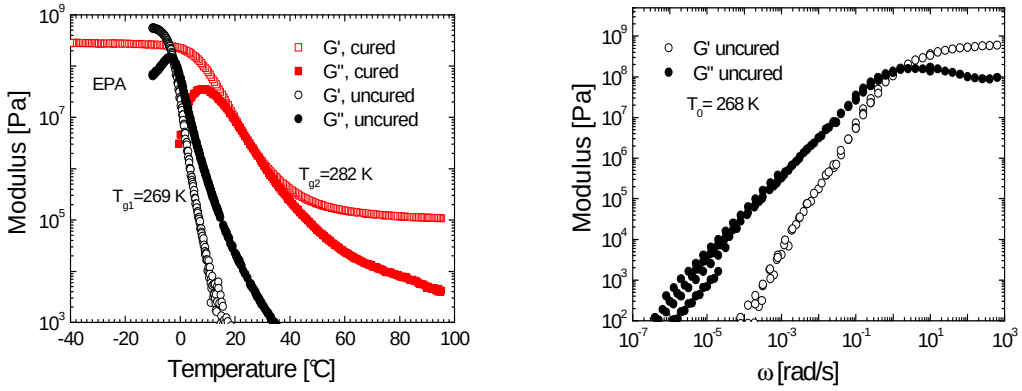

Figure 39. Temperature dependent modulus curves of EPA (uncured and cured) measured by DMTA at 1 Hz frequency (left), Master curves of uncured EPA (right) at a reference temperature of 268 K.

Blend of Reactive diluent TPGDA and Oligomer EPA

As an example for the viscoelastic properties of a mixture of an oligomer and a reactive diluent, EPA and TPGDA were mixed in a weight ratio 2:1. The concentration of PI in the mixture was 0.1 wt %. The mixture was cured with 10 s of UV irradiation (equivalent to UV dose of 3.85 kJ/m^2). The temperature dependent modulus curves of the mixture in both uncured and cured state are shown in Figure 40. The temperature dependent shear modulus curves of both uncured and cured mixture exhibit only one glass transition region and a single loss modulus peak over the measured temperature range. This indicates that TPGDA and EPA are homogeneously miscible in the reactive mixture and on curing forms cross-linked

networks with no significant phase separation. The broadening of the relaxation time spectrum of the cured system is rather related to other inhomogeneities of the network or contributions from composition fluctuations which are typical for polymer blends, than to a reaction-induced macroscopic phase separation.

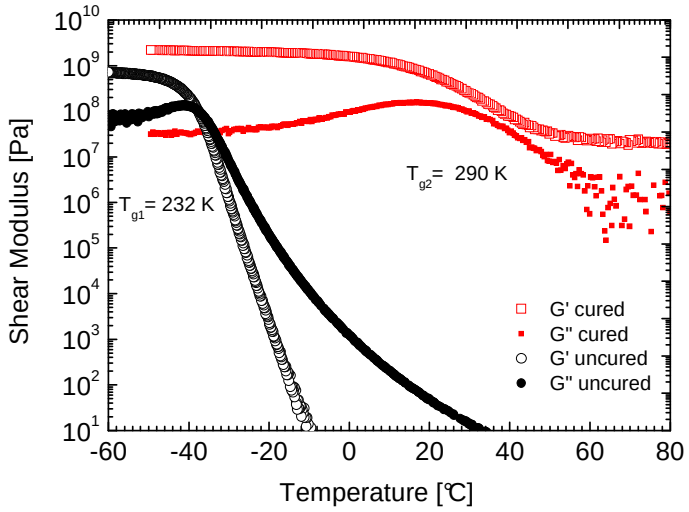

Figure 40. Temperature dependent modulus curves of reactive blend EPA/TPGDA in a ratio 2:1 (uncured and cured).

The G' and G'' curves of EPA, TPGDA and mixture of EPA and TPGDA in uncured state are plotted together in Figure 41. The T_g of the mixture was found to be 232 K, determined from the position of the peak of its G'' curve. This value lies in between the T_gs of the oligomer (269 K) and the monomer (193 K). The T_g of the mixture was then calculated theoretically from Fox equation for homogeneous polymer mixture, given as:

$$\frac{1}{T_{g,mixture}} = \frac{W_A}{T_{gA}} + \frac{W_B}{T_{gB}} \qquad (37)$$

where W_A and W_B are the weight fraction of each of the homo-polymers A and B in the mixture, whose glass transition temperature is given by T_{g_A} and T_{g_B} respectively. The predicted value of T_g from Fox equation was found to be 238 K, which is close to the experimental value. This indicates that the given reactive blend EPA/TPGDA is homogeneously mixed and has only one phase.

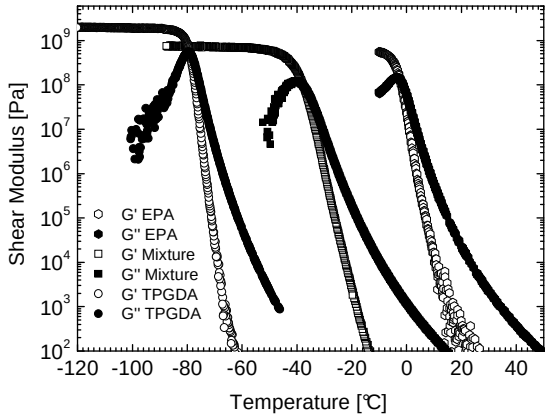

Figure 41. Comparison of temperature dependent shear modulus of uncured EPA, TPGDA and blend of EPA and TPGDA in a weight ratio 2:1.

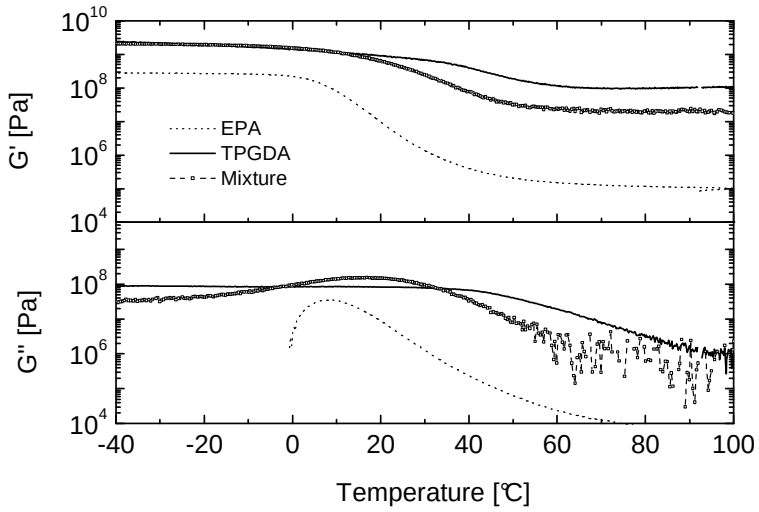

Figure 42. Comparison of temperature dependent shear modulus of cured EPA, TPGDA and blend of EPA and TPGDA in a weight ratio 2:1.

Figure 42 shows the G' and G'' curves of the polymer mixture and each of its component in cured state. As it can be observed, on cross-linking both the G' and G'' curves of each of the polymers are considerably broadened with an equilibrium storage shear modulus at higher temperatures (rubber plateau). This indicates that these acrylate polymers form highly cross-linked networks on radiation curing. By extension of rubber theory to highly cross-linked systems, the storage modulus (G') in the "rubbery region" can be used to calculate the cross-link density (ν_e) by the following relationship:

$$G' = 3\nu_e RT \quad (38)$$

where R is the gas constant and T is temperature in degrees Kelvin at which G' is taken (here 373 K). Cross-link density is the number of moles of elastically effective network chains per cubic centimeter of material. The values of the cross-link density and T_g of these polymers are summarized in Table 6. It has to be noted here, that the thus calculated cross-link densities are only relative quantities, since theory of rubber elasticity is not fulfilled for highly cross-linked polymers. However, it can be seen that TPGDA exhibit the highest cross-link density and the polymer mixture has a crosslink density in between the monomer and the oligomer. This finding is also supported by the order of their T_g's, TPGDA>mixture>EPA.

Table 7. Tg, shear modulus, cross-link density of TPGDA, EPA and EPA/TPGDA (2:1).

Cured Polymer Film	T_g cured (K)	Shear Modulus (at rubber plateau) G' (MPa)	Crosslink density (mol/cm^3)
TPGDA	320	104.6	11.2×10^{-5}
EPA	282	0.1	1.07×10^{-5}
EPA/TPGDA	290	17.2	1.84×10^{-5}

The very low crosslink density of pure oligomer is attributed to its high viscosity (18.9 Pa.s @ 49°C), which retards the conversion and cross-linking at early stages under the given curing conditions (as will be discussed in the following section). Another possible reason is the initial high molecular weight of EPA oligomer which leads to longer network chains and a lower cross-linking density. This is consistently expressed by the small change of T_g on curing.

The master curves of the uncured and cured polymer mixture are shown in Figure 43. The master curve of the cured film corresponds to EPA/TPGDA (2:1) blend with 0.5 wt % PI cured with 100 s of UV irradiation (38.5 kJ/m^2 UV dose). The master curve of the uncured mixture was constructed at a reference temperature of 233 K for a series of measurements from 213 K to 293 K. The master curve of the cured polymer mixture was constructed at a reference temperature of 293 K for a series of measurements done from 184 K to 353 K. The

temperature dependence of the shift factors is shown in Figure 96 in the appendix. The master curves also depicts only one glass transition zone in case of both uncured and cured polymer mixture, as also seen in temperature dependent modulus curves. The master curve of the cured mixture is considerably broadened as compared to the uncured mixture. The broadened curve with only one glass transition zone indicates again that the mixture forms almost homogeneous networks with a broad distribution of molecular relaxation processes without any reaction induced phase separation.

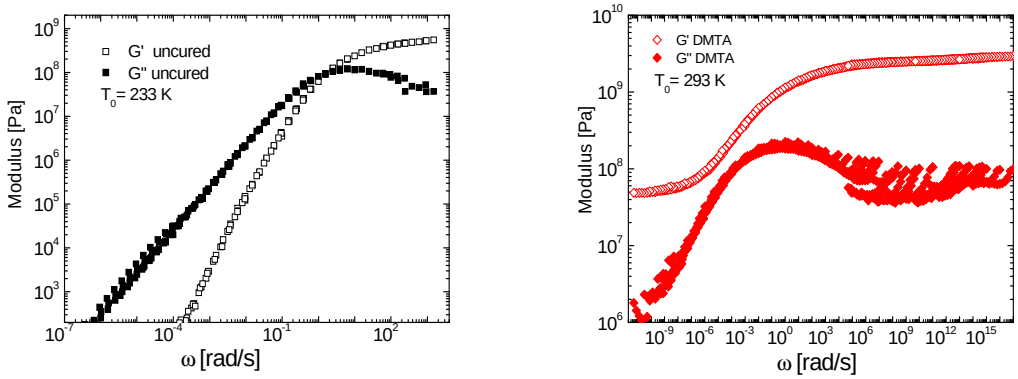

Figure 43. Master curves of uncured EPA/TPGDA (left) at a reference temperature of 268 K, master curves of cured EPA/TPGDA (right) at a reference temperature of 293 K.

Urethane Acrylate (UA)

Figure 44 shows the shear modulus and loss modulus curves of the uncured and cured UA. The oligomer was mixed with 0.1 wt % of photoinitiator and cured for 10 s (equivalent to UV dose of 3.85 kJ/m^2). The temperature dependent storage modulus of uncured UA shows two transitions, a dominant glass transition step at lower temperatures (240 K) and a weak transition at higher temperatures (257 K). The loss modulus curve shows a well defined peak corresponding to the glass transition at lower temperatures, whereas only a shoulder can be seen at higher temperatures. This can be possibly, either due to entanglements of UA chains ($\overline{M}_n$ = 2294 g/mol) or the given UA is a two phase system. It has been also previously reported by many authors (*87-90*) that UA exists as a two phase system, comprising of a soft (containing the macrodiol) and a hard segment (polyacrylates and/or diacrylated diisocyanate segments). The glass transition zone at lower temperatures is attributed to the soft segments and that at higher temperatures is due to hard segments. A small transition at higher temperatures suggests that the hard segments are present only in minute quantities in the

given UA. The T_g of the soft UA segments was found to be 240 K. In case of cured UA, it can be seen that both the G' and G'' curves broadens significantly, with an indication of two broad glass transition regions. The G'' data gets noisy at high temperatures. The loss modulus curve seems to be consisting of two peaks: one at lower temperatures (≈241 K) and the other at higher temperatures (≈276 K). This indicates that possibly there is still some phase separation in the cured system, similar to the uncured UA. Interestingly, the lower glass transition, related to the soft segments seems to be almost unchanged by the cross-linking. This is not surprising, since the macrodiols are possibly not changed by the cross-linking. An alternative explanation of the two transitions and the extreme broadening of cured UA can be a transition from entanglement or gel like macromonomer to a cross-linked system with a broad distribution of chain lengths between the cross-links.

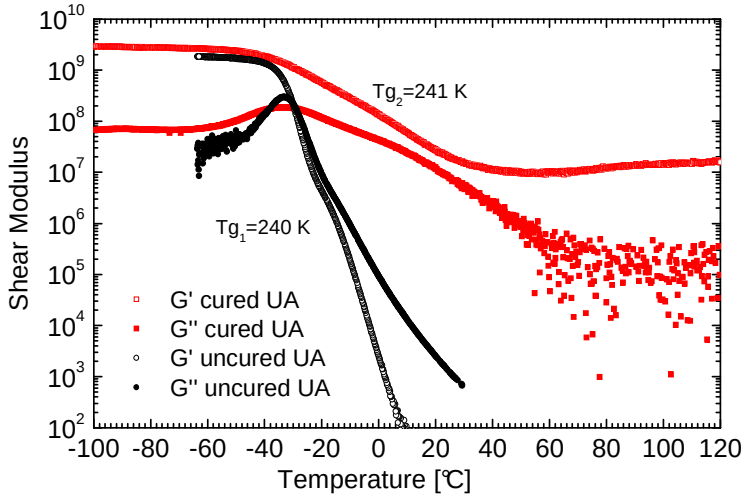

Figure 44. Temperature dependent modulus curves of UA (uncured and cured) measured by DMTA at 1 Hz frequency.

Master curves of the uncured and cured UA are shown in Figure 45. The temperature dependent shift factor curves are shown in Figure 97 in the appendix. The master curve of the uncured UA was constructed at a reference temperature of 243 K for a series of measurements done from 218 K to 298 K. The master curve of the cured UA was constructed at a reference temperature of 243 K for a series of measurements done from 213 K to 323 K. The frequency dependent storage modulus curve of uncured UA, similar to temperature dependent modulus curve shows two transition zones. The frequency dependent shear modulus curves of the cured UA are very broad and are spread over a frequency range of 26 decades. They seem to

be consisting of two transition regions. The possible explanation to this behaviour is same as discussed before.

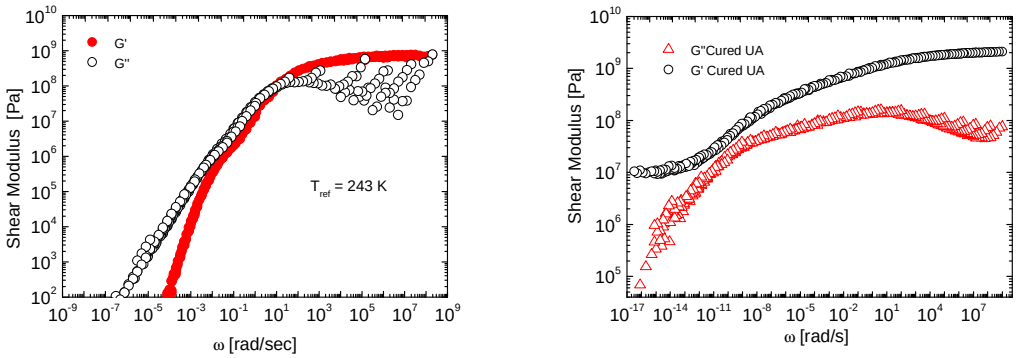

Figure 45. Master curves of uncured UA (left) at a reference temperature of 243 K, Master curves of cured UA (right) at a reference temperature of 243 K.

Blend of Reactive diluent TPGDA and Oligomer UA

UA and TPGDA were mixed in a weight ratio of 2:1. The matrix was mixed with 0.5 wt % of PI and cured for 100 s (equivalent to UV dose of 38.5 kJ/m^2). Figure 46 shows the temperature dependent modulus curve of the uncured and cured mixture. The shear modulus of uncured mixture has a similar shape like that of the oligomer UA. The presence of two transition steps in G' and a strong and weak peak in G'' indicates that the diluted UA is also a two phase system. The glass transition temperature of the uncured UA shifts to lower temperature on dilution. Both the peaks (strong & weak) in G'' curve shows a shift of 22 ± 2 K on dilution. On curing, it can be seen that both the shear modulus curves (G' and G'') are considerably broadened with a very weak indication of two transition regions. This indicates that the UA/TPGDA blend forms cross-linked network with broad heterogeneity in distribution of molecular weight of the cross-linked networks and possibly the hard segments are now a part of the cross-linked network. The second possibility is that the UA networks dominate the hard segment networks (present in minute quantity) so that they are not clearly distinguished. The frequency dependent modulus behaviour of this mixture was not studied in detail as the focus was on the systems based on EPA/TPGDA matrix.

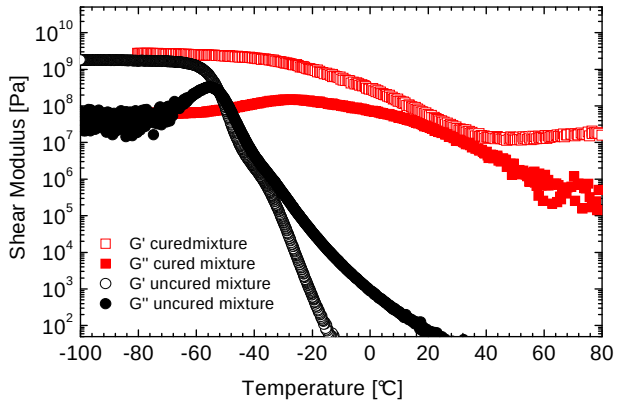

Figure 46. Temperature dependent modulus of uncured and cured blend of UA/TPGDA in a weight ratio 2:1.

5.2 Combined US/NIR Experiments

5.2.1 Modulus-Conversion Curves

In the following chapter, results of the combined US/NIR experiments for the monomer TPGDA, the oligomers EPA and UA and mixtures of the monomer and the oligomers are exemplary discussed. The construction of the combined modulus conversion curves from the simultaneously measured conversion-time and modulus-time curves is demonstrated.

UV Curing Process

The combined US/NIR measurements were performed as follows: the cleaned US cell (with 2-butanone) was placed inside an aluminium box in a dark chamber. To maintain an inert atmosphere free of oxygen gas, the aluminium box was ventilated with nitrogen gas with a flow rate of 10 l/min. The temperature of the cell was maintained at 20°C by a water cooling thermostat. Once all the conditions were stable, US reference measurement was done with empty quartz cell. Then the sample was spread on the quartz cell with the help of a razor plate. The thickness of the sample was controlled by tesa tapes of thickness 300 µm, fixed on the four sides of the cell. The sample was irradiated after 10 minutes of its application on the US cell, assuming that the concentration of oxygen gas in the box is minimized. The UV dose was controlled by an electronic shutter. The sample was allowed to post cure (after irradiation) for 6 hrs under the same conditions before it was taken off from the quartz substrate. The decrease in concentration of acrylate bonds and increase of modulus of the film throughout the curing was recorded *in situ* by the combined US/NIR method.

Reactive Diluent: TPGDA

TPGDA was mixed with 0.1 wt % of PI and was irradiated with UV light for 10 s (equivalent to UV dose of 3.85 kJ/m^2). The simultaneously measured conversion-time and modulus-time curves are shown in Figure 47. It can be seen that, this acrylate based reactive diluent is highly reactive with a high rate of polymerization at the beginning of irradiation. Using Equation 3, the maximum rate of polymerization was found to be 5.38 $mol \cdot l^{-1} \cdot s^{-1}$. The conversion reaches a value of about 80 % within 2 s of irradiation, above which it slows down and is finally retarded at a value of 90 %, whereas, the modulus of TPGDA starts to increase significantly after 2 s of irradiation and continues to increase thereafter.

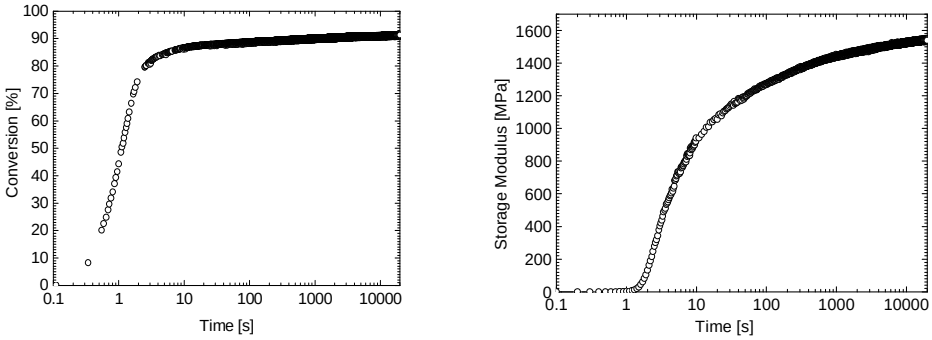

Figure 47. Conversion vs. time (left) and modulus vs. time (right) curves of TPGDA irradiated for 10 s.

For better interpretation of the dependency of modulus of the polymer film on chemical conversion, these two quantities (conversion and modulus) were plotted against each other (Figure 48). It can be seen that on curing, the increase of storage modulus does not follow the chemical conversion linearly. The increase in modulus is insignificant till the polymer reaches a conversion of 70 %. At this point the modulus shows a drastic change and continues to increase thereafter, whereas, conversion stops before completion (i.e, at 90 %). This is because of vitrification of the reacting polymer resin that changes the rate of polymerization from reaction-controlled to diffusion-controlled process, therefore, retarding further conversion of acrylate double bonds. The modulus-conversion curve provides a clear indication of the so-called “autodeceleration” phenomena, which is related to the slowing down of the polymerization by a “negative-feedback” of the vitrification of the sample. This experimental curve was later tried to fit with an empirical model which will be discussed in chapter 5.8.

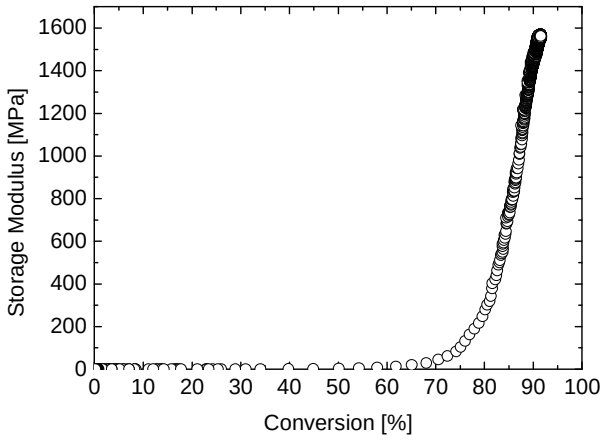

Figure 48. Modulus-conversion curve of the monomer TPGDA irradiated for 10 s.

Oligomer-EPA

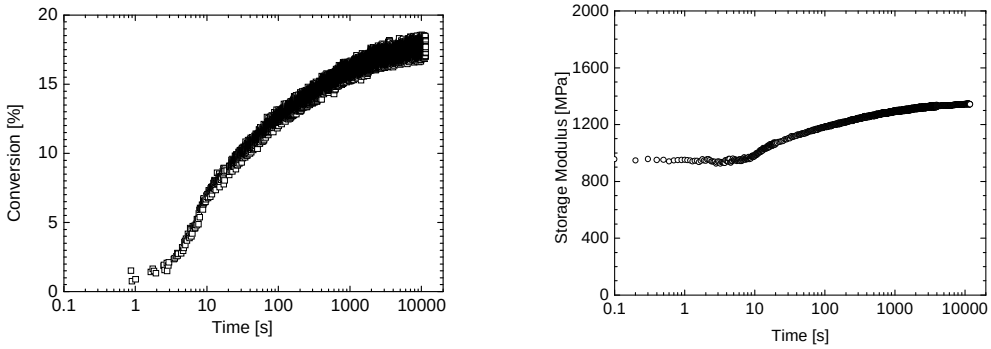

Figure 49. Conversion vs. time (left) and modulus vs. time curve of EPA irradiated for 10 s.

EPA is a highly viscous resin, therefore, to ease its application, the US cell was heated to 40°C prior to its application. After the resin was applied, the cell was cooled back to 20° C. The EPA resin was mixed with 0.1 wt% of PI and was irradiated for 10 s (equivalent to UV dose of 3.85 kJ/m^2). The curing conditions of EPA were identical to that of TPGDA. The conversion-time curves and modulus-time curves are given in Figure 49. The high viscosity of the resin is reflected from its high initial storage modulus of 950 MPa. It has to be noted here that the ultrasonic shear modulus was measured at 5 MHz, and the high initial modulus reflects that some of the segmental motions are already frozen at this frequency, although the sample is still liquid and above its thermal glass transition temperature (268 K). This is also seen in the conversion–time curve. The reaction proceeds slowly and at 10 s the conversion is only 8 % in contrast to 89 % in case of the low molecular weight monomer TPGDA

($\overline{M}_n = 480 g/mol$). The final conversion measured after 3 hrs of post curing was 19 % only, and the final storage modulus was 1340 MPa, the change being only 48 % of its initial value.

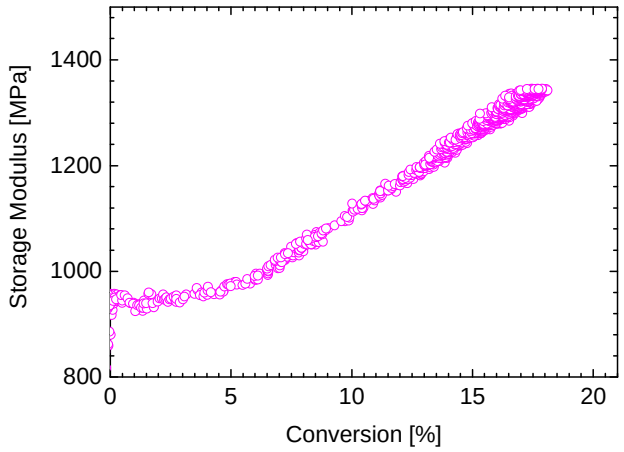

Figure 50. Modulus-conversion curve of EPA irradiated for 10 s.

Figure 50 shows the modulus plotted against conversion. It can be seen that due to the high viscosity of EPA resin and retardation of chemical reaction due to mobility restrictions, the modulus-conversion curve has a different shape than for TPGDA. It suggests that for oligomers with a high US modulus and viscosity at t=0, chemical reaction is almost diffusion controlled from the beginning of polymerization. The conversion in such cases is retarded at an early stage taking an extremely low final value.

Mixture of EPA and TPGDA

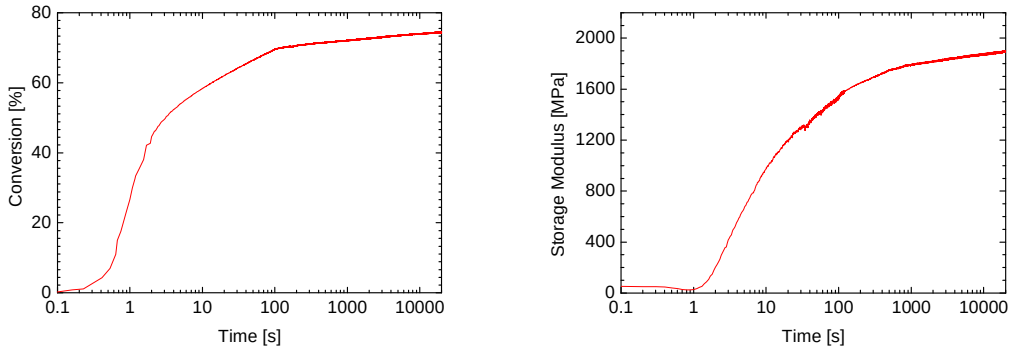

Figure 51. Conversion vs. time (left) and modulus vs. time(right) curve of a mixture of EPA and TPGDA in a weight ratio 2:1.

The mixture of EPA and TPGDA in a weight ratio 2:1 was mixed with 0.5 wt % of PI and was irradiated for 100 s (equivalent to UV dose of 38.5 kJ/m^2). A high concentration of PI and a increased irradiation time was chosen for this mixture, as the conversion with 0.1 wt % PI and 10 s irradiation was below 50 % (i.e, around 48 %).The conversion and modulus as a function of time are given in Figure 51. In comparison to the pure EPA, the initial modulus of EPA at t=0 is reduced to 51 MPa due to dilution with 33 wt % of TPGDA. Dilution decreased the viscosity and thus, the initial storage modulus of the EPA resin. The lowering of viscosity increased the mobility of the reacting polymer chains, thereby, decreasing the glass transition temperature, which leads to an increase in the rate of reaction, as seen in conversion–time curve. This leads to a final conversion of 75 % and storage modulus of 1800 MPa. Interestingly, the slope of the conversion-time curve changes at 100 s. Since the UV irradiation was stopped at this time, the decrease of the slope is related to the transition from a light curing phase to a dark reaction phase (as discussed in chapter 2.1.3), with a decreasing radical concentration. This transition was not so significant in case of pure TPGDA and pure EPA, since these samples were irradiated only for 10 s and the concentration of radicals produced was comparatively less. Figure 52 shows the modulus-conversion curves. It can be seen that the modulus starts to build up strongly only after 40 % acrylate bonds have been reacted. The modulus continues to increase with conversion till 75 % of conversion, after which it becomes independent of conversion, as the conversion is retarded due to vitrification of the polymer resin.

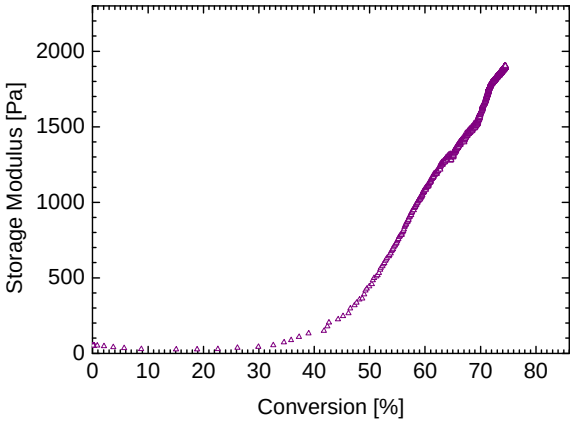

Figure 52. Modulus-conversion curve of a mixture of EPA and TPGDA in a weight ratio 2:1 irradiated for 100 s.

In the modulus-conversion curve of diluted EPA, the cross-over from a mass-controlled to a diffusion-controlled reaction regime is at a lower conversion value than for a pure TPGDA,

but at a considerably higher conversion value than for the pure EPA. This can be explained by a mixing law for the viscoelastic properties. Interestingly, the change from a light curing phase to a dark reaction phase at about 70 % conversion is also indicated by a change in the slope of modulus-conversion curve.

Oligomer: UA

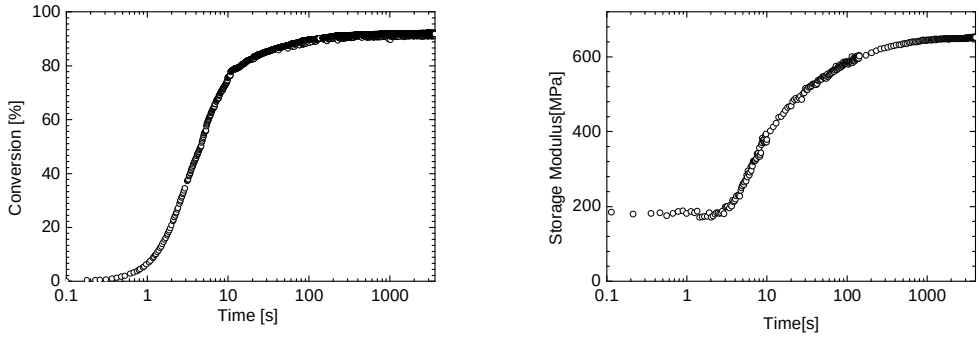

Figure 53. Conversion vs. time (left) and modulus vs. time curve of UA irradiated for 10 s.

The conversion and modulus curves of UA as a function of time are shown in Figure 53. UA was mixed with 0.1 wt % PI and was irradiated for 10 s. The curing conditions were identical to that of pure TPGDA and pure EPA. It can be seen that the initial modulus of UA is 200 MPa. This can be related to the high viscosity (3 Pa.s @ 60°C) and high molecular weight ($\overline{M}_n = 2294 g/mol$) of UA oligomer at room temperature, as in case of the EPA. However, the conversion–time curve of UA indicates that under the same curing conditions, the UA oligomer is more reactive than the EPA oligomer. It attains a conversion of 80 % within 10 s of UV irradiation and the polymerization ends up at a final conversion of 90 % of its acrylate bonds. The final modulus of the UA polymer is 640 MPa, which indicates that it is a rubber like elastic film. The dependency of modulus of UA on its chemical conversion is shown by the combined curve in Figure 54. It can be seen that in case of UA, the modulus maintains its initial value (200 MPa) till 40 % of conversion, after which it slowly starts to increase with conversion. This can be again interpreted as the onset of the diffusion controlled reaction. After 90 % of acrylate bonds in the resin are reacted, the reaction slows down whereas, the modulus continues to increase. It can be seen that the increase in modulus of UA with conversion is less as compared to TPGDA, although both the resins reach a similar final conversion of about 90 %. This is because, UA is a flexible polymer forming an elastic network, whereas, TPGDA is a glassy polymer.

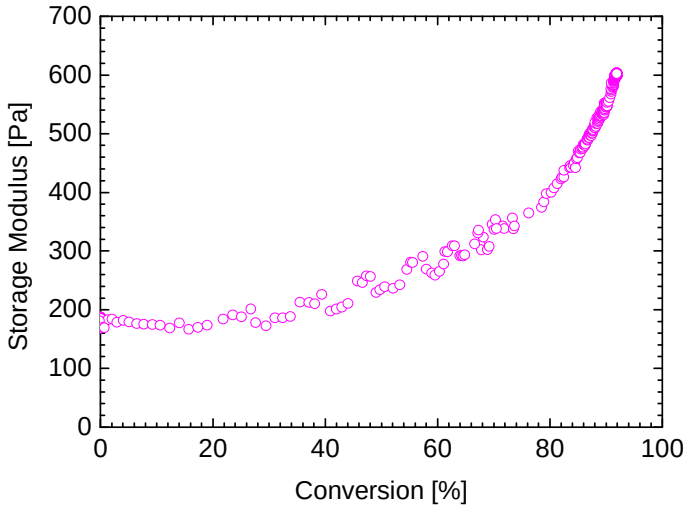

Figure 54. Modulus-conversion curve of UA irradiated for 10 s.

Although, the conversion in case of EPA in Figure 49 reaches only about 18 %, its higher modulus as compared to UA can be explained by the higher glass transition temperature of its reaction mixture and the partially cured EPA.

Mixture of UA and TPGDA

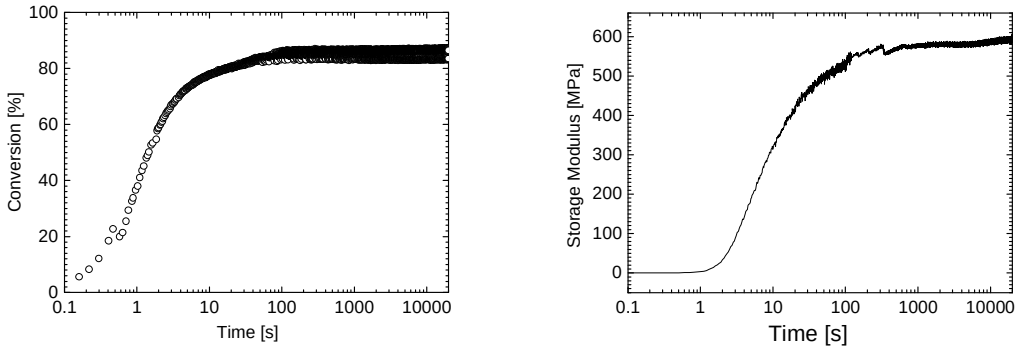

Figure 55. Conversion vs. time (left) and modulus vs. time (right) curve of UA.

The mixture of UA and TPGDA in a weight ratio 2:1 was mixed with 0.5 wt% PI and was irradiated for 100 s (equivalent to UV dose of 38.5 kJ/m^2). The curing conditions were kept identical to that of the mixture of EPA and TPGDA for a comparison between them. As seen in case of EPA/TPGDA mixture, the rate of reaction of UA oligomer also increases on dilution with TPGDA. However, in contrast to EPA/TPGDA mixture, the difference in final conversion of pure UA and the mixture of UA and TPGDA was not very big (only 4 %).

From the modulus–time curves (Figure 55) it can be seen that the initial modulus of UA is lowered (to 0.1 MPa) on dilution with TPGDA, due to similar reasons as discussed for the mixture of EPA and TPGDA. However, its final modulus (600 MPa) is close to the final modulus of the pure UA polymer (640 MPa). This suggests that similar to its base oligomer, the mixture of UA and TPGDA also forms an elastic network on curing. Figure 56 shows the modulus-conversion curve. It can be seen that on dilution, the modulus of the mixture starts to rise after 60 % conversion of acrylate bonds and continues to increase thereafter. As in other cases, the conversion is retarded at later stages due to vitrification of the reacting polymer.

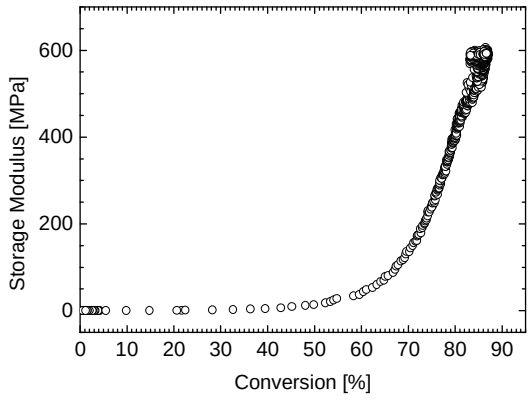

Figure 56. Modulus-conversion curve of the polymer mixture UA and TPGDA in a weight ratio 2:1 irradiated for 100 s.

5.2.2 Effect of Reactive Diluent Concentration

Reactive diluents play an important role in UV curing chemistry. They not only dilute the oligomers and decrease the viscosity, but also actively participate in cross-linking mechanism and impact the final properties of the coatings significantly. Therefore, in order to better optimise the final properties of coatings, it is necessary to understand the influence of reactive diluent on curing kinetics. This section will deal in detail a series of reacting mixtures prepared by varying the weight percentage of epoxy acrylate EPA and reactive diluent TPGDA in the ratio of 100/0, 80/20 and 67/33 respectively. The concentration of photoinitiator TPO-L in each of the above mixtures was 0.1 wt % with respect to the matrix and curing time was 10 s with an equivalent UV dose of 3.85 kJ/m^2.

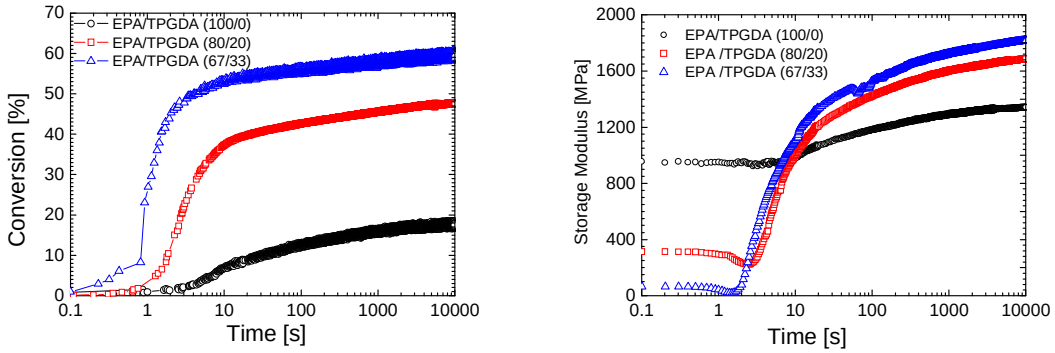

Figure 57. Conversion vs. time (left) and modulus vs. time (right) curves of varied ratios of EPA/TPGDA mixtures.

Figure 57 shows the conversion-time and modulus-time curves of the curing of EPA/TPGDA mixtures, measured simultaneously and *in situ* by combined US/NIR method. It can be seen from the conversion–time curves that the rate of conversion of acrylate coatings increases with dilution of EPA and the final conversion is significantly higher for higher diluent content. Such a behaviour was also reported by Kou et al. for hyperbranched acrylate polymer diluted with trimethylolpropane triacrylate (TMPTA) (*91*). In the modulus-time curves, it can be seen that the initial shear modulus of the EPA resin decreases with dilution, which can be attributed to the decrease in viscosity and the related shear modulus of the mixture, as discussed before. The 100 % EPA resin has an initial storage shear modulus (G') of 1 GPa, which reduces significantly for a mixture of EPA with 33 wt % of TPGDA. It can be seen that the modulus-time curves become steeper with dilution and lead to higher final modulus at higher conversion. Figure 58 shows the modulus-conversion curves of the given mixtures. From this figure, important informations can be derived about the interdependency of shear modulus and conversion kinetics on dilution of an oligomer. For pure EPA it can be observed that the polymerization of acrylate double bonds stops already at about 20 % of conversion and is followed by only a small change in modulus from about 950 to 1400 MPa. This can be attributed to the high viscosity of 100 % EPA resin (18.9 Pa .s @ 49 °C), which is related to a high initial US modulus and hinders the propagation of the reacting polymer chains and the radicals. This results in a low conversion and only a moderate increase in its shear modulus.

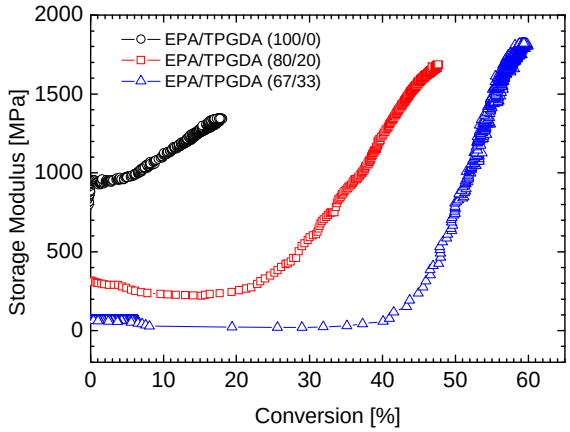

Figure 58. Modulus-conversion curves of EPA/TPGDA mixed in different weight ratios.

For a higher content of TPGDA (33 wt %), it can be observed that the shear modulus shows a significant change from an initial value of 65 Pa to a final value of 1.8 GPa, the change being significant only after 40 % of double bond conversion. This is due to decrease in viscosity of the EPA resin on dilution with TPGDA, which results in an increase in the mobility of reactive polymer chains and the radicals, increasing the rate of polymerization. The lower viscosity shifts the vitrification of the polymer coatings to higher conversion values, as observed in Figure 58. TPGDA having a low molecular weight and the same functional end groups as EPA, is expected to have a higher mobility within the EPA networks as compared to EPA itself. Therefore, TPGDA can increase the reaction rate by forming cross-link networks with EPA. This result in higher final conversion of acrylate double bonds with higher network density (Figure 42) and a higher final shear modulus with increase in the content of TPGDA. Thus, the modulus-conversion curves in Figure 58 illustrate the onset of diffusion controlled reaction and the final conversion including the associated initial and final moduli. The onset of diffusion controlled reaction for 0 wt %, 20 wt % and 33 wt % of the reactive diluent is at ~ 5 %, 25 % and 45 % conversion respectively. The related final conversions are also in the same order, ~ 18%, ~ 48 % and ~ 60 %.

Figure 59 shows the scratch test results of the cured films which support these findings. It gives the permanent deformation which is a measure of hardness of the film and the elastic deformation which is a measure of elasticity of the film. It can be seen that as the TPGDA concentration in the matrix increases, the permanent deformation of the matrix increases and the elastic deformation decreases. This means that on addition of TPGDA, the EPA films become harder and their elasticity decreases. This is in accordance with the previous findings.

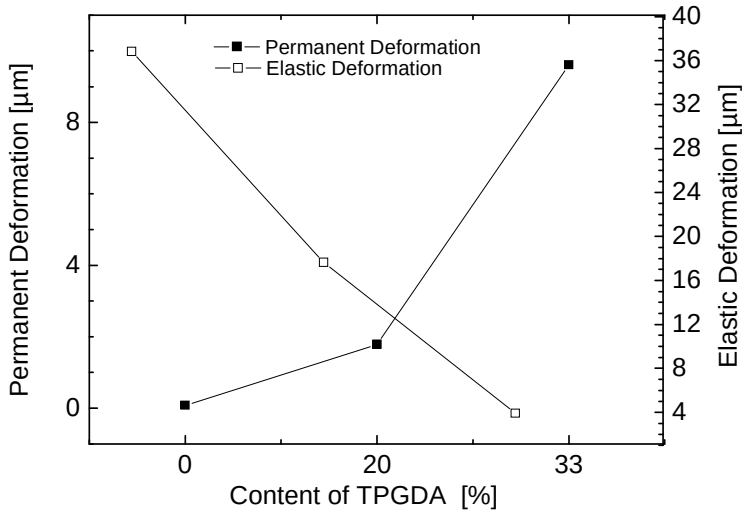

Figure 59. Scratch test data of EPA/TPGDA films at different weight ratios of EPA and TPGDA.

5.2.3 Effect of UV Dose and Photoinitiator Concentration

In this section, the effects of the concentration of photoinitiator and the duration of UV irradiation (total amount of UV dose) on the rate of polymerization and mechanical shear modulus of polymer coatings, as studied by combined US/NIR method will be discussed. The effects of these two parameters on chemical conversion and reaction kinetics of UV curing polymers has also been studied by groups like C. Decker et. al. (*23*) and W. Shi et.al. (*91*). However, with the combined US/NIR it was possible to measure both the changes in conversion and shear modulus of acrylates simultaneously and to study how the above parameters affect the interrelationships between them. For this purpose, a mixture of EPA and TPGDA in the weight ratio 2:1 with the stabilising agent MEHQ (0.25 wt %) and the dispersing agent Disperbyk–108 (1 wt %) was taken. The amount of PI was varied from 0.1, 0.5 to 1.0 wt % with respect to the matrix and the UV dose was varied from 3.85, 38.5 to 385 kJ/m^2 by increasing the time of exposure of UV light by 10 s, 100 s and 1000 s respectively.

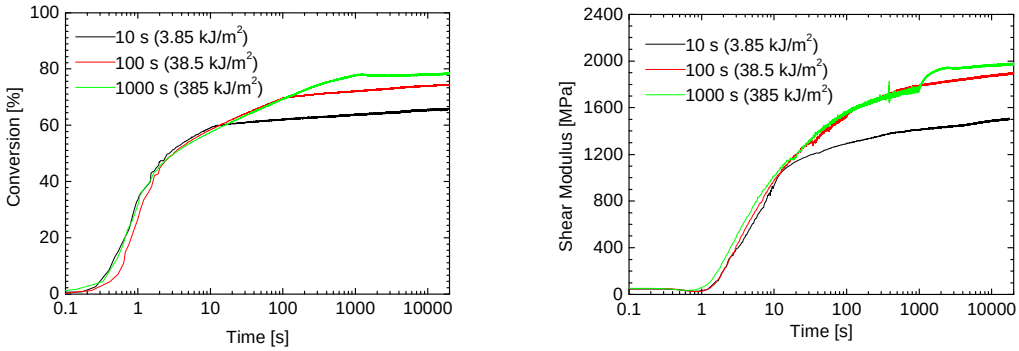

Figure 60. Conversion vs. time (left) and modulus vs. time (right) curves of EPA/TPGDA in a weight ratio 2:1 at different UV doses.

Figure 60 shows the conversion-time and modulus-time curves of EPA/TPGDA with 0.5 wt % of TPO-L, cured under different irradiation times. With increase in duration of UV irradiation, the extent of curing of the films increases without any change in the chemical kinetics in the light curing phase, as seen from the shape of the conversion-time curves in Figure 60. This shows that for the same UV intensity, an increase of the time of UV exposure prolongs the period of dissociation of photoinitiator molecules producing a higher total number of primary radicals. These newly formed radicals are more reactive and mobile than the polymer chain radicals and are capable of reacting with larger number of acrylate double bonds in their surroundings. This increases the extent of curing and shear modulus of the films. As soon as the UV irradiation is stopped, the production of initiator radicals is also stopped. This phenomenon is clearly marked by the sudden drop in slope of conversion curves (described as starting of "dark reaction" in chapter 2.1.3). The sudden rise in modulus corresponding to 1000 s irradiation time, after light curing phase is an experimental error due to strong cooling of the quartz cell by the thermostat.

In the present case, the reaction kinetics is already diffusion controlled when the dark reaction phase starts, and the effect of "negative feedback" of vitrification on the conversion process is already evident. These findings are clearly illustrated in the modulus-conversion curves in Figure 61. The onset of diffusion controlled reaction is at about 40 % conversion for all the samples, reflecting the same radical density at the same amount of UV dose. The final conversion at the end of the light curing phase clearly depends on the total UV dose, i.e duration of UV irradiation. The beginning of dark reaction phase is clearly marked by the change of shape of the curves on stopping the UV irradiation at 10, 100 and 1000 s.

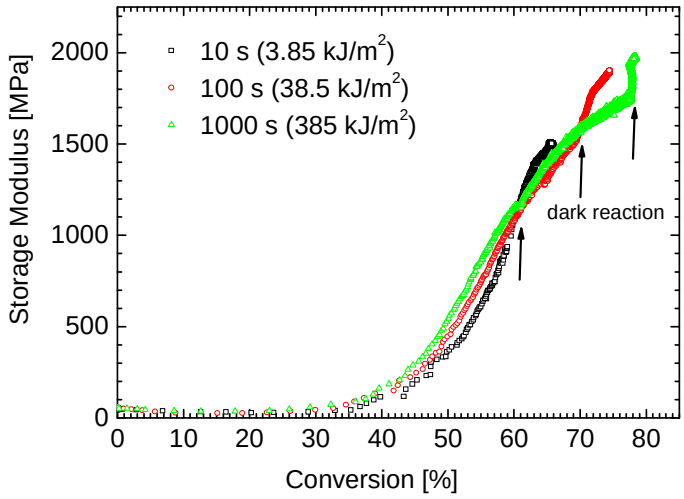

Figure 61. Modulus-conversion curves of EPA/TPGDA mixture with varied duration of UV irradiation (or total UV dose).

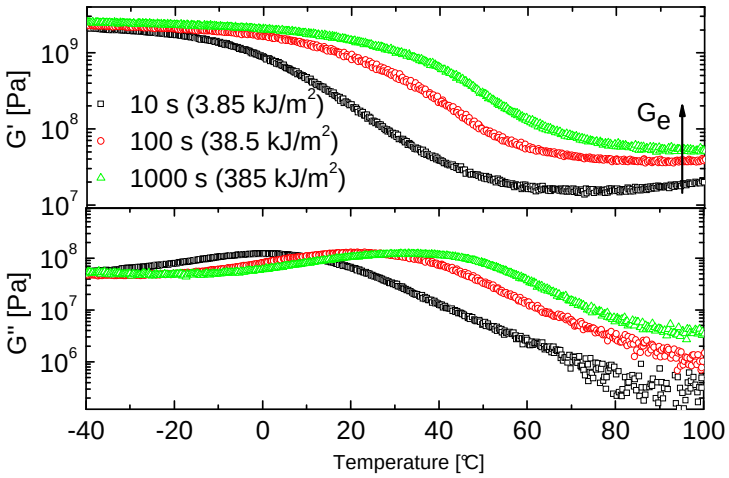

Figure 62. Temperature dependent shear modulus of the cured EPA/TPGDA films cured at varied UV doses.

Figure 62 presents the temperature dependent shear modulus curves of EPA/TPGDA coatings cured at varied UV doses. The shift in the position of rubber plateau (equilibrium storage modulus) to higher values with higher UV doses indicates that the cross-link density of the polymer film is increased on increasing the duration of UV irradiation. An increase in the T_g of the coatings with irradiation time is indicated by the shift in the position of maximum of

the loss modulus curves (G'') towards higher temperatures. The T_g as a function of UV irradiation time is plotted in Figure 63.

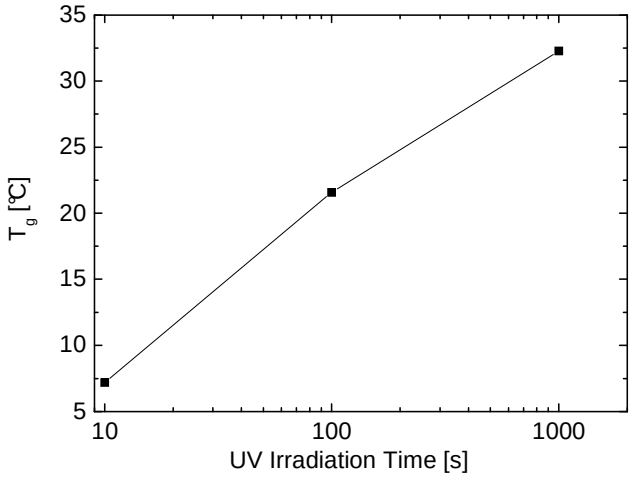

Figure 63. T_g as a function of UV irradiation time for EPA/TPGDA coatings.

For a detail study of the effect of photoinitiator concentration on curing kinetics of polymer coatings, the conversion-time and modulus-time curves of EPA/TPGDA resin (in a weight ratio 2:1) at three different concentrations of the photoinitiator-TPO-L, all cured with 100 s of UV irradiation are given in Figure 64.

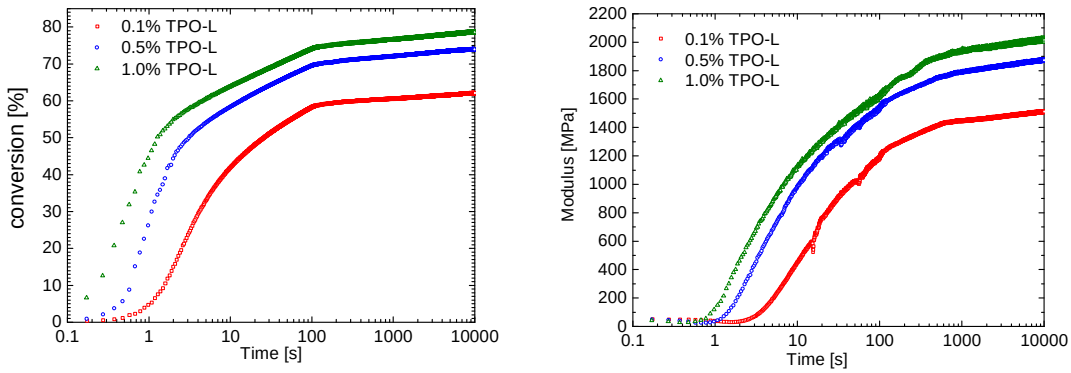

Figure 64. Conversion vs. time (left) and modulus vs. time (right) curves of EPA/TPGDA in a weight ratio 2:1 at different concentrations of TPO-L.

It can be seen that on increasing the concentration of photoinitiator in the reacting polymer mixture, the rate of polymerization (Figure 65) and the final conversion values of the films increases (Figure 64). The modulus-time curves (Figure 64) also give similar results. The rate

of increase of shear modulus and the final modulus increases with increase in the concentration of TPO-L.

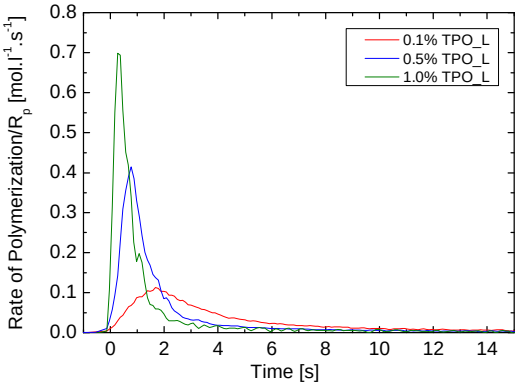

Figure 65. Rate of polymerization of EPA/TPGDA (2:1) coatings at three different concentrations of photoinitiator (TPO-L).

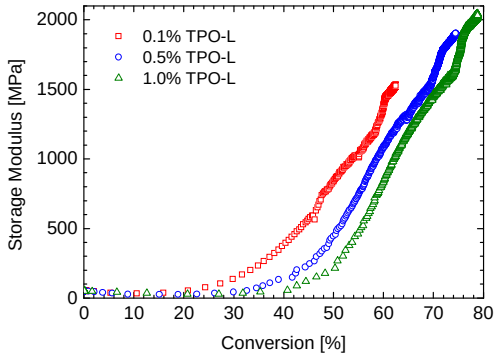

Figure 66. Modulus-conversion curves of a mixture of EPA/TPGDA (2:1) at different concentrations of TPO-L and 100 s of UV irradiation.

Figure 66 presents the modulus-conversion curves of the given polymer mixtures. It shows the influence of photoinitiator concentration on the interdependency of conversion and modulus development at 100 s of UV irradiation. It can be seen that at a lower concentration of TPO-L, the modulus starts to increase at lower conversions as compared to that at higher concentrations of TPO-L. This behaviour can be explained as follows: for the same UV irradiation time, the number of initiator radicals produced is proportional to the concentration of photoinitiator. For a low initiator concentration it can be assumed that the probability of radical termination at the beginning of the polymerization is lower as compared to its rate of propagation. Thus, the network grows faster at the beginning of the reaction. An additional

auto-acceleration effect also cannot be excluded, so the diffusion controlled region –indicated by an increase in G'- is reached earlier. The low value of final conversion is obvious due to the low concentration of total radicals produced. With increase in the TPO-L concentration, the number of primary radicals produced is increased. The high concentration of initiator radicals increases the rate of polymerization (as seen in Figure 65) as well as leads to a higher probability of radical termination. This shifts the diffusion controlled region to higher conversions, which is indicated by the increase in modulus at considerably higher conversions for high TPO-L content in the modulus-conversion curves. Higher final conversion at higher photoinitiator concentration is obvious from its high total radical density.

Another possible effect for a low modulus of coating at high conversions can be the heat of reaction. At high radical concentrations and high polymerization rate, the heat of reaction produced is high, which is not able to dissipate fast enough, causing heating up of the resin. This causes softening of the reacting resin and thus lowering the values of modulus at the same conversion.

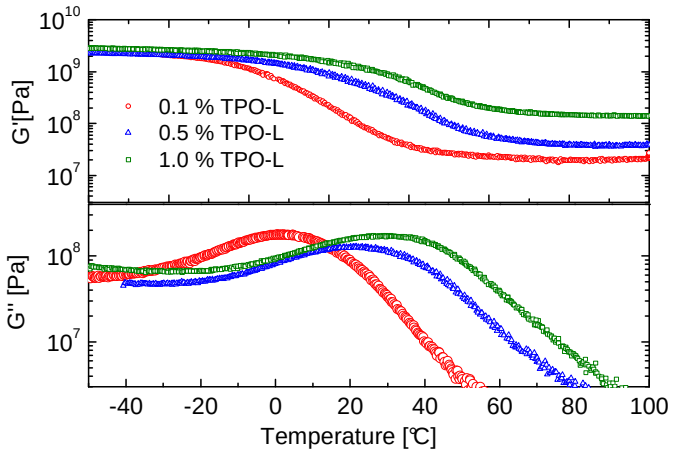

Figure 67. Temperature dependent shear modulus of the EPA/TPGDA films cured at varied concentration of TPO-L and 100 s of UV irradiation.

Figure 67 presents the temperature dependent shear modulus curves of the polymer mixtures at different concentrations of TPO-L measured by DMTA. It can be seen that on increasing the TPO-L concentration the cross-link density of the polymer increases, marked by a shift in the position of rubber plateau to higher values of storage modulus. In addition to this, the maxima of the loss modulus curves shifts to higher temperatures at higher TPO-L concentration, indicating that the T_g of the polymer increases with PI concentration.

Figure 68 shows the final conversion and final modulus values of the EPA/TPGDA coatings plotted as a function of total UV irradiation time for different concentrations of the photoinitiator-TPO-L. As seen before, the final conversion and final modulus is increased with increase in photoinitiator content at each UV dose. It can be seen that the difference between the conversion values and the modulus values for 0.1 wt % and 0.5 wt % photoinitiator concentrations respectively, at each of the UV dose, is larger than that of the difference between 0.5 wt % and 1.0 wt % photoinitiator values. This indicates that 1.0 wt % TPO-L concentration is near to the optimum concentration of photoinitiator in the given polymer mixture.

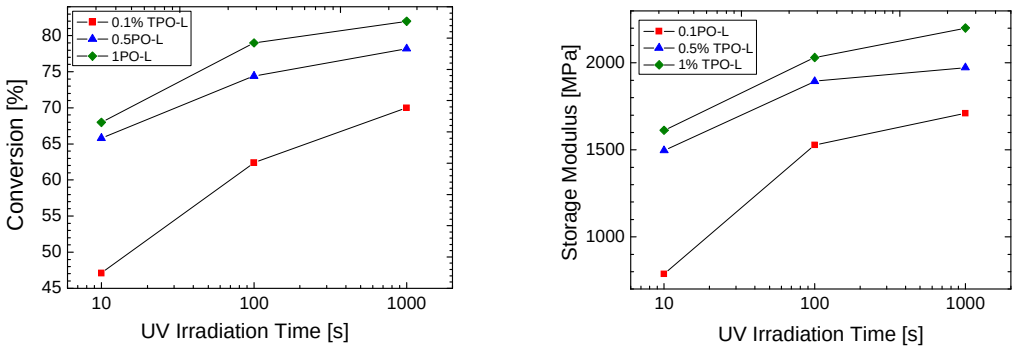

Figure 68. Final conversion (left) and final modulus (right) as a function of UV irradiation time at three different concentrations of TPO-L in EPA/TPGDA polymer mixture.

When the final modulus and the glass transition temperature of the cured coatings at different concentrations of TPO-L and at different UV irradiation time are plotted against conversion, it is found that they exhibit a linear dependence on final conversion (Figure 69). This implies that for the EPA/TPGDA coating systems the final modulus depends mainly on the conversion reached during the reaction. The increase in T_g with conversion can be attributed to the increase in crosslink density of the coatings with conversion, as discussed before.

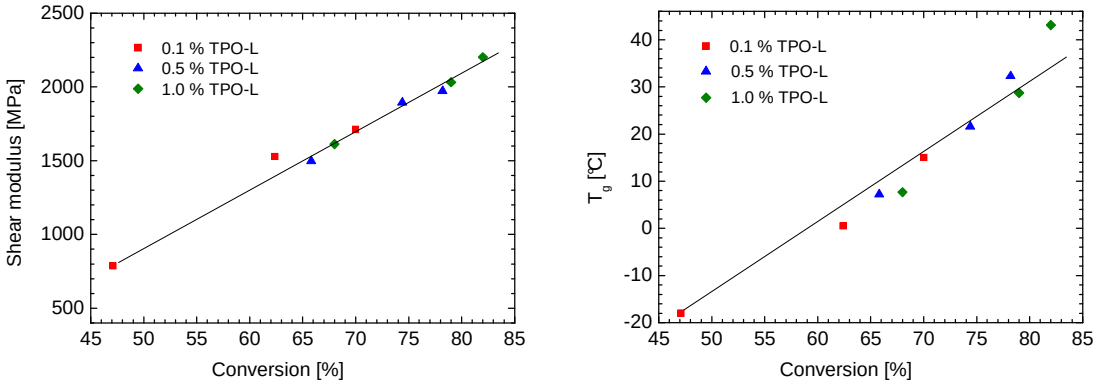

Figure 69. Final modulus vs. final conversion (left) and Tg of cured coatings vs. final conversion (right) at three different conc. of TPO-L for a mixture of EPA/TPGDA (2:1).

Figure 70 presents the scratch test results of the cured coatings, obtained with UST technique. It can be seen that the permanent and plastic deformation also shows a linear dependence on conversion, except the values at very low conversions where the sample is exceptionally rubbery and changes the scratch mechanism. The elastic deformation, irrespective of the curing parameters, decreases linearly with increase in conversion, whereas the plastic deformation increases with conversion. These results are correlated with the shear modulus as a function of conversion. The harder the sample (or higher the crosslink density), the lower is its elasticity. As the diamond tip of the measurement device moves laterally on the film surface with a defined velocity and load, the deformations formed in case of a soft and elastic film are ‘healed ‘back immediately with low permanent deformation. Whereas, in case of hard films, the deformations formed do not return to their original positions. Sometimes it is also possible that as the diamond tip moves over the surface of the film, it scratches out some film material from inside out, that follows the needle in front. This material piles up on the sides of the tip and gives an impression of negative permanent deformation. It should be noted that the scratch resistance results can be different from other methods.

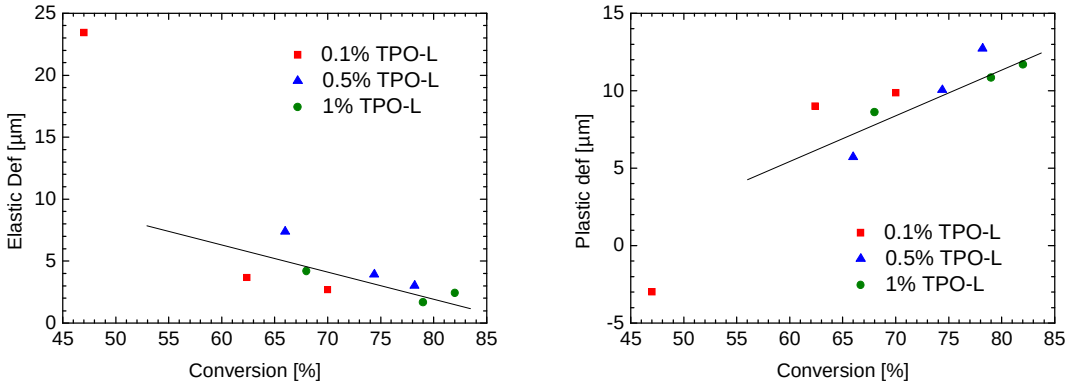

Figure 70. Elastic and plastic deformation measured with UST for samples cured with different UV doses and photoinitiator content.

The influence of photoinitiator concentration was also studied for the same resin mixture EPA/TPGDA in the weight ratio 2:1, filled with 15 wt % ALMAL nanoparticles and irradiated for 100 s (appendix Figure 98). The photoinitiator was varied in the weight percentage of 0.1, 0.25, 0.5, 0.75 and 1.0 wt % with respect to the matrix, keeping the concentration of other additives constant. Figure 71 shows the final conversion and modulus values plotted as a function of TPO-L content for the filled coating systems. It can be seen that like in unfilled polymer mixtures, both conversion and modulus of the filled system increases with increase in TPO–L content. The glass transition temperature also followed a similar pattern (Figure 99 in the appendix). These results suggest that for the given polymer mixture the nanoparticles do not interfere with its curing chemistry at varied concentrations of photoinitiator.

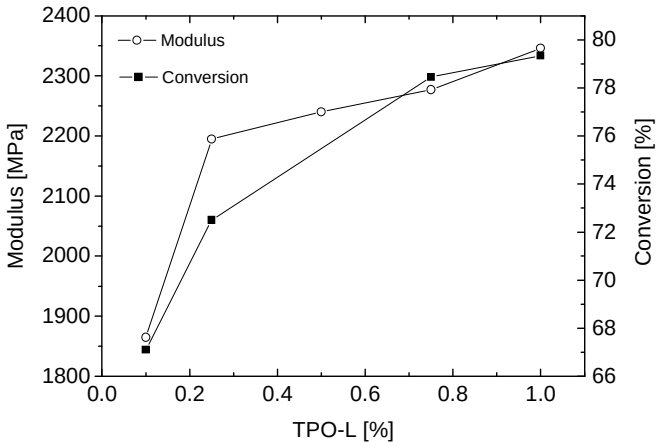

Figure 71. Final modulus and conversion values of EPA/TPGDA coatings filled with 15 wt % ALMAL nanoparticles at different concentrations of TPO-L.

5.2.4 Effect of Different Types of Nanoparticles

In this section the effects of different types of nanoparticles on the curing kinetics and final properties of the EPA/TPGDA coatings is discussed. For this purpose the following 5 types of nanoparticles were taken: inorganic silica nanoparticles (Aerosil), methacrylate functionalised silica (SIMA) nanoparticles, methacrylate functionalised alumina (ALMA) nanoparticles, aluminium-maleate nanoparticles (ALMAL) and aluminium-oxalate (ALOXAL) nanoparticles. Five different curing formulations were made by adding 15 wt % of each of these nanoparticles to the base matrix. The base matrix consisted of mainly EPA/TPGDA base resin in the ratio 2:1, TPO-L in a concentration of 0.5 wt % with respect to the base resin, Disperbyk 108 (1 wt %) and MEHQ (0.25 wt %). All these curing formulations were cured under similar conditions with 100 s of UV irradiation.

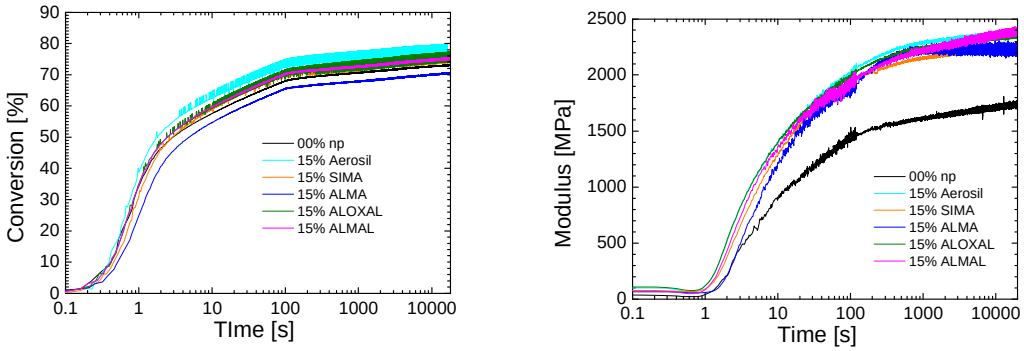

Figure 72. Conversion-time curves (left) and modulus-time curves (right) of EPA/TPGDA coatings with different types of nanoparticles.

In the conversion-time curves (Figure 72), it can be seen that the addition of nanoparticles did not influence the reaction kinetics of the EPA/TPGDA films significantly. The final conversion values of the films with different types of nanoparticles are close to that of the film without nanoparticles (only matrix), the absolute values being within the order of magnitude of the error limits (±3 %). This indicates that, for a given concentration of nanoparticles, the conversion is independent of the types of nanoparticles.

In the modulus-time curves (Figure 72) it can be seen that the modulus of the EPA/TPGDA polymer film is increased on addition of nanoparticles. As in the case of conversion, the values of the final moduli of the polymer films each with 15 wt % of different types of nanoparticles are almost the same; the differences being within the order of magnitude of the error limits (±150 MPa). This indicates that also the modulus depends mainly on the total

concentration of nanoparticles rather than on its type. The modulus-conversion curves in Figure 73 also show a similar effect and indicate that for a given concentration of nanoparticles, the chemical conversion and the shear modulus of the polymer films is independent of the type of nanoparticles.

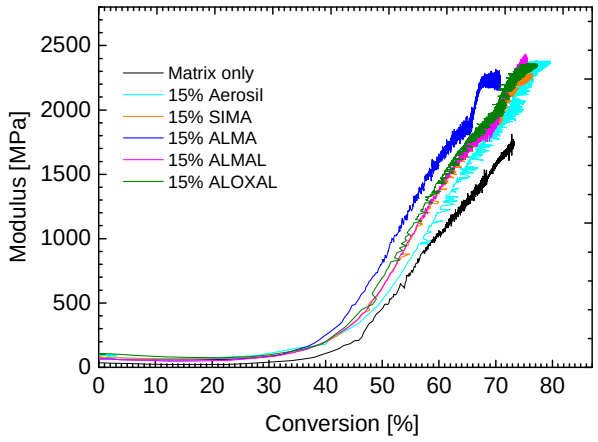

Figure 73. Modulus-conversion curves of EPA/TPGDA polymer films in presence of different types of nanoparticles.

Figure 74 presents the glass transition temperature of the polymer films as a function of the type of nanoparticles. It can be seen that the glass transition temperature of all these polymer films are close to each other (21-26°C). This is in agreement with their conversion values which are also close to each other.

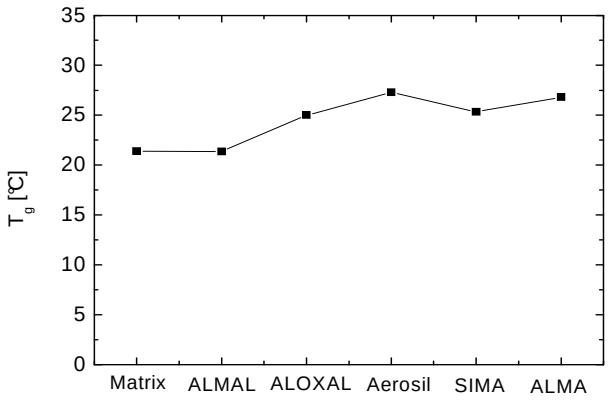

Figure 74. T_g values as a function of different types of nanoparticles in EPA/TPGDA coatings.

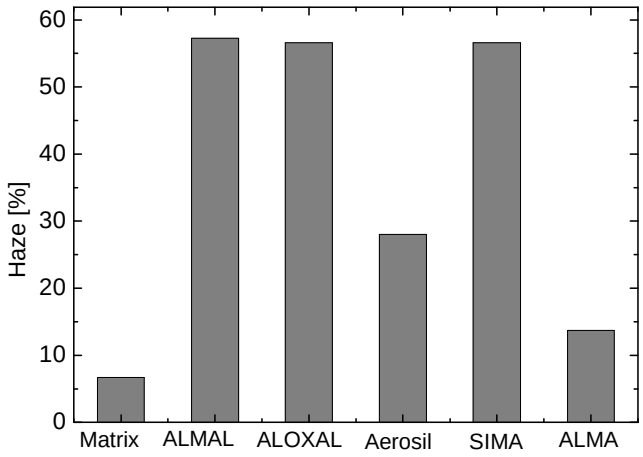

Figure 75. Haze values as a function of different types of nanoparticles in EPA/TPGDA coatings.

Figure 75 presents the results of haze measurements of these polymer films. It can be seen that among all the polymer-nanocomposite films, the film with ALMA nanoparticles has the least haze and is most transparent, followed by the film with Aerosil nanoparticles. Whereas, the polymer film with SIMA nanoparticles exhibits the highest haze among all the polymer-nanocomposite films. To study this unexpected discrepancy between the particles with the same functional groups, SEM studies were done. Figure 76 presents the SEM pictures of the polymer films with SIMA and ALMA nanoparticles. It can be seen that the ALMA nanoparticles in acrylate films are better dispersed and have lower tendency to agglomerate as compared to SIMA nanoparticles which form agglomerates of size between 200-400 nm. As per the light scattering theory given by Mie (*92*), higher the particle size, higher is the difference between the refractive indices of the particle and the matrix and higher is the light scattering and thus, the haze of the system. Therefore, the polymer films with SIMA nanoparticles exhibit higher haze than the films with ALMA nanoparticles.

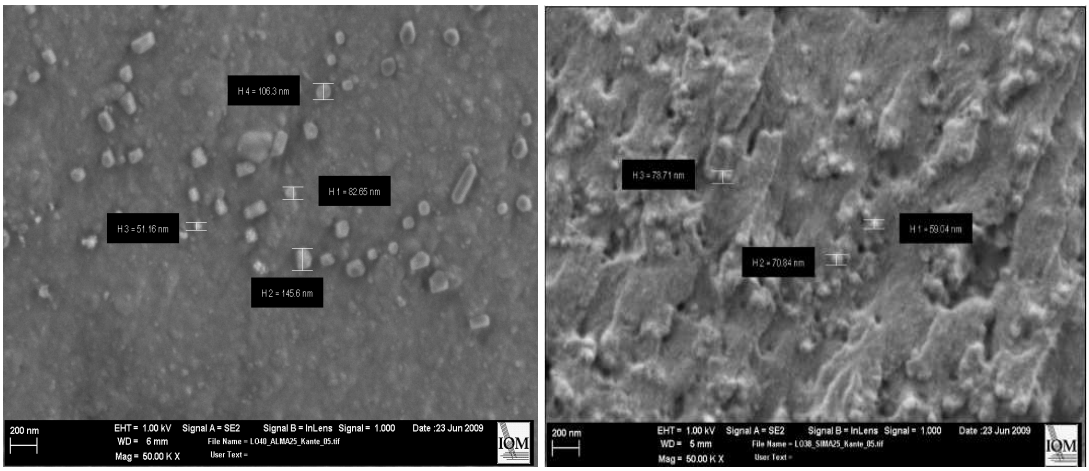

Figure 76. SEM pictures: ALMA-nanoparticles in EPA/TPGDA-system with 200 nm resolution (left), SIMA nanoparticles in EPA/TPGDA-system with 200 nm resolution (right).

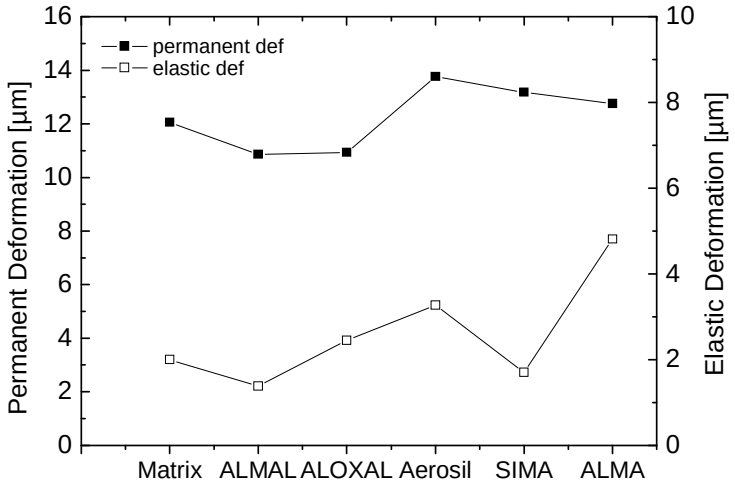

Figure 77. Scratch test results of EPA/TPGDA coatings containing different types of nanoparticles.

Figure 77 presents the scratch test results of these polymer films as a function of the type of nanoparticles. Generally, a film is said to be scratch resistant, if it exhibits high elastic deformation (i.e, recoverable deformation) and a low permanent deformation. It was found that among all the types of polymer-nanocomposite films, the film with ALOXAL nanoparticles exhibited better properties. It showed an increase in elasticity and at the same time decrease in the plastic deformation as compared to the pure EPA/TPGDA films (i.e,

without nanoparticles). Therefore, ALOXAL nanoparticles were found to have better scratch resistance properties.

Thus, from the above data, it was found that the selection of the types of nanoparticles for UV curable polymer systems depends largely on the desired final properties of the coatings.

5.2.5 Effect of Nanoparticle Concentration

In the previous section, the effects of same concentration of different types of nanoparticles were studied. In this section, it is aimed to study the effects of the same type of nanoparticles at varied concentrations, on the curing kinetics and final properties of coatings. For this purpose, a series of formulations were made by taking EPA/TPGDA in the weight ratio 2:1 as the base matrix and functionalised SIMA nanoparticles as the filler. The concentration of SIMA was varied from 0-25 wt % with respect to matrix and the concentration of photoinitiator was 0.5 wt % with respect to matrix. The dispersing agent Disperbyk 108 (1 wt %) and the stabilising agent MEHQ (0.25 wt %) were also added. Each of these formulations was irradiated for 100 s with a total UV dose of 38.5 kJ/m^2.

Figure 78 shows the conversion–time curves and the modulus-time curves of EPA/TPGDA resin at varied concentrations of SIMA nanoparticles. Surprisingly, it was found that the variation of SIMA nanoparticles concentration did not have any influence on the reaction kinetics of the base resin and the conversion is comparable at all the concentrations of SIMA. As discussed before, the transition from the light curing phase to dark reaction phase is indicated for all the samples. In contrast to this, shear modulus of the films increases with increasing the concentration of SIMA nanoparticles. This behaviour can be explained by a considering a mixing law based on the modulus of the matrix and the nanoparticles.

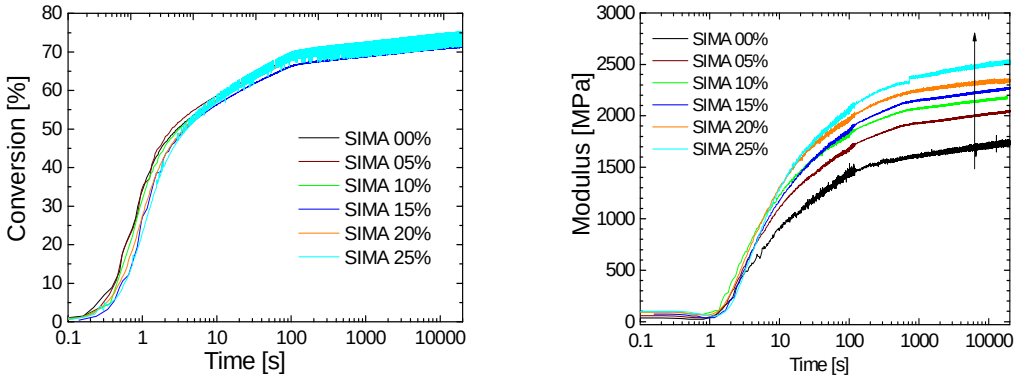

Figure 78. Conversion–time curves (left) and modulus–time curves (right) of EPA/TPGDA coatings at different concentrations of SIMA nanoparticles.

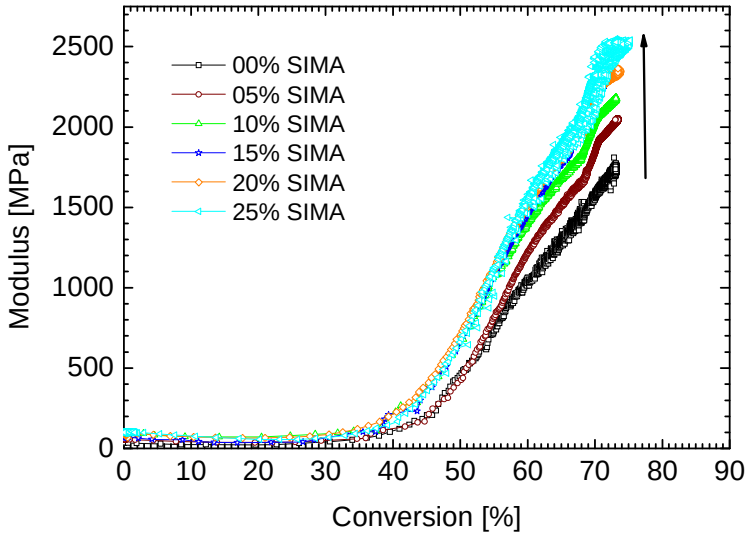

Figure 79. Modulus-conversion curves of EPA/TPGDA coatings at different concentrations of SIMA nanoparticles.

This mixing law is also consistently expressed in the modulus-conversion curves in Figure 79. It is expected that the modulus of a mixture of two components of the polymer nanocomposite should lie in between the extremes of serial and parallel mixing laws. In case of serial interaction both the components are connected linearly to each other and in case of parallel interaction the two components are parallel to each other. According to parallel interaction, the total stress experienced by the polymer composite is the sum of stresses in the matrix and the nanoparticles multiplied by their relative volume fractions as given in equation 38. The strain of the matrix is equal to the strain of the inorganic component.

$$\varepsilon = \varepsilon_1 = \varepsilon_2,\ \sigma = \Phi_1\sigma_1 + \Phi_2\sigma_2 \tag{38}$$

where ε_1, σ_1, ε_2, σ_2 are the strain and stress in the inorganic part and organic part of the composite respectively, Φ_1, Φ_2 are the volume fractions of the inorganic and organic component of the matrix respectively. Thus, the shear modulus of the composite in case of parallel interaction $G_{parallel}$ can be given as,

$$G_{parallel} = \Phi_1 G_1 + \Phi_2 G_2 \tag{39}$$

It is to be noted that in SIMA nanoparticles, the weight percentage of silica core (the inorganic part) is about 82 % and the organic ligands is about 18 %. The density of SIMA nanoparticles is 1.63 g/cm^3 and that of the matrix is 1.08 g/cm^3. Silica nanoparticles are hard spheres of modulus of 31 GPa which is much higher than the modulus of the matrix (1.7 GPa).

In case of serial interaction, the stress in the matrix and the nanoparticle is same and the strain is additive,

$$\varepsilon = \Phi_1\varepsilon_1 + \Phi_2\varepsilon_2,\ \sigma = \sigma_1 = \sigma_2 \tag{40}$$

And the shear modulus G_{serial} is given as,

$$\frac{1}{G_{serial}} = \frac{\Phi_1}{G_1} + \frac{\Phi_2}{G_2} \tag{41}$$

The shear modulus calculated from both parallel and serial interactions with the data given above is compared with that of the measured shear modulus values of the SIMA–EPA/TPGDA polymer-nanocomposite in Figure 80. It can be seen that the measured values lie closer to the value calculated from serial interaction. Thus, possibly the increase in modulus on addition of nanoparticles closely follows the serial interaction. This means that the particles in the matrix are almost independent of each other and the interaction between the particles and the matrix is weaker. And for a given stress the inorganic component (with a very high shear modulus of 31 GPa) undergo smaller deformation as compared to the organic part. This is different from the usual assumption that the nanoparticles built a large interface and influence the matrix properties tremendously.

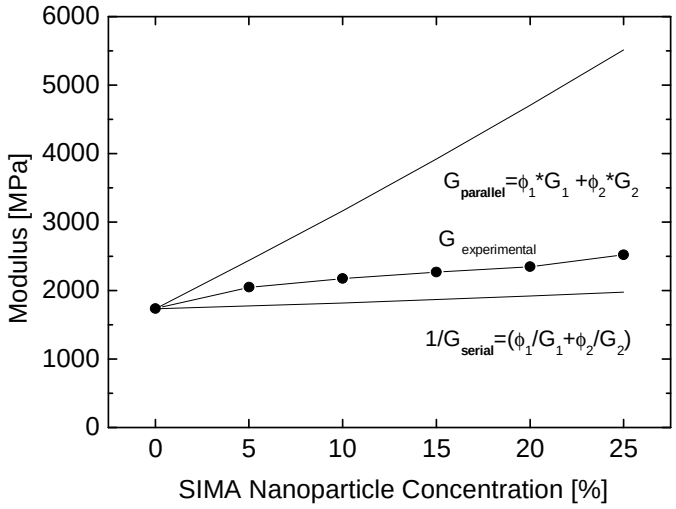

Figure 80. Comparison of shear modulus of EPA/TPGDA coatings at various concentrations of SIMA nanoparticles, with parallel and linear mixing laws.

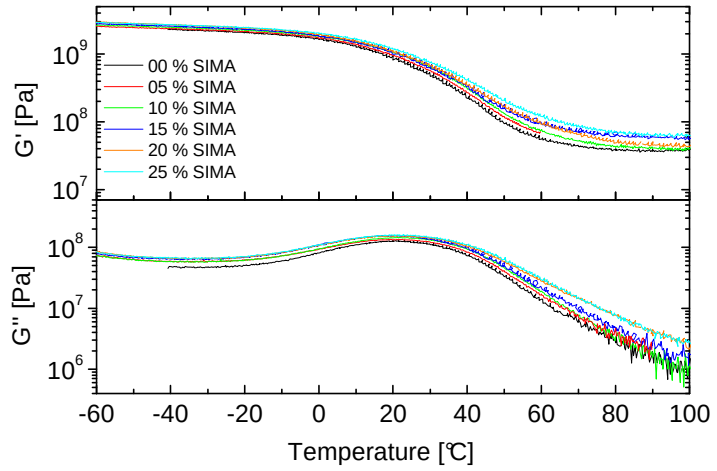

Figure 81. Temperature dependent shear modulus of the EPA/TPGDA films at different concentrations of SIMA nanoparticles.

Figure 81 gives the temperature dependent shear modulus of the given series as measured by DMTA. If observed carefully, it can be seen that the addition of SIMA nanoparticles increases the equilibrium storage modulus G_e of the EPA/TPGDA matrix slightly, though no linear trend can be found between them. This can be either due to participation of SIMA nanoparticles in cross-linking process or is merely a physical effect as seen above in case of shear modulus measured by US (serial interaction). Now, if we consider the loss modulus curves, it can be seen that the position of the loss modulus maximum (T_g) does not vary with

the concentration of SIMA nanoparticles. This indicates that the SIMA nanoparticles do not influence the cross-link density of the polymer matrix. So, the observed increase in the value of equilibrium shear modulus is probably a physical effect due to increased concentration of nanoparticles in the matrix.

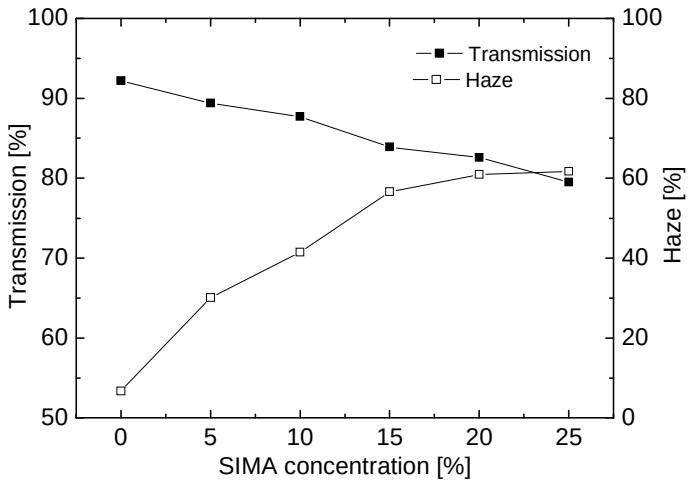

Figure 82. Transmission (left) and haze (right) value of EPA/TPGDA films at different concentrations of SIMA nanoparticles.

Figure 82 shows the optical properties of the EPA/TPGDA coatings with increased concentration of nanoparticles measured by Haze experiment. It can be seen that, with increase in nanoparticle concentration the transmission of light through the films is decreased and the turbidity or the haze value of the films is increased. Figure 83 shows the haze values of EPA/TPGDA films with increasing ALMAL nanoparticles concentrations at two different film thicknesses (25 and 100 µm). It can be seen that the haze decreases with decrease in the thickness of the films. For the same formulation, the 100 µm thick film is hazier than the 25 µm thin film. The films of 25 µm thickness are more transparent (haze value below 20 %) even with 25 wt % of nanoparticles and can be considered as transparent coatings. This is in accordance with the Lambert–Beer's law according to which the transmission of light is inversely proportional to the thickness of the sample.

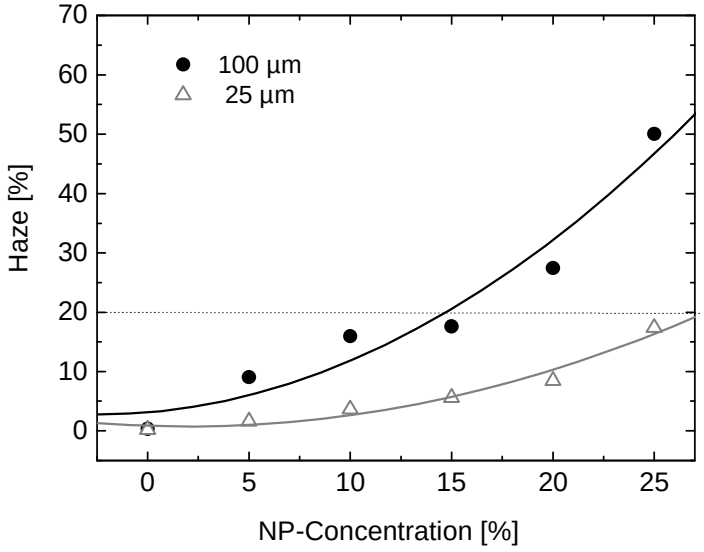

Figure 83. Comparison of haze values of EPA/TPGDA/ALMAL polymer films at two different film thicknesses.

Figure 84 shows the volume abrasion test results of EPA/TPGDA coatings at different concentrations of SIMA. It can be seen that the extent of abrasion after 4000 rotations reduces with increase in the concentration of SIMA nanoparticles. This is because of increased surface hardness of the EPA/TGDA films due to addition of high modulus SIMA nanoparticles. The increased surface hardness acts against the external abrasive force, thus reducing the volume abrasion.

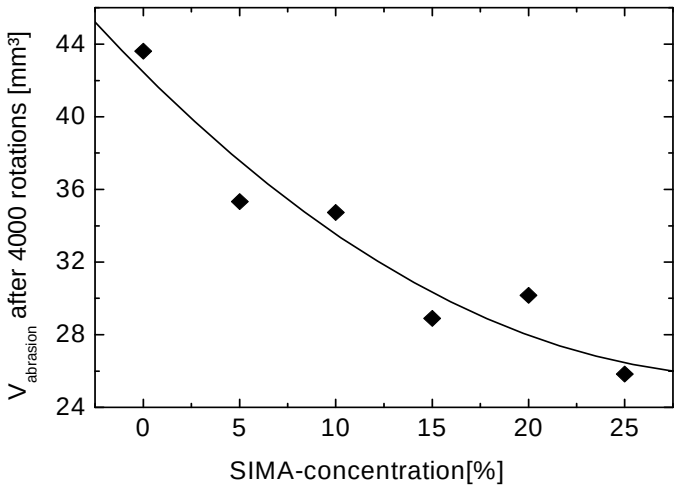

Figure 84. Volume abrasion after 4000 rotations as a function of SIMA nanoparticles concentration in EPA/TPGDA coatings.

Thus, it can be observed that on varying the concentration of nanoparticles the mechanical strength of the films, like its volume abrasion resistance is considerably increased without affecting the reaction kinetics of the films.

5.2.6 Effect of Type of Base oligomer

In this chapter, the curing kinetics and physical properties of polymer-nanocomposites in two different base matrices are compared. Epoxy acrylate and urethane acrylate each diluted with TPGDA in a weight ratio 2:1 were taken as the base matrices. Both of these acrylate matrices differ considerably in their chemical and physical properties. Urethane acrylate on curing forms a soft and elastic elastomer with a glass transition temperature much below room temperature (-31 °C), whereas epoxy acrylate forms a highly cross-linked and hard network with a glass transition temperature much higher than the room temperature (67 °C). EPA films behave like glassy polymers at room temperature as compared to rubber like elastic UA films. A series of curing formulations were made by adding ALMAL nanoparticles in a concentration of 0-25 wt % in each these base matrices. The concentration of photoinitiator in each of the formulations was 0.5 wt %, the dispersing agent Disperbyk 108 was 1 wt % and the stabilising agent MEHQ was 0.25 wt % with respect to the matrix. All the formulations were irradiated for 100 s (equivalent to 38.5 kJ/cm^2 UV dose). The conversion and modulus time curves are given in the appendix in Figure 100 and 101.

Similar to the previous chapters, it was seen that the nanoparticles concentration did not affect the curing kinetics of any of the matrices (see appendix). The average final conversion was 86 % for UA/TPGDA and 74 % for EPA/TPGDA coatings. The final modulus of the coatings at varied concentrations of ALMAL is shown in Figure 85. It can be seen that both the matrices respond in a similar manner and the modulus increases on increasing the concentration of nanoparticles (as observed in previous chapter). The possible explanation for this increase in modulus is similar to that discussed in previous chapter. But the impact of nanoparticles on the modulus of low modulus UA/TPGDA coatings is higher than on the EPA/TPGDA coatings. The modulus in case of UA/TPGDA increases from about 600 MPa (0 % ALMAL) to 1200 MPa on addition of 25 % of ALMAL, which is an increase of 100 %. Whereas, in case of EPA/TPGDA coatings the modulus increases from a value of 1900 MPa (0 % ALMAL) to a value of 2600 MPa with addition of 25 % ALMAL nanoparticles, which is only about 37 % of its initial value. The possible reason for this difference can be attributed to the different mechanical behaviour (expressed by mixing laws) for a rubber like and a glassy matrix respectively.

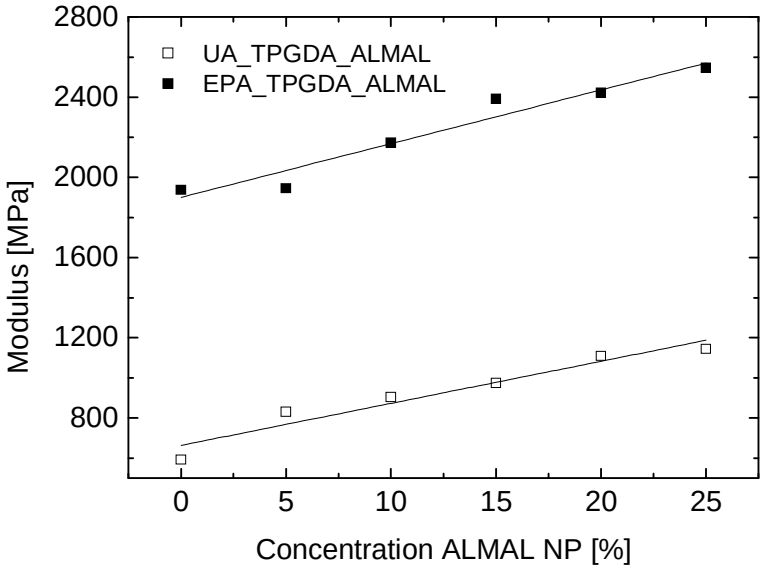

Figure 85. Modulus as a function of concentration of ALMAL nanoparticles in EPA/TPGDA and UA/TPGDA polymer matrices.

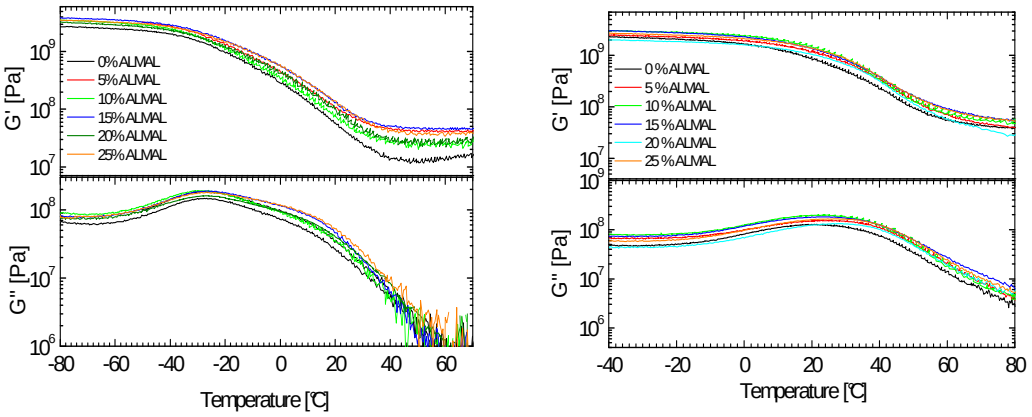

Figure 86. Temperature dependent shear modulus of UA/TPGDA (left) and EPA/TGPDA (right) at varied concentration of ALMAL nanoparticles.

The temperature dependent modulus curves of UA/TPGDA and EPA/TPGDA with varied amount of ALMAL nanoparticles (Figure 86) show similar behaviour as discussed in chapter 5.2.5. The physical interaction between the nanoparticles and the matrix increased the equilibrium shear modulus (in the rubber plateau) in both the matrices without any effect on the position and shape of loss modulus maximum. UA/TPGDA is found to have a two phasestructure at all the compositions of ALMAL nanoparticles as was discussed in chapter 5.1.2.

Figure 87 and 88 shows the elastic deformation and the results from volume abrasion test of UA/TPGDA and EPA/TPGDA polymer-nanocomposite films respectively. It can be seen that on addition of nanoparticles the elastic deformation of the UA/TPGDA films is reduced, i.e, the films with higher content of ALMAL are less elastic and are harder than the one without any nanoparticles. At the same time the volume abrasion of UA/TPGDA shows a linear increase with nanoparticles content. The possible explanation for this observation is as follows: The UA films are inherently elastic with low modulus values (rubber-elasticity). Such elastic films are capable of redirecting most of the impact energy back to the impacting object without undergoing significant destruction in itself. This is supported by the very low value of volume abrasion of UA/TPGDA (5 mm^3 after 4000 rotations). On addition of nanoparticles the films become harder with increased modulus and decreased elasticity. But the increase in hardness is not sufficient enough to withstand the energy of the rotating wheel of Taber abraser. This allows the sandpaper to take off more material from the film surface, increasing the volume abrasion and thus, decreasing the abrasion resistance.

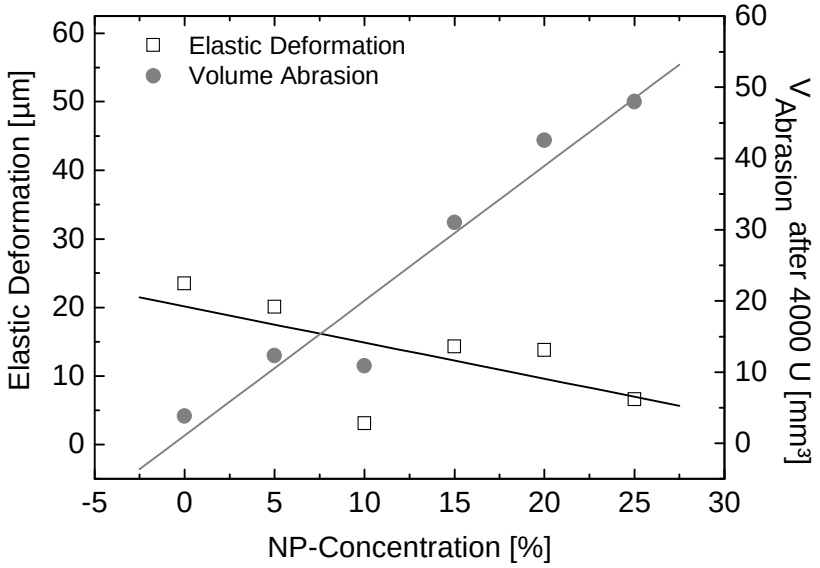

Figure 87. Volume abrasion and elastic deformation of UA/TPGDA films at different concentrations of ALMAL nanoparticles.

In contrast to UA/TPGDA, the elastic deformation of the EPA/TPGDA coatings remains almost constant at varied amounts of ALMAL and the volume abrasion decreases with increase in nanoparticles content. The possible explanation for such behaviour is as follows: EPA/TPGDA films (even without nanoparticles) features a high T_g and high final modulus values. These films are already so hard that the nanoparticles content do not have any further

effect on the elasticity of these films. The hardness of these films is further increased with addition of nanoparticles. As compared to UA/TPGDA, the EPA/TPGDA films with high content of nanoparticles are much harder and are capable to withstand any external force without undergoing much volume loss. This decreases the volume abrasion of EPA/TPGDA films at high concentrations of nanoparticles. Thus, for a film to be abrasion resistant, it should be either elastic with low modulus (like UA/TPGDA) or should be very hard to withhold the force applied by the sandpaper, which is the case with EPA/TPGDA at high concentrations of ALMAL.

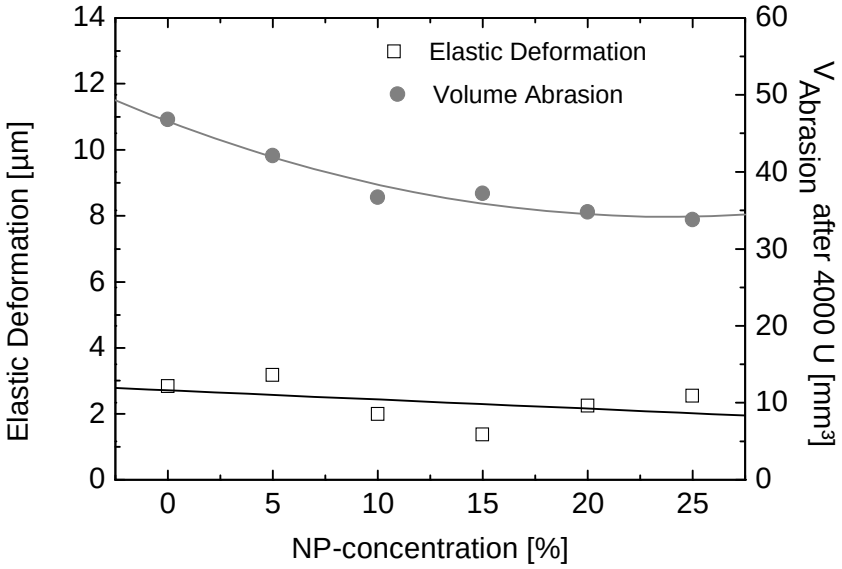

Figure 88. Volume abrasion and elastic deformation of EPA/TPGDA films at different concentrations of ALMAL nanoparticles.

Figure 89 shows the haze values of the EPA/TPGDA and UA/TPGDA coatings with different concentrations of ALMAL, measured with 100 µm thick film. As it can be seen, the haze increases with addition of nanoparticles but the effect is more pronounced in case of UA/TPGDA films. Both the matrices have zero haze and are completely transparent when cured without nanoparticles. But as the nanoparticles are added, haziness of the films increases. The glassy EPA films are transparent till 15 % of ALMAL concentration (haze below 20%). The higher value of haze of UA films at low concentrations of ALMAL shows that the degree of aggregation of nanoparticles in an elastic matrix is possibly higher as compared to that in a glassy matrix like that of EPA.

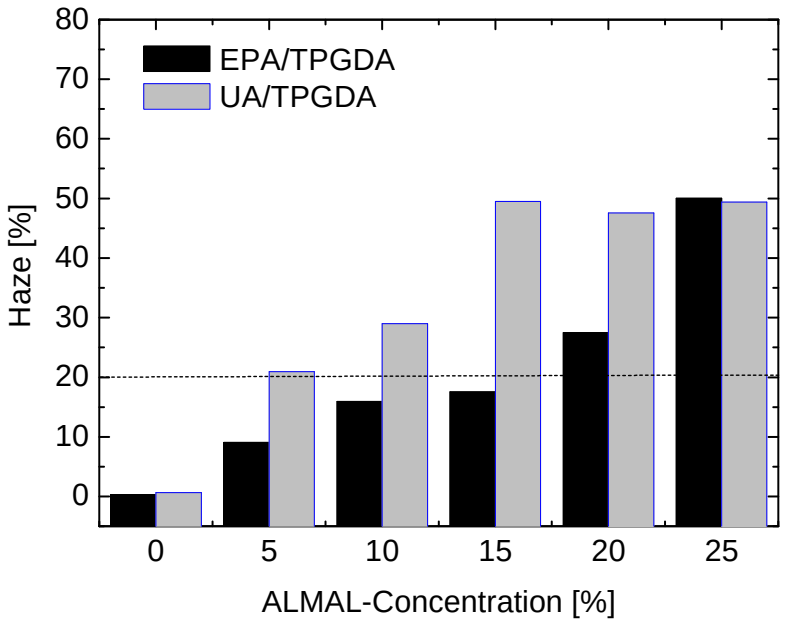

Figure 89. Haze values of UA/TPGDA and EPA/TPGDA films at different concentration of ALMAL nanoparticles.

Thus, the extent of improvement of properties of polymer films by addition of nanoparticles depends largely on the base oligomer/resin. Though, the nanoparticles do not interfere with the chemical kinetics they increase the mechanical properties considerably. If a resin is soft and have a low modulus like urethane acrylate, its modulus and hardness can be increased by addition of nanoparticles, but in turn it reduces its abrasion resistance. On the other hand in case of glassy films like that of EPA, the abrasion resistance increases with increase in its hardness on addition of nanoparticles without impacting its elasticity. Thus, if a transparent film with high mechanical properties is desired, glassy materials like EPA with nanoparticles can prove to be better choice than the one with elastic UA.

5.3 Modelling of Combined Conversion-Modulus Curve

5.3.1 The Empirical Model

In this chapter a physical model is described to fit the experimental modulus-conversion curves. The model was first described by the group of Alig et al, in 2006 (*26*) for a chemo-rheological simple acrylate polymer cured isothermally. This model was developed using the three well known empirical equations, Dibenedetto, Vogel-Fulcher and Havriliak-Negami

equations (*93-95*). It establishes a relationship between shear modulus and conversion of thermosetting or UV cured polymers by taking into account the changes in glass transition temperature and relaxation time of a coating as it is cured. In our case, the glass transition temperature of the acrylate polymer increases continuously as its cross-link density increases. When the glass transition temperature of a polymer during curing exceeds the temperature of cure (T_{cure}) the sample vitrifies. In this region (time interval) the curing reaction shifts to diffusion controlled regime and the reaction rate slows down. The extent of cure has been related uniquely to glass transition temperature of thermosetting polymers (*96-100*) by many research groups. Various models have been developed describing the relationship between these two quantities. In the present model DiBenedetto equation was used to describe the dependence of glass transition temperature $T_g(p)$ on conversion p. It can be given as follows:

$$T_g(p) = \left(\frac{\lambda \cdot p}{1-(1-\lambda)\cdot p} \cdot \left(T_{g,1} - T_{g,0}\right) \right) + T_{g,0} \tag{42}$$

The meaning of these quantities is given in chapter (2.2.2). Usually, the curing reaction slows down due to diffusion restrictions and is retarded before the polymer is 100 % cured and does not reach $T_{g,1}$.

As a resin is polymerized, its cross-link density and the characteristic relaxation time of molecular rearrangements increases. The relaxation time can thus be related to the extent of cure. At first the characteristic relaxation time can be related to curing temperature by Vogel-Fulcher equation as follows:

$$\log(\tau(T_{VF})) = \log(\tau_0) + \frac{B}{T_{cure} - T_{VF}} \tag{43}$$

where T_{VF}, T_{cure}, τ, τ_0, B are the Vogel-Fulcher temperature, the temperature of curing, relaxation time of molecular rearrangements, the relaxation time at time $t = 0$ and a constant specific for a given polymer, respectively. Since the Vogel temperature can be related to glass transition temperature, its conversion dependence can be expressed by:

$$T_{VF}(p) = T_g(p) - c_2 \tag{44}$$

The values of τ_0, B, c_2 and T_{VF} are constants depending on the actual material.

From equations 43 and 45 the dependence of relaxation time on conversion $\tau(p)$ for an isothermal curing reaction can be given as:

$$\log(\tau(p)) = \log(\tau_0) + \frac{B}{T - (T_g(p) - C_2)} \tag{45}$$

For an isothermal curing experiment the complex shear modulus G^* can be expressed by a time-dependent relaxation function $\Phi(t')$ in its general form by:

$$\frac{G^*(\omega, T_{cure}, p) - G_\infty(p)}{G_\infty(p) - G_0(p)} = \int_0^\infty \frac{d\Phi(t', T_{cure}, p)}{dt'} e^{-i\omega t} dt' \tag{46}$$

In case of a curing reaction, Φ is a function of conversion and the temperature of cure. For simplification it is assumed that Φ has a constant shape, i.e. it does not depend on the curing time and is only a function of relaxation time ($\Phi\left(\frac{t'}{\tau}\right)$). The temperature of the system is defined by the curing temperature T_{cure}.

As already mentioned in chapter 2.2, the relaxation function in time-domain is given by the well known KWW function (equation 27). The relaxation time distribution parameter β given by KWW function is assumed to be constant during curing. The relaxation time is a function of curing temperature and conversion $\tau(T_{cure}, p)$ (equations 43 & 45). Alternatively, $G^*(\omega, p)$ can be expressed by the empirical HN function in the frequency domain:

$$\frac{G^*(\omega, p) - G_\infty(p)}{G_\infty(p) - G_0(p)} = -\frac{1}{(1 + (i\omega\tau(p))^\beta)^\gamma} \tag{47}$$

where β, γ are constants for chemically stable polymers depending on the actual material. Here it is assumed that β and γ do not change during curing. In order to describe an isothermal curing experiment at a fixed frequency ω = constant, $\tau(p)$ is replaced by equation 45.

5.3.2 Fitting of Shear Modulus-Conversion Curve

The model was applied here to fit the modulus-conversion curves of simple and homogeneous systems like pure TPGDA and a mixture of EPA and TPGDA in a weight ratio 2:1. In order to fit the modulus-conversion curves of TPGDA, the experimental known parameters were kept fixed and the unknown quantities were obtained by fitting. The fixed quantities are the

ultrasonic frequency $\omega = 3.14 \cdot 10^7\ s^{-1}$ and the temperature of curing $T_{cure} = 293K$. The glass transition temperature of uncured $T_g(p=0) = 193K$ and cured $T_g(p=1) = 320K$ monomer was determined by DMTA. The limiting values of $G_0 = 2.9Pa$ and $G_\infty = 5 \cdot 10^9\ Pa$ were taken from the HN fit of the master curve of uncured and cured monomer respectively. The values of the constants $B = 623.6K$ and $c_2 = 43K$ were obtained from VF fit of shift factors a_T as a function of temperature above T_g for uncured monomer. The four quantities λ, γ, β and τ_0 were set as free fitting parameters. Figure 90 gives the experimental and the fitted curve of TPGDA with $\lambda = 0.4$, $\gamma = 0.07$, $\beta = 0.99$ and $\tau_0 = 4 \times 10^{-12} s$. The G'' curve is shown to illustrate the relaxation maximum which occurs during the 'reaction induced glass transition'.

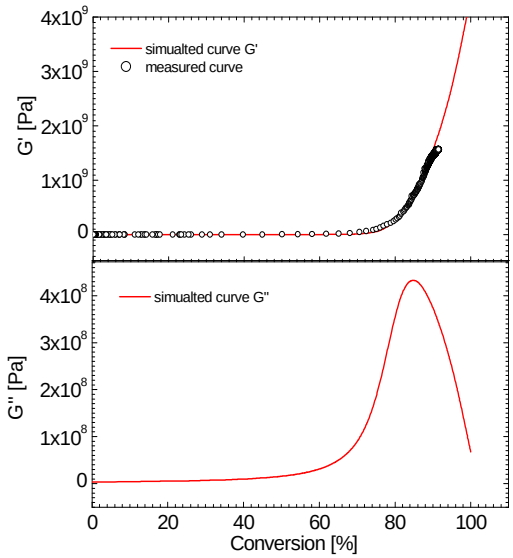

Figure 90. Experimental and simulated modulus-conversion curves of TPGDA at T_{cure}=293 K.

This model was further applied to fit the modulus-conversion curves of a homogeneous polymer mixture EPA/TPGDA in a weight ratio 2:1. The US radial frequency and temperature of cure were again kept fixed. The glass transition temperature of uncured $T_g(p=0) = 232K$ and cured $T_g(p=1) = 295K$ polymer mixture was determined by DMTA. The limiting value of $G_0 = 5111Pa$ and $G_\infty = 2.87 \cdot 10^9\ Pa$ was taken from the HN fit of the master curve of uncured and cured polymer mixture respectively. The values of constants $B = 4791K$ and $c_2 = 144K$ were obtained from VFT fit of shift factors a_T as a function of

temperature above T_g for cured polymer mixture. The fit yields $\lambda = 0.45$, $\gamma = 0.6$, $\beta = 0.9$ and $\tau_0 = 1 \times 10^{-19} s$ were set as free fitting parameters. Figure 91 shows the experimental and the simulated curve of the polymer mixture EPA/TPGDA. The simulated G'' curve as a function of conversion is also shown. The deviation from the theoretical curve at about 60 % conversion is related to the cross over from a light curing phase to a dark reaction phase. Such changes in the reaction mechanism are not included in the model. This deviation is also obvious for TPGDA in Figure X, but less pronounced.

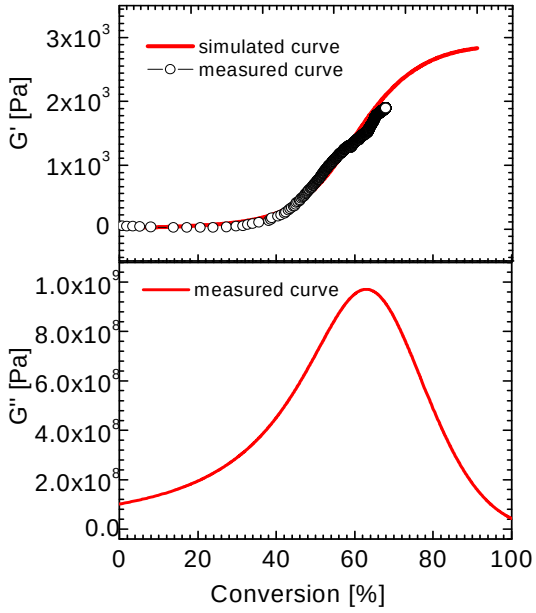

Figure 91. Experimental and simulated modulus-conversion curves of a polymer mixture EPA/TPGDA in a weight ratio 2:1 at T_{cure}=293 K.

It was found that the given empirical model fits well for the systems with single glass transition temperature (homogeneous systems). If desired to use it for a system with two or more phases as in the case of UA, it has to be extended. Furthermore, the extreme broadening of the relaxation time distribution, which has been found for all the UV cured systems investigated, has to be incorporated. For reaction mixtures with high molecular weight reactive oligomers, further modification of the model seems to be necessary.

6 Conclusion and Future Research

This work's aim was to study the photo-curing kinetics and network formation of UV-curable acrylate resins in real time using combined Ultasound/NIR measurements. This method enabled the study of chemical conversion and mechanical modulus (here shear modulus) at the same time and on the same sample, which minimises the errors due to two experiments. This allows studying the interdependency of chemical reaction and rheological properties during curing. These complimentary informations are of great importance, as it allows a UV curing formulator to characterize the resins based on the relationship between their reaction kinetics and the resulting mechanical properties. On the other hand, this combination provides information leading to better understanding of photo-curing kinetics, like the onset of diffusion controlled reactions and the transition between the light curing phase and the dark reaction. With fast acquisition rate of both the measurement techniques-Ultrasound reflectometry (US) and Near Infra Red spectroscopy (NIR), it was possible to study the fast curing kinetics of reactive acrylates in the time scale of milliseconds. In addition to the cure kinetics, final properties of coatings like scratch resistance, abrasion resistance and haze were also studied. The frequency dependent (master curves) and temperature dependent viscoelastic properties of the uncured and cured samples were studied in detail using DMTA.

UV curing was studied for two acrylate systems: the hard and brittle epoxy acrylate (EPA) and the soft elastomer urethane acrylate (UA), both of them diluted with the reactive diluent tripropylene glycol diacrylate (TPGDA). These acrylate resins exhibit a characteristic absorbance band at 1621 nm in the NIR region (900- 2200 nm) which corresponds to CH_2=CH- acrylate double bonds. As the acrylate resin polymerizes, the intensity of this band decreases. Conversion is calculated from the change in area (in case of UA) or change in height (in case of EPA) of this acrylate band. In order to correctly determine the values of conversion and to minimise the errors due to base line shift and overlapping neighbouring bands, the spectral region from 1500 nm to 1800 nm was fitted with 9 Gaussian and 1 cubic functions in case of UA and with 3 Gaussian and 1 linear fit in case of EPA. US reflection technique measures the real time changes in acoustic reflection coefficient of the US shear waves as these waves are reflected at the interface between the sample and the substrate (fused quartz of the US cell). The shear modulus of the coatings is then calculated from the complex reflection coefficient of the US shear waves using the acoustic impedance of the substrate.

The changes in curing kinetics and network formation of the acrylate resins on variation of chemistry of curing formulation and curing conditions are summarised below:

- *Effect of reactive diluent*: Addition of reactive diluent TPGDA in EPA lowers its viscosity and increases the mobility of the reactive chain radicals. This leads to an increase in the rate of polymerization and the rate of formation of polymer networks. The modulus-conversion curves showed that the reaction shifts from a rather diffusion controlled regime to an extended interval of mass controlled reaction on dilution. The final conversion as well as final modulus of the films increases with increase in concentration of the reactive diluent TPGDA. DMTA analysis indicates that the cross-link density of EPA increases with addition of low molecular weight TPGDA. This is also reflected from a decrease in the elasticity and increase in the permanent deformation of the films in the scratch tests.
- *Effect of PI and duration of UV irradiation*: Increase in the concentration of photoinitiator and time of UV irradiation (total UV dose) were found to have similar impact on the final properties of the EPA/TPGDA film. Increased time of UV irradiation increased the final conversion and modulus of the film without affecting the curing kinetics and interdependency of modulus and conversion of the reacting resin in the light curing phase. On the other hand with increase in PI concentration, both the rate of polymerization and the rate of network formation were increased and the dependency of modulus on the extent of conversion was changed. This is attributed to an increase in concentration of primary radicals which accelerates the rate of polymerization increasing the crosslink density of the film.

The influence of different types and concentration of nanoparticles on the properties and curing kinetics of EPA matrix and UA matrix are summarised as follows:

- *Effect of different types of nanoparticles*: A series of UV curing experiments with different types of nanoparticles like ALMAL, ALOXAL, Aerosil, ALMA and SIMA (15 wt % with respect to the matrix) in EPA/TPGDA base matrix showed that the chemical conversion and shear modulus of the films is independent of the type of nanoparticles. The values of the final conversion and glass transition temperature of pure EPA/TPGDA film and those with nanoparticles were close to each other, indicating no significant impact of nanoparticles on the chemical kinetics of the base resin. The shear modulus of the EPA/TPGDA film increased on addition of nanoparticles, irrespective of the type of nanoparticles. It was found that the film with ALMA nanoparticles had the lowest value of haze (< 20%) and the film was

transparent, whereas all other films exhibited higher values of haze (> 20%). The SEM pictures showed that the ALMA nanoparticles are better dispersed in the matrix and has lowest degree of agglomeration, whereas SIMA nanoparticles which have the same functional groups as ALMA formed agglomerates of size 200-400 nm. From the scratch test results it was found that as compared to other polymer-nanocomposite systems, the film with ALOXAL nanoparticles showed improved scratch resistance properties. Thus, it can be concluded that different types of nanoparticles impart different final properties to the films, though they do not interfere with the chemical kinetics.

- *Effect of concentration of nanoparticles*: It was found that the final modulus of the EPA/TPGDA films increased with increase in the concentration of SIMA nanoparticles without any change in kinetics of network formation and conversion. This phenomenon was discussed using the serial and parallel models for the modulus. It was found that the experimentally determined modulus values were close to the prediction of the serial model. The constant value of the glass transition temperature, determined from the maximum of the loss modulus curves, also indicates that there is no significant change in the structure of the polymer networks and it is merely a mixing effect. It was found that both an increase in concentration of nanoparticles and the thickness of the films decreases the optical transparency, thereby increasing the haze of the films. It was further found that the mechanical properties of the films like, the modulus and volume abrasion resistance increased with nanoparticle concentration.
- *Effect of type of base oligomer*: The study of UV-curing kinetics of two different base matrices i.e, a rubber-elastic UA/TPGDA network and a glassy EPA/TPGDA network in presence of ALMAL nanoparticles showed a similar trend in chemical kinetics and mechanical properties during curing. It was found that the chemical kinetics of both the matrices were independent of the concentration of nanoparticles. The final properties of the films were found to depend mainly on the inherent nature of the matrix. The shear modulus of UA/TPGDA networks at room temperature represents entropy-elastic behaviour, whereas the shear modulus of the EPA/TPGDA network is dominated by energy-elasticity in the glassy state. The nanoparticles were found to have greater impact on the soft UA matrix as compared to the glassy EPA matrix. The nanoparticles decreased the surface elasticity (in the scratch test) of the UA/TPGDA films whereas no significant effect was seen in case of EPA/TPGDA. Insufficient

hardness and the loss of elastic behaviour due to addition of nanoparticles lead to a decrease in volume abrasion resistance of UA/TPGDA films. On the other hand, in case of EPA/TPGDA, addition of nanoparticles increased its hardness, increasing the volume abrasion resistance of the films. The rubber-elastic UA/TPGDA films had higher value of haze as compared to glassy EPA/TPGDA. This indicates higher degree of agglomeration in case of rubbery matrix.

It was found that the nanoparticles mainly improved the mechanical properties of the polymer coatings, without affecting the cure kinetics. Finally an empirical fit model based on combined Dibenedetto, Vogel-Fulcher and Havriliak-Negami equations was applied to model the interdependency of modulus and conversion for homogeneous systems like TPGDA and mixture of TPGDA and EPA. Some ideas for its improvement are given.

Future Research

This combined US/NIR measurement method has a great potential as a qualitative tool in polymer research and material development. It can be used to compare the cure efficiency of different reactive diluents, photoinitiators and different matrix systems. This will be helpful in formulating an organic coating with controlled reaction kinetics and desired properties. As far as the interpretation in terms of “chemical reaction controlled reaction kinetics”, “light curing phase” and “dark reaction phase” is concerned, this combined method has still not used its potential for better understanding of basic radiation curing kinetics. All the measurements discussed above were done at a single temperature (i.e, at room temperature). It will be interesting to study the cure kinetics of the resins at varied temperatures. This method can be further extended to study the cure kinetics of interpenetrating networks and study how the cure kinetics of each of its component affects its network formation. This set up used a microwave powered continuous Mercury vapour UV-Lamp with a broad UV spectrum (200-600 nm). Replacing this broad range UV lamp with a monochromatic source like laser radiation or an LED will further facilitate to study more complex reactions and to compare the results to the corresponding kinetic equations. The wavelength range of the used near-infrared spectrometer (900-2200 nm) limits its use to acrylates only. This can be further extended till mid-IR region to study the cure kinetics of epoxies and water based urethanes. Further, the model given above can be extended for predicting the dependency of modulus on conversion in case of complex and multiphase systems.

7 List of Abbreviations and Symbols

A	Area
A_{us}	Amplitude of US shear waves
ALMAL	Aluminium maleate, Bis- Aluminium dihydroxy maleate nanoparticles
ALMA	3-Methacryloxy(propyl)trimethoxysilane modified aluminium oxide nanoparticles
ALOXAL	Bis- Aluminium dihydroxy oxalate nanoparticles
Aerosil	Silica nanoparticles
a_T	Shift factor
B	Activation Temperature
c_t	Speed of sound through quartz bar
DMTA	Dynamic mechanical thermal analysis
EPA	Epoxy acrylate
F	Force
G*	Complex dynamic shear modulus
G’	Storage shear modulus
G’’	Loss shear modulus
G_e	Equilibrium shear modulus
$G_{parallel}$	Shear modulus of serial interaction
G_{serial}	Shear modulus of parallel interaction
I_a	Absorbed irradiance
I_0	Incident irradiance
K	Bulk modulus
k_p	Propagation rate constant

k_t	Termination rate constant
KCL	Kinetic chain length
l	Film thickness
L^*	Complex dynamic longitudinal modulus
$[M]_{t_i}$	Concentration of monomer at the onset of dark reaction
MEHQ	Hydroquinone monomethyl ether
n_{p}	Refractive index of particles
n_{m}	Refractive index of matrix
PI	Photoinitiator
$[PI^{\bullet}]_0$	Concentration of polymer radicals at the end of UV exposure
$[PI^{\bullet}]$	Concentration of polymer radicals
$P(t)$	Conversion at time t
R	Gas constant (8.314 J/mol.K)
r	Reflection coefficient
R_p	Rate of Polymerization
r_i	Rate of Initiation
$(R_p)_{t_i+t}$	Rate of dark polymerisation at time $t_i + t$
SIMA	3-Methacryloxy(propyl)trimethoxysilane modified silica nanoparticles
T	Temperature
T	Time
T_g	Glass transition temperature
T_{VF}	Vogel–Fulcher temperature
T_g	Glass transition temperature

$T_{G,0}$	Glass transition temperature of uncured sample
$T_{G,1}$	Glass transition temperature of cured sample
$T_G(p)$	Glass transition temperature at conversion P
T_{cure}	Temperature of cure (293 K)
TPO-L	Ethyl - 2, 4, 6 – Trimethylbenzoylphenylphosphinate
TPGDA	Tripropylene glycol diacrylate
US	Ultrasound reflectometry
UST	Universal surface tester
UA	Urethane acrylate
UV	Ultra-violet radiation
$V_{Abrasion}$	Volume abrasion
W_A	weight fraction of homo-polymer A
W_B	weight fraction of homo-polymer B
X	Wavelength
X_0	Area under acrylate band at time zero
X_t	Area under acrylate band at time t
$X(t)$	Height of Gaussian function of the band 1621 nm at time t
$X(0)$	Height of Gaussian function of the band 1621 nm at time 0
Z	Acoustic impedance
$\mathbf{\Phi}_i$	Quantum yield of initiation
ϕ	Phase shift of the reflected US waves
$\mathbf{\Phi}$	Relaxation function
$\mathbf{\Phi}_2$	Volume fraction of organic component of the matrix

$\mathbf{\Phi}_1$	Volume fraction of inorganic component of the matrix
$\mathbf{\Phi}_p$	Volume fraction of particles
ε_{PI}	Molar extinction coefficient of photoinitiator
E	Strain
ε_1	Strain of inorganic component of the polymer nanocomposite
ε_2	Strain of organic component of the polymer nanocomposite
Σ	Shear stress
σ_1	Stress of inorganic component of the polymer nanocomposite
σ_2	Stress of organic component of the polymer nanocomposite
Ω	Radial Frequency
γ	Shear angle
υ	Poisson's ratio
P	Density
Λ	Constant in debenedetto equation
H	Viscosity
$\tau(p)$	Relaxation time as a function of conversion
δ	Phase lag between stress and strain
Ω	Specific resistance
ν_e	Cross-link density

8 References

1. A. Goldschmidt, H. J. Streitberger, *BASF Handbook On Basics Of Coating Technology*. (Vincentz Network, Hannover, Germany, 2003).
2. R. Schwalm, *UV Coatings - Basics, Recent Developments and New Applications.* (Elsevier, ed. 1st 2007).
3. P. Gloeckner, T. Jung, S. Struck, K. Studer, *Radiation Curing-Coatings and Printings Inks*. (Vincentz Network, Hannover, Germany, 2008).
4. A. Endruweit, M. S. Johnson, A. C. Long, *Polym. Composite* **27**, 119 (2006).
5. J. A. Johnson, C. O. Bliss, *Radtech Report*, 21 (2006).
6. M. Kutschera, R. Sander, P. Herrmann, U. Weckenmann, A. Poppe, *JCT Research* **3**, 91 (2006).
7. E. Beck, *Euro. Coat.* **9**, 10 (2006).
8. A. M. S. Chowdhury, M. M. Rahman, H. C. Das, M. N. Islam, M. A. Khan, *Polym. Plast. Technol. Eng.* **45**, 1295 (2006).
9. M. H. Bland, N. A. Peppas, *Biomaterials* **17**, 1109 (1996).
10. G. Wisanrakkit, J. K. Gillham, *J. Appl. Polym. Sci.* **41**, 2885 (1990).
11. I. Alig, K. Nancke, C. P. Johari, *J. Polym. Sci. Poly. Phys.* **32**, 1465 (1994).
12. M. R. Kamal, S. Sourour, *Thermochim. Acta* **14**, (1976).
13. A. Nebioglu, M. D. Soucek, *J. Polym. Sci. Poly. Chem.* **44**, 6544 (2006).
14. F. Karasu, M. Aydin, M. A. Kaya, D. K. Balta, N. Arsu, *Prog. Org. Coat.* **64**, 1 (2009).
15. I. V. Khudyakov, W. S. Fox, M. B. Purvis, *Ind. Eng. Chem. Res.* **40**, 3092 (2001).
16. T. F. Scott, W. D. Cook, J. S. Forsythe, *Polymer* **44**, 671 (2003).
17. T. Scherzer, S. Mueller, R. Mehnert, A. Volland, H. Lucht, *Polymer* **46**, 7072 (2005).
18. T. Scherzer, S. Mueller, R. Mehnert, A. Volland, H. Lucht, *Nucl. Instrum. Meth. B* **236**, 123 (2005).
19. R. P. Slopek, Master Thesis, Georgia Institute of Technology (2005).
20. C. Decker, *J. Polym. Sci. Poly. Chem.* **30**, 913 (1992).
21. C. Decker, *Prog. Polym. Sci.* **21**, 593 (1996).
22. C. Decker, *Polym. Int.* **45**, 133 (1998).
23. C. Decker, *Macromol. Rapid. Commun.* **23**, 1067 (2002).
24. C. Decker, *J. Coatings. Tech.* **59**, 97 (1987).
25. B. S. Chiou, S. A. Khan, *Macromolecules* **30**, 7322 (1997).
26. I. Alig, P. A. M. Steeman, D. Lellinger, A. A. Dias, D. Wienke, *Prog. Org. Coat.* **55**, 88 (2006).
27. I. Alig, D. Lellinger, J. Sulimma, S. Tadjbakhsch, *Rev. Sci. Instrum.* **68**, 1536 (1997).
28. D. Lellinger, S. Tadjbakhsch, I. Alig, *Macromol. Symp.* **184**, 203 (2002).

29. I. Alig, H. Oehler, D. Lellinger, *Adhaesion* **5**, 36 (2005).
30. M. L. Digar, S. L. Hung, T. C. Wen, A. Gopalan, *Polymer* **43**, 1615 (2002).
31. P. J. Flory, *Principles of Polymer Chemistry*. (Cornell University Press, London, 1971).
32. C. Li, R. M. Nagarajan, C. C. Chiang, S. L. Cooper, *Polym. Eng. Sci.* **26**, (1986).
33. T. A. Speckhard *et al.*, *J. Appl. Polym. Sci.* **30**, 647 (1985).
34. C. Decker, D. Decker, *Pure Appl. Chem.* **34**, 605 (1997).
35. U. Kolczak, G. Rist, K. Dietliker, J. Wirz, *J. Am. Chem. Soc.* **118**, 6477 (1996).
36. S. Jockush, N. J. Turro, *J. Am. Chem. Soc.* **120**, 11773 (1998).
37. I. Gatlik *et al.*, *J. Am. Chem. Soc.* **121**, 8332 (1999).
38. M. Spichty *et al.*, *J. Photoch. Photobio. A.* **142**, 209 (2001).
39. S. Jockusch, N. J. Turro, *J. Am. Chem. Soc.* **121**, 3921 (1999).
40. J. Lalevee, X. Allonas, S. Jradi, J. P. Fouassier, *Macromolecules* **39**, 1872 (2006).
41. S. Zhu, Y. Tian, A. E. Hamielec, *Macromolecules* **23**, 1144 (1990).
42. C. Decker, B. Elzaouk, D. Decker, *Pure Appl. Chem.* **33**, 173 (1996).
43. M. D. Goodner, C. N. Bowman, *Macromolecules* **32**, 6552 (1999).
44. K. S. Anseth, C. M. Wang, C. N. Bowman, *Macromolecules* **27**, 650 (1994).
45. W. Funke, *Brit. Polym. J.* **21**, 107 (1989).
46. L. Lecamp, B. Youssef, C. Bunel, P. Lebaudy, *Polymer* **40**, 1403 (1999).
47. C. N. Bowman, N. A. Peppas, *Chem. Eng. Sci.* **47**, 1411 (1992).
48. D. L. Kurdikar, N. A. Peppas, *Macromolecules* **27**, 4084 (1994).
49. J. Fournier, G. Williams, C. Duch, G. A. Aldridge, *Macromolecules* **29**, 7097 (1996).
50. K. C. Cole, *Macromolecules* **24**, (1991).
51. K. C. Cole, J. J. Hechler, D. Noel, *Macromolecules* **24**, (1991).
52. C. S. Chern, G. W. Poehlein, *Polym. Eng. Sci.* **27**, (1987).
53. C. M. W. Kristi S. Anseth, Christopher N. Bowman, *Macromolecules* **27**, 650 (1994).
54. E. Rabinowitch, *Trans. Faraday Soc.* **33**, (1937).
55. Y. Choe, *Macromol. Res.* **11**, 311 (2003).
56. W. Jenninger, J. E. K. Schawe, I. Alig, *Polymer* **41**, 1577 (2000).
57. S. Rice, *In Diffusion-Limited Reactions*. (Elsevier, New York, 1985).
58. J. D. Ferry, *Viscoelastic Properties of Polymers*. (John Wiley & Sons, ed. 3rd Edition, 1980).
59. G. Strobl, *The Physics of Polymers*. (Springer, ed. 2nd, 1997).
60. F. Kohlrausch, *Pogg. Ann. Phys.* **199**, (1863).
61. G. Williams, D. C. Watts, *Faraday Soc.* **66**, (1971).
62. S. Havriliak, S. Negami, *Polymer* **8**, 161 (1967).

63. S. Havriliak, S. Negami, *J. Polym. Sci. Part C* **4**, (1966).
64. L. R. G. Treloar, *The Physics of Rubber Elasticity*. (Oxford, ed. 3rd, 1975).
65. E. Stark, K. Luchter, M. Margoshes, *Appl. Spectrosc. Rev.* **22**, 335 (1986).
66. D. G. Rogers, E. Marand, D. J. T. Hill, G. A. George, *High Perform. Polym.* **11**, 27 (1999).
67. S. J. Park, G. H. Kwak, M. Sumita, J. R. Lee, *Polym. Eng. Sci.*, (2000).
68. J. M. R. Fontoura *et al.*, *J. Appl. Polym. Sci.* **90**, 1273 (2003).
69. L. A. R. Guadarrama, *Eur. Polym. J.* **43**, 928 (2007).
70. D. Fischer, T. Bayer, K. J. Eichhorn, M. Otto, *Fresenius J Anal Chem* **359**, 74 (1997).
71. H. W. Siesler, Y. Ozaki, S. Kawata, H. M. Heise, *Near Infrared Spectroscopy, Principles, Instruments, Applications.* (Wiley-VCH, Weinheim 2002).
72. W. P. Mason, W. O. Baker, H. J. McSkimin, J. H. Heiss, *Phys. Rev.* **75**, 936 (1949).
73. I. Alig, D. Lellinger, *Chem. Innov.* **1**, 12 (2000).
74. I. Alig, H. Oehler, D. Lellinger, S. Tadjbach, *Prog. Org. Coat.* **58**, 200 (2007).
75. G. E. Kron, *Publ. Astron. Soc. Pac.*, 76 (1966).
76. W. V. Bhagwat, N. R. Dhar, *J. Phys. Chem.* **35**, 2383 (2002).
77. C. D. Vladimir VIvanov, *Polym. Int.* **50**, 113 (2001).
78. **www.innowep.com**.
79. C. R. Mendonca, D. S. Correa, T. Baldacchini, P. Tayalia, E. Mazur, *Appl. Phys. A* **90**, 633 (2008).
80. A. D. Gianni *et al.*, *J. Coat. Technol. Res.* **6**, 177 (2009).
81. L. Keller *et al.*, *Polymer* **45**, 7437 (2004).
82. N. G. Salleha, H. J. Glaesel, R. Mehnert, *Radiat. Phys. Chem.* **63**, 475 (2002).
83. H. J. Glaesel *et al.*, *Macromol. Chem. Phys.* **201**, 2765 (2000).
84. F. Bauer, H.-J. Glaesel, E. Hartmann, E. Bilz, R. Mehnert, *Nucl. Instrum. Meth. B* **208**, 267 (2003).
85. F. Bauer *et al.*, *Nucl. Instrum. Meth. B* **265**, 87 (2007).
86. H. J. Glaesel, E. Hartmann, L. Wennrich, T. Hoeche, M. R. Buchmeiser, *Macromol. Mater. Eng* **292**, 70 (2007).
87. J. Dai, X. Gao, G. Jiang, *Makromol. Chem.* **192**, 177 (1991).
88. B. Nabeth, I. Corniclion, J. P. Pascault, *J. Polym. Sci. Poly. Phys.* **34**, 401 (1996).
89. P. H. Barbeau, J. F. Gerard, B. Magny, J. P. Pascault, G. Vigier, *J. Polym. Sci. Poly. Phys.* **37**, 919 (1999).
90. J. Yang, Z. Wang, Z. Zeng, H. Yuan, Y. Chen, *Chinese J. Polym. Sci.* **19**, 175 (2001).
91. H. Kou, A. Asif, W. Shi, *Journal of Appl. Polym. Sci.* **89**, 1500 (2003).
92. G. Mie, *Annalen der Physik* **330**, 377 (1908).
93. W. Vogel, *Phys. Z.* **22**, 645 (1921).

94. G. S. Fulcher, *J. Am. Ceram. Soc.* **8**, (1925).

95. A. T. Dibenedetto, *J. Polym. Sci. Poly. Phys.* **26**, 1949 (1987).

96. S. L. Simon, J. K. Gillham, *J. Appl. Polym. Sci.* **51**, 1741 (1994).

97. S. L. Simon, J. K. Gillham, *J. Appl. Polym. Sci.* **47**, 461 (1993).

98. S. Montserrat, *J. Appl. Polym. Sci.* **44**, 545 (1992).

99. A. Hale, C. W. Macosko, H. E. Bair, *Macromolecules, Vol. 24, No. 9, 1991* **24**, 2610 (1991).

100. J. P. Pascault, R. J. J. Williams, *J. Polym. Sci. Poly. Phys.* **28**, 85 (1990).

9 Appendix

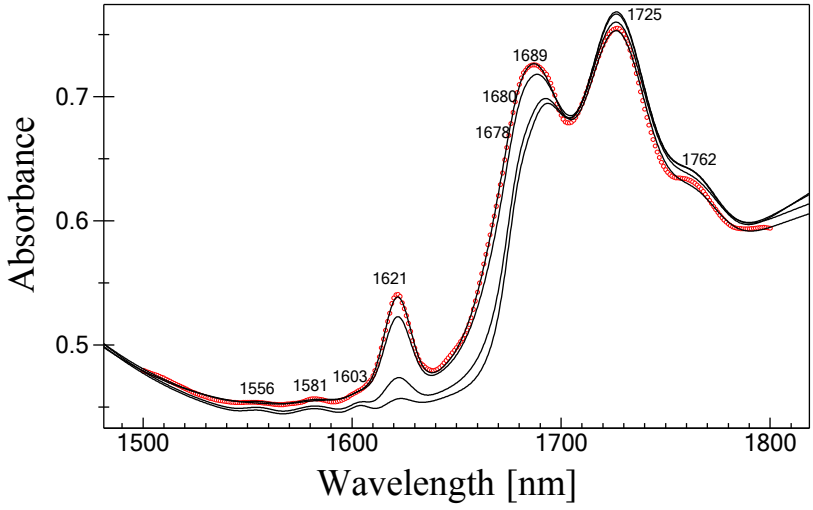

Figure 92. Fit of an NIR spectrum from 1500-1800 nm with 9 Gaussian fit function (in red circles).

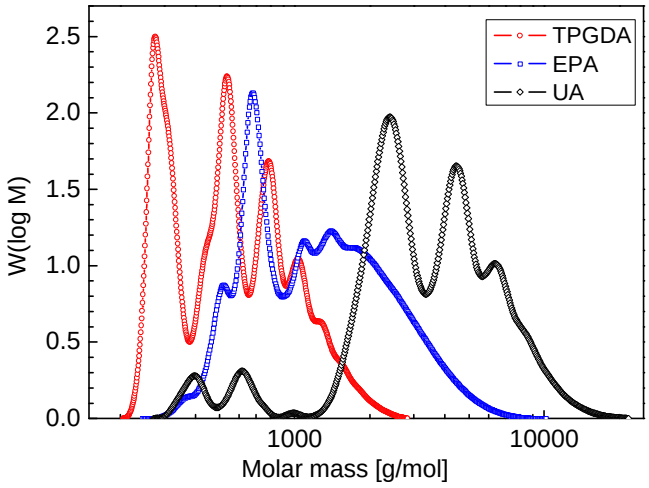

Figure 93. GPC chromatogram of TPGDA, EPA and UA in THF.

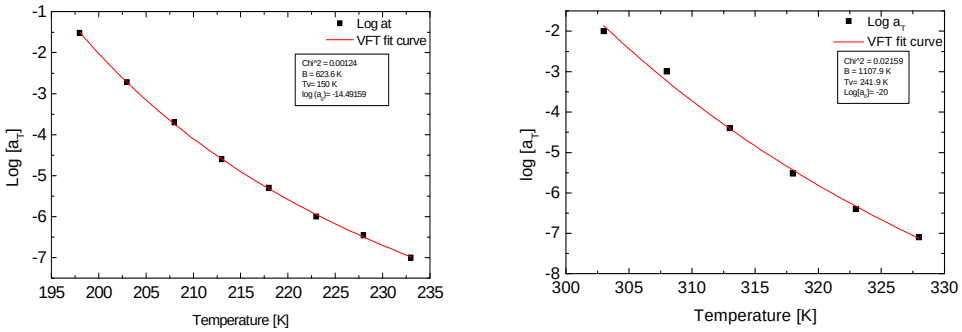

Figure 94. VFT fit of frequency shift factors vs. temperature for uncured TPGDA (left) and cured TPGDA (right).

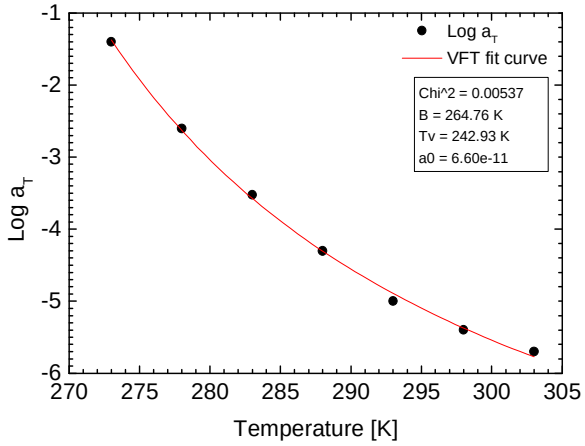

Figure 95. VFT fit of frequency shift factors vs. temperature for uncured EPA.

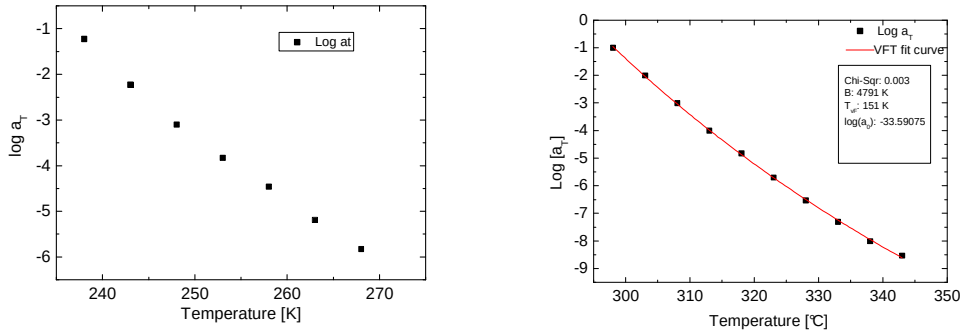

Figure 96. Frequency shift factors vs. temperature for uncured EPA/TPGDA (left) and cured EPA/TPGDA (right).

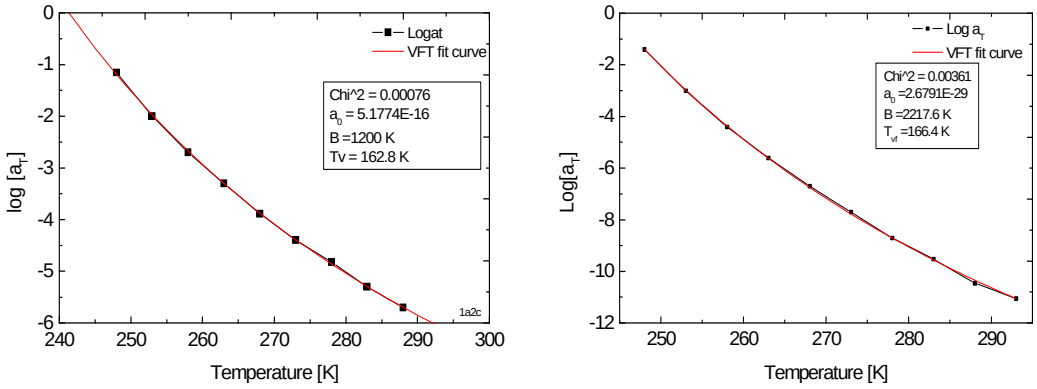

Figure 97. VFT fit of frequency shift factors vs. temperature for uncured UA (left) and cured UA (right).

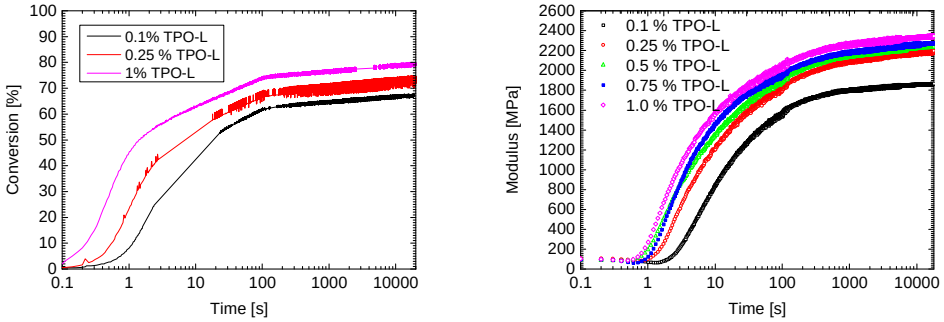

Figure 98. conversion-time curves (left) and modulus-time curves (right) of the cured EPA/TPGDA coatings filled with 15 wt % of ALMAL at different concentrations of photoinitiator-TPO-L.

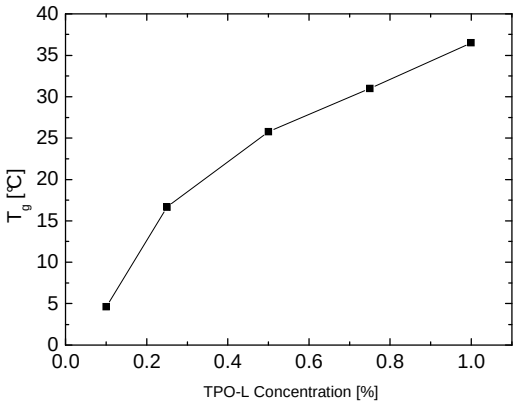

Figure 99. Glass transition temperature of the cured EPA/TPGDA coatings filled with 15 wt % of ALMAL nanoparticles as a function of different concentration of photoinitiator-TPO-L.

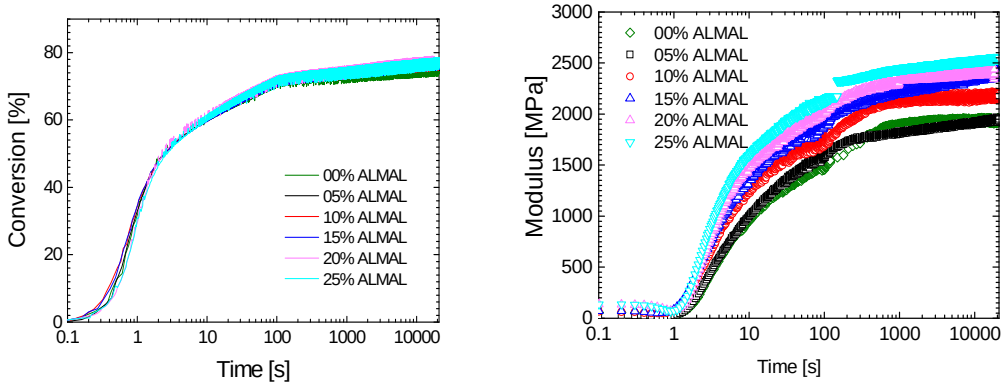

Figure 100. Conversion-time curves (left) and Modulus-time curves (right) of the EPA/TPGDA coatings at different concentrations of ALMAL nanoparticles.

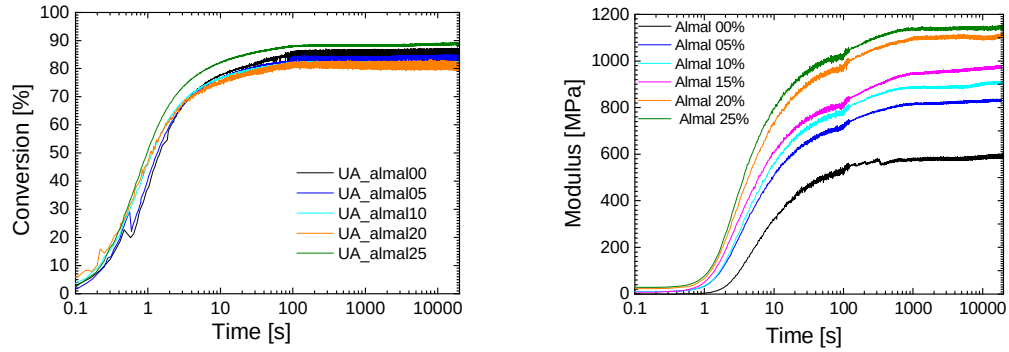

Figure 101. Conversion-time curves (left) and Modulus-time curves (right) of the UA/TPGDA coatings at different concentrations of ALMAL nanoparticles

Curriculum Vitae

Name and Address:	Suman Agarwal Neckarstrasse 15 64283 Darmstadt
Date of Birth:	14.06.1982
Place of Birth:	Cuttack, India
Nationality:	Indian
Email:	suman.agl@gmail.com

Academic Career

05/1997	10th, Seventh Day Adventist High School, Khurda, India
07/1997 - 06/1999	12th, Prannath College, Khurda, India
07/1999 - 06/2002	Bachelors in Chemistry (BSc.) Ravenshaw College, Cuttack, India
07/2003 - 08/2005	Masters in Chemistry (MSc.) Utkal University, Bhubaneswar, India
08/2005 - 08/2007	Masters of Technology (M. Tech.) in "Modern Methods of Chemical Analysis", Indian Institute of Technology Delhi, India
02/2006 - 07/2006	Minor project: "Effect of Hydrocarbon phases on the size of nanoparticles synthesized by reverse micellar route" Indian Institute of Technology Delhi, India
09/2006 - 05/2007	Master Thesis: "EPR investigation of catalyst free SWNT and endofullerene doped peapods", TU-Darmstadt, Germany
11/2007 - 1/2011	Doctorate at German Polymer Institute, Darmstadt Thesis: "In Situ Monitoring of UV curing of Acrylate Coatings by Combined US/NIR"

Work Experience

04/2007 - 05/2007	"Analysis of the PMMA films by Raman spectroscopy" at Degussa, Darmstadt
10/2009 - 03/2010	Guided Practical classes for Master Students on "Dielectric Spectroscopy of Polymers" German Polymer Institute-TUD, Darmstadt

Darmstadt, 26. November 2011

Presentations:

- "In Situ Monitoring of UV-Curing by Combined NIR & US Spectroscopy"
  S. Agarwal, H. Oehler, D. Lellinger and I. Alig, 2nd Baekeland Symposium on Thermosets, Antalya, Turkey, November 2009

- „Einfluss Von Bindersystem Und Nanofüllern Auf Härtung Und Eigenschaften Von UV - Lacken"
  S. Agarwal, H. Oehler, D. Lellinger and I. Alig, DKI - Kolloquim, Darmstadt, Germany, March 2010

- "In Situ Monitoring of UV-Curing of Acrylate Coatings"
  S. Agarwal, H. Oehler, D. Lellinger and I. Alig, MSE 2010, Darmstadt, Germany, August 2010

Poster Presentations:

- "Kinetic study of photoinduced quasi-simulatenous interpenetrating polymer networks", *M. De Brito, X. Allonas, Céline Croutxé-Barghorn, S. Agarwal, I. Alig*, ESPS, Mulhouse, France, November 2010.
- "Monitoring of UV-Curing of Acrylate Coatings by Combined US/NIR Spectroscopy"
  S. Agarwal, I. Alig, 2nd Postgraduate Workshop, Technical University Darmstadt, Germany, 1st July 2009.

Suman Agarwal

Neckarstrasse 15

64283 Darmstadt

Darmstadt, 26.11.2010

Eidesstattliche Erklärung

Affirmation

Ich erkläre hiermit an Eides Statt, dass ich meine Dissertation selbständig und nur mit den angegebenen Hilfsmitteln angefertigt habe.

I declare that I have made my dissertation independently and only with the specified tools.

Darmstadt, 26. November 2010

Suman Agarwal

Neckarstrasse 15

64283 Darmstadt

Darmstadt, 26.11.2010

Erklärung

Declaration

Ich erkläre hiermit, noch keinen Promotionsversuch unternommen zu haben.

I hereby declare that this Doctor thesis has not been submitted previously for a comparable academic award.

Darmstadt, 26. November 2010